Anette Johannessen

Characterizing the damage mechanisms of orthopedic joint prostheses

Master's thesis in Materials Science and Engineering
Supervisor: Ida Westermann
Co-supervisor: Ragnhild Elizabeth Aune
June 2021

Master's thesis

NTNU
Norwegian University of Science and Technology
Faculty of Natural Sciences
Department of Materials Science and Engineering

NTNU
Norwegian University of
Science and Technology

Anette Johannessen

Characterizing the damage mechanisms of orthopedic joint prostheses

NTNU
Norwegian University of
Science and Technology

Preface

This is a master's thesis governed by the Norwegian University of Science and Technology (NTNU). Three used hip joint prostheses were examined using various metallurgical methods. The aim was to characterize the damage mechanisms present in the materials, understand why these arose and compare the damage mechanisms to relevant literature.

The main supervisor for this project was Ida Westermann. She has provided valuable guidance, ideas and feedback throughout the project work. Co-supervisor Ragnhild Elizabeth Aune has provided the prostheses used in this project. I have greatly appreciated their contributions to this project.

I would also like to thank Berit Vinje Kramer along with Yingda Yu, Håkon Wiik Ånes, Pål Christian Skaret and Cristian Torres Rodriguez. They have taught me how to use the equipment and software needed for this thesis. They have also patiently provided help and guidance when needed.

Anders Sundal from Ortomedic and Dr. Åke Hamberg have helped me identify the prostheses in this project. Dr. Hamberg has also provided much valuable information about common prosthesis materials, the use of these and potential issues.

All utilized equipment, tools and chemicals have been provided and financed by NTNU.

Anette Johannessen

Trondheim, June 2021

Summary

English

This project investigated three used hip joint prostheses with the goal of understanding which damage mechanisms were present and why these arose. A series of metallurgical examinations were executed to reveal surface characteristics, microstructure and material properties.

Two of the prostheses were from a CoCrMo alloy and were referred to as prosthesis Co and prosthesis Co-o. The last prosthesis was made from stainless steel and was referred to as prosthesis SS. Prosthesis Co-o had a fatigue fracture at the stem, that originated from cyclic stresses during use. The prosthesis had an uneven surface, which provided many stress raisers where fatigue cracks could initiate, and very large grains that allowed crack propagation to develop rapidly. Prosthesis Co also had unfavourably large grains. Prosthesis SS had larger grains in the direction perpendicular to the stem length than in the parallel direction. This was unfavourable as the typical loads for a hip prosthesis would cause cracks to propagate in the direction in which there were fewer grain boundaries to impede them. All prostheses had discoloration and surface layers from corrosion. Tribo-corrosion had likely happened in between the femoral heads and necks of prostheses Co and Co-o. All prostheses had larger damages to the surfaces that likely originated post use.

Norwegian

Dette prosjektet undersøkte tre brukte hofteleddsproteser med hensikt å forstå hvilke skademekanismer som var til stede og hvorfor disse oppsto. En rekke metallurgiske undersøkelser ble benyttet for å avdekke overflatekarakteristikk, mikrostruktur og materialegenskaper.

To av protesene besto av CoCrMo og refereres til som protese Co og protese Co-o. Den siste protesen besto av rustfritt stål og refereres til som protese SS. Protese Co-o hadde et utmattingsbrudd på stammen, forårsaket av syklisk belastning ved bruk. Protesen hadde ujevn overflate, hvilket ga mange punkter med økt spenning der sprekker kunne initiere, samt svært store korn som tillot rask sprekkutvikling. Protese Co hadde også uhensiktsmessig store korn. Protese SS hadde større korn i vinkelrett retning på protesens lengde enn parallelt. Dette var uheldig da typiske belastninger for en hofteprotese vil gi sprekkutvikling i den retningen hvor det er færre korngrenser som kan hindre dette. Alle protesene hadde misfarge og overflatelag som følge av korrosjon. Det hadde mest sannsynlig oppstått tribokorrosjon i overgangen mellom nakke og hode for protesene Co og Co-o. Alle protesene hadde større overflateskader som sannsynligvis ikke oppsto under bruk, men i etterkant.

Contents

1 Abbreviations

Table 1 below lists the abbreviations used in this thesis.

Table 1: *This table lists the upcoming abbreviations*

Abbreviation	Meaning
NTNU	Norwegian University of Science and Technology
MoM	Metal on Metal
MoP	Metal on Polyethylene
CoC	Ceramic on Ceramic
BCC	Body Centered Cubic
HCP	Hexagonal Close Packed
FCC	Face Centered Cubic
UHMWPE	Ultra High Molecular Weight Polyethylene
ZTA	Zirconia Toughened Alumina
PMMA	Polymethyl Methacrylate
UTS	Ultimate Tensile Strength
WHO	World Health Organization
EU	European Union
wt%	Weight percentage
at%	Atomic percentage
XRF	X-Ray Fluorescence
SEM	Scanning Electron Microscopy
SE	Secondary Electrons
BSE	Backscatter Electrons
EDS	Energy Dispersive x-ray Spectroscopy
EBSD	Electron Backscatter Diffraction
PE	Perpendicular
PA	Parallel
HV	Hardness Vickers
Ext.	External
Int.	Internal
R_a	Average roughness
R_q	Root mean square roughness
R_z	Mean peak to valley height

2 Introduction

As modern day technology advances, so do the possibilities within the medical sector. Joint prostheses are now a common way to increase mobility and reduce pain for patients suffering from osteoarthritis and other conditions affecting the joints. Looking only at hip joint prostheses, 9870 prostheses were implanted in Norway in 2019[27]. There is a broad selection of designs and materials to choose from, allowing each patient to be paired with a suitable model.

The vast material selection signify the need for thorough testing before putting them to use. It is possible to test each material short term, but there is a need for universal in vitro test methods to determine long time consequences of utilizing a material. Many materials are just now displaying their long term properties. In order to develop such test methods, data must be collected from the various materials. This master's thesis is part of collecting such data.

This project examines three used hip joint prostheses using metallurgical methods. The aim is to reveal present damage mechanisms and understand why these arose. The present damage mechanisms will also be compared to the literature and between the different prostheses to reveal patterns.

Much of the research that is already done on various materials are focused on the medical repercussions. Common failures include fractures, loosening and inflammatory immune responses[27]. This project will direct its focus on the materials rather than the human body. This will reveal the effects of use on the material itself, contributing to a better understanding of the use of joint prostheses.

3 Background

3.1 Joint prostheses

Throughout everyday life, the human joints are exposed to a variety of stresses. Loads from daily activities, general movement and exercise are usually manageable for the human body and do not cause any issues. However, the joints can get worn down, fracture or in other ways cease to sustain normal function. In these cases there may be a need to replace the joints with artificial alternatives. By replacing damaged joints, the patients can improve their mobility, reduce pain levels and significantly heighten their quality of life. There are numerous joint prostheses on the market today, providing the luxury of choosing a suitable shape, size and material combination for each individual patient.

The joint prostheses investigated in this project are hip joint prostheses, illustrated in Figure 1 below. Components that make up the modern day hip joint prostheses are an acetabular cup, a liner that is typically made from polyethylene, a femoral head and a femoral neck and stem. Each of these parts may consist of different materials.
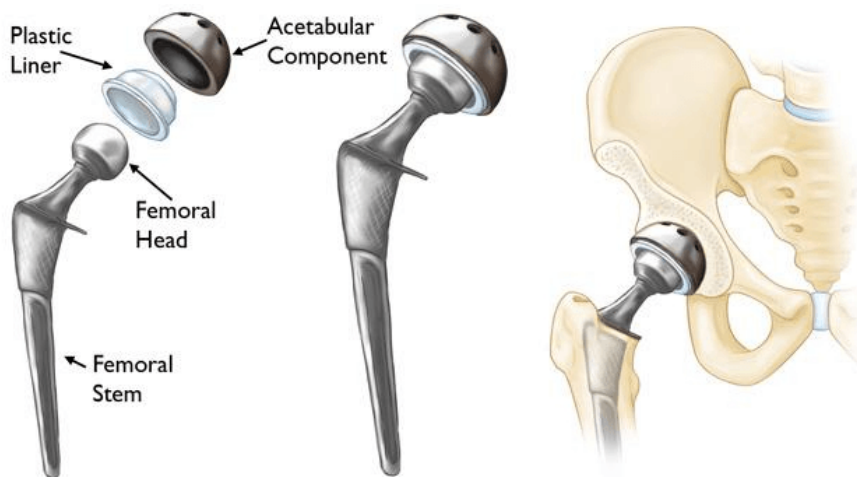

Figure 1: The components of hip joint prostheses[14]

Over 95 percent of most types of hip prostheses inserted in Norway survives for over ten years. Over 80 percent survives for 15 years and 60 percent survives for 30 years. Prostheses inserted in 1999 and later display higher survival rates than older insertions according to the data in Norway so far. The top five causes of revision surgery in the time period of 2015-2019 were loose acetabular components, infection, luxation, loose femoral components and fracture of the prostheses. These causes are listed in descending order and also reflect the year of 2019 alone. [27]

3.2 Material selection

Joint prostheses are typically composed of a combination of materials. The general material categories, which are to be further specified within this section, are metals,

polyethylenes and ceramics. Traditionally, the composition of hip joint prostheses is referred to as XoY, where X is the material used for the femoral head and Y is the material used for the liner. If a liner is not used, Y refers to the acetabular cup. MoM refers to metal on metal, MoP refers to metal on polyethylene and so on.

According to the 2020 report from the national register for joint prostheses in Norway, the most common material used for the acetabular cup in hip joint prostheses inserted from 2015 - 2019 was polyethylene. For the femoral stem, metal was the most used material in the same time period [27].

3.2.1 Polyethylene

Polyethylene is typically used as a liner, an acetabular or a tibial component in joint prostheses [61][19]. The main advantage to this material is reduced friction, which allows the joint to move more effortlessly [40][46][61]. It also has a high impact strength [40][61]. The most commonly used polyethylene today is *Ultra High Molecular Weight Polyethylene*, shortened UHMWPE [27][40][5]. This polymer displays wear rates that are lower than other tested polymers, but this is still a significant issue [40][5].

Wear debris from polyethylene components is one of the most prominent challenges for joint prostheses today [5][4]. When wear debris is released into the human body, this can cause an inflammatory response that results in osteolysis, a case of bone loss around the prosthesis. This could cause the prosthesis to loosen, called aseptic loosening [64][46]. Loosening of the acetabular component and the femoral component were the first and fourth most frequent causes for revision surgery of hip joint prostheses in Norway in 2019 [27].

3.2.2 Metal

There is a great variety of metal alloys available on the joint prosthesis market today. Statistics from 2015 to 2019 show that the 7 most frequently used femoral components in primary surgeries for hip joint prostheses were all made from metal. Titanium was most frequently used each of these years, followed by stainless steel and CoCrMo [27]. Metal can be used for all components of joint prostheses [31][5].

Titanium is beneficial for use in joint prostheses due to great corrosion resistance, high strength and excellent biocompatibility [5][44]. Due to poor wear resistance, titanium is not used for articular surfaces such as femoral heads in hip joint prostheses [5][46]. At temperatures above $883°C$, pure titanium is stable at the β phase with a body centered cubic (BCC) unit cell, and below this temperature α phase and the hexagonal close packed (HCP) unit cell is stable. Alloy elements can affect this temperature balance [43][44]. Alloys based on CoCr are frequently used for joint prostheses as they have high strength and high resistance to corrosion and wear [5][46]. A major drawback to these alloys is metal ions releasing into the human body [6][66]. Largely elevated levels of chromium or cobalt can be hazardous to the human body. Cobalt toxicity can lead to neurologi-

cal issues, vision or hearing loss, tinnitus and cardiomyopathy, among other symptoms [34][42]. CoCrMo alloys typically have face centered cubic (FCC) or hexagonal close packed (HCP) unit cells. HCP is theoretically stable at the lower temperatures, but a meta stable FCC phase is typically found at room temperature [67][56][43]. The most frequently used stainless steel alloys in joint prostheses are austenitic and generally contain molybdenum, manganese, chromium, nickel and carbon [5][51]. They are not as biocompatible as titanium, but will resist oxidation well and are easy to machine into the desired shape [5][36].

Damage mechanisms for metal components depend on the design and material combination. One of the typical damage mechanisms for metals in joint prostheses is third body abrasive wear. Wear particles that form with relative movement will govern wear rates. Also, the presence of synovial fluid combined with repeated relative motion accommodates tribocorrosion [5][40]. Surface fatigue and fretting wear could also occur, along with the risk of crevice corrosion in the case of MoM configurations [4][28][6].

3.2.3 Ceramic

Ceramic components can be used for the acetabular cup, the femoral head and sometimes also as a liner in hip joint prostheses [5][46]. Common ceramic materials used are alumina and zirconia toughened alumina [5][40].

Alumina displays excellent biocompatibility along with a high wear and chemical resistance. Alumina components used to have issues with fracture, but due to improvements in manufacturing methods regarding porosity and grain size, this issue has been significantly improved. [5][40]

Zirconia was thought to be a superior alternative to alumina due to a higher fracture toughness and bending strength. However, this material proved prone to fractures, likely caused by a phase transformation during use [21][30][5]. The solution was to combine the qualities of zirconia and alumina with zirconia toughened alumina, shortened ZTA. ZTA consists of 25 wt% zirconia and 75 wt% alumina. The final product is less prone to cracking and has now been on the market for about 20 years [5][40].

Advantages of ceramic components include great wear resistance, high hardness and great biocompatability [45][5]. The significant downsides are squeaking sounds if combined in a CoC configuration and the need for proper manufacturing to avoid a risk of fracture. Less prominent occurences include intergranular erosion and mild surface fatigue [45][5].

3.3 Environment of the human body

When securing a joint prosthesis to the human skeleton, there are two common ways to cohere it. One method is to cohere the prosthesis using a bone cement. This bone cement is usually acrylic and based on polymethyl methacrylate (PMMA) [18][54].

The other common method used to secure joint prostheses is based on pressing the prosthesis into the bone. These prostheses have porous surfaces and the goal is for the bone to grow into them [38][54]. The human bone mainly consists of collagen, type I, and calcium hydroxyapatite crystals[55][38]. In terms of strength and ductility, the femur bone, especially relevant for hip joint prostheses, can be used as an example. The bone surrounding the internal cavity has an engineering elongation of 1.07 - 2.83 % and an engineering ultimate tensile strength (UTS) of 68-174 MPa[7][46].

The environment in the joints will have a temperature of about $32°C$, which is lower than the core body temperature of $37°C$ [53][24]. The joint will be lubricated by a synovial fluid keeping a pH of about 7.4 - 7.8[41][53]. This fluid mainly consists of phospholipids, hyaluronic acid and lubricin[47][32].

3.4 Manufacturing and design

Most metal parts for joint prostheses are manufactured by forging or casting [35][65]. The modern day forging process involves heating of the metal before using machines to press it into the desired shape. Forging closes pores in the material and will crush and redistribute impurities, resulting in a dense product with a more uniform particle distribution [26][39]. Following the forging or casting, the metal will typically undergo polishing and possibly also coating to meet the design criteria [65][35]. Ceramic components are usually sintered from powder before being polished [35][15].

In order to achieve as little friction as possible, the bearing surfaces, for example the femoral head of a hip joint prosthesis, are polished to a very low surface roughness on a nanometer scale [35][65]. The need for this is due to the fact that there no longer is a natural articular cartilage within the joint. Components that are in contact with the human bone, such as uncemented femoral stems, have a porous coating that the bone can grow into [38][54]. When the bone has grown into the prosthesis, the prosthesis is securely fastened.

In previous years, the femoral head, neck and stem of hip joint prostheses were all in one piece of material. They were so called monoblock pieces. Today, these are rarely in use anymore as modular joint prostheses have replaced them [27] [1] [49]. For modular hip joint prostheses, the femoral head and sometimes also the femoral neck can be replaced, allowing different material combinations, neck lengths and head diameters adjusted to each individual patient [49][8][48].

3.5 Legislation

Correct material selection, design and application are important components in making sure that joint prostheses and other medical devices are safe to use. Combined with the fact that a number of providers will benefit financially on various medical devices, a solid

legislation is crucial.

The world health organization, shortnened WHO, released the document *WHO Global Model Regulatory Framework for Medical Devices including in vitro diagnostic medical devices* in 2017, meant to guide its member countries in building or improving their own legislation. One of the main points of this document is to categorize and follow up medical devices based on their level of potential hazard. Other important parts of the document are advice on how to incorporate routines for proper labelling and advertising, reporting errors and withdrawing deficient or unsafe products. [62]

Up until now, there has been three directives governing the use of medical devices in the European Union (EU) region. These were all released in the time frame of 1990 to 1998 [9], so two new directives are to gradually replace these up until 2025[10]. The first directive is the *Regulation (EU) 2017/745* on medical devices, released May 26th 2021. The second directive, *Regulation (EU) 2017.746* on in vitro diagnostic medical devices, is to be released in 2022 [10]. These new regulations require more transparency, through public databases and so called implant cards. They insert stricter pre market control and hold manufacturers accountable for financial compensation to patients in the case of deficient products [11]. Annex 1 in *Regulation (EU) 2017/745* lists many of the important requirements for medical devices today. Some points include performing a risk management plan for each device and paying attention to toxicity and biocompatibility when selecting materials [12].

3.6 Damage mechanisms

This section briefly explains the damage mechanisms that are relevant for this thesis.

3.6.1 Adhesive and abrasive wear

Wear is the occurrence of material loss, often due to two surfaces moving against one another. There are multiple types of wear, adhesive and abrasive wear being two central mechanisms. Adhesive wear happens when there is adhesion between two surfaces, so that motion causes material to loosen from one surface and stick to the other. [60]

Abrasive wear can happen when one surface slides against another. Peaks on one surface will dig into the other, loosening material as they slide [60]. This mechanism alone is called two body abrasive wear. If wear debris or other hard particles get in between the two surfaces during the sliding process, this is called third body abrasive wear [52].

Figure 2 and Figure 3 below illustrate abrasive and adhesive wear.
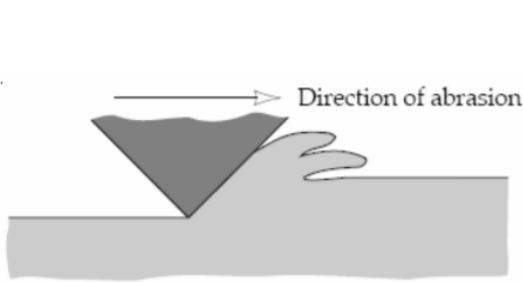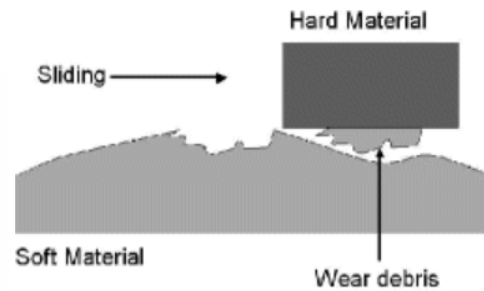
Figure 2: Two body abrasive wear [22]   Figure 3: Adhesive wear [29]

3.6.2 Surface fatigue

Surface fatigue happens when a surface is exposed to repeated alternating loads causing stresses in the material. This stress can cause microscopic physical changes and initiate cracks. A material is not able to survive as high stresses in this environment as it would in a static load case. At a set stress level, a component will be able to survive a certain amount of load cycles before failing. This is often described using *stress versus life* curves, so called *S-N* curves. Examples of these are shown in Figure 4 below. Some materials, such as low alloy steels, tend to have a stress limit under which fatigue failure does not usually occur. This stress limit, called a *fatigue limit* or *endurance limit*, can be clearly seen in an S-N curve as the curve flattens out at this stress level. [17]
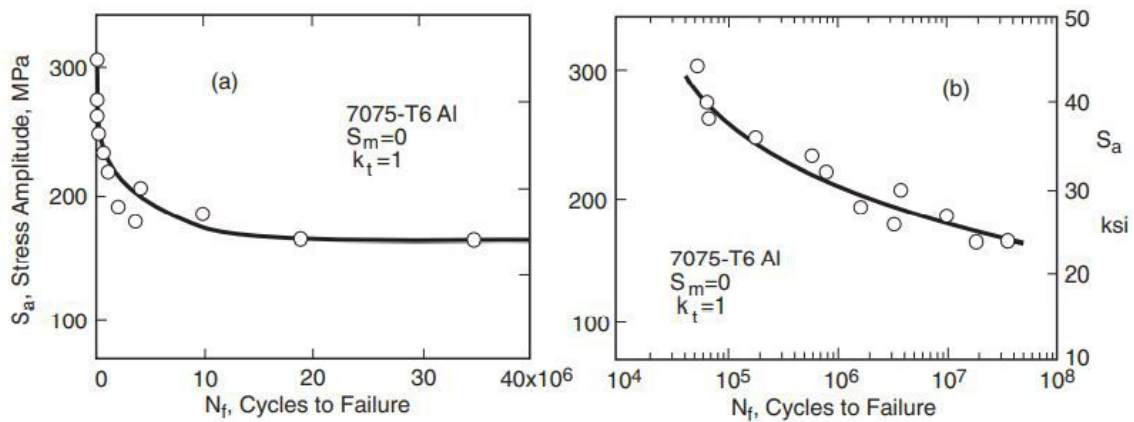

Figure 4: S-N curves from rotating bending tests of an aluminium alloy. Curve (a) has the cycle numbers plotted on a linear scale and curve (b) has the cycle numbers plotted on a logarithmic scale [17]. Note that low allow steels, from BCC unit cells, will display a different trend in their S-N curves than aluminium from FCC unit cells

Fatigue crack growth can be described by Equation 1 below, called the *Paris equation*.

$$\frac{da}{dN} = C(\Delta K)^m \tag{1}$$

In this equation, a and N represent crack length and the number of cycles, so $\frac{da}{dN}$ is the fatigue crack growth for a single load cycle. ΔK is the stress intensity range and C and m

are material constants.

Section 3.6.7 describes how a fatigue crack propagates in a material. Materials that are somewhat ductile, contain low amounts of voids or inclusions, have small grain sizes and have dense networks of dislocations are more resistant to fatigue.

3.6.3 Fretting fatigue

Fretting is a type of surface damage that occurs when two surfaces are in small relative motions to one another and are simultaneously exposed to cyclic loads. In severe cases this will lead to crack initiation and propagation. [17]

3.6.4 Galvanic corrosion

Galvanic corrosion occurs when two metals of different electrochemical potentials are in contact with each other and with an electrically conducting electrolyte. Due to an electrochemical process, the rate of deterioration, the corrosion rate, will increase for the metal with the lowest potential and decrease for the metal with the highest potential [3]. A simple illustration of galvanic corrosion with iron and tin is shown in Figure 5 below.
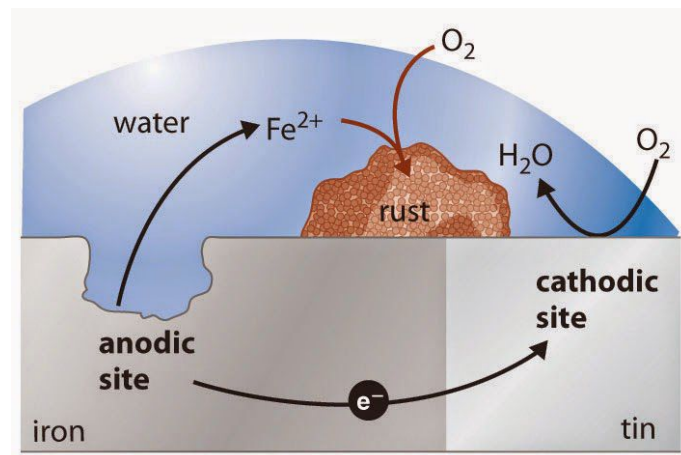

Figure 5: A simple illustration of galvanic corrosion with iron and tin [59]

If a metal alloy consists of elements that have electrochemical potentials far apart, selective corrosion can occur. The metal can become weak and porous as the less noble element disappears, making it more unreliable and prone to mechanical failure [3].

3.6.5 Crevice corrosion

Crevice corrosion can happen in cases where components or structures have small crevices where liquid can enter and become stagnant. Crevice corrosion typically occurs on materials that are either initially passive or can easily be passivated. In the case of water based liquids, OH^- is produced when the metal as a whole corrodes, a process which

stops inside the crevice as there is depletion of the oxygen required to sustain the process shown in Equation 2.

$$O_2 + 2H_2O + 4e^- \rightarrow 4OH^- \qquad (2)$$

Simultaneously, there is a dissolution of the metal, M, that is independent of oxygen. This produces metal ions as seen in Equation 3 below.

$$M \rightarrow M^+ + e^- \qquad (3)$$

When the supply of OH^- inside the crevice ceases, the charge equilibrium must be upheld through other means. If the liquid contains chloride, Cl^- will be used to sustain the charge equilibrium in the crevice as seen in Equation 4. This causes the pH in the crevice to gradually diminish, as the metal chloride reacts with water and forms hydrochloric acid. This is shown in Equation 5.

$$M^+ + Cl^- \rightarrow M^+Cl^- \qquad (4)$$

$$M^+Cl^- + H_2O \rightarrow MOH + HCl \qquad (5)$$

This creates an aggressive environment that attacks the surface oxide film. Active corrosion at a higher corrosion rate follows. [3]

3.6.6 Tribocorrosion

Tribocorrosion is the case of a material being exposed to both wear and corrosion simultaneously. The combined effects of corrosion and wear will differ from the individual effects. In the case of a passive metal with an oxide film on the surface, wear can remove parts of this surface layer. This temporarily depassivates small areas in which corrosion rates can be high when exposed to corrosive environments. [2]

3.6.7 Fracture

Fracture is caused by crack propagation from stresses to the material. The two general fracture modes for metals are ductile and brittle fractures.

Metals that absorb high amounts of energy and are able to plastically deform display ductile fractures. This is usually the preferred fracture mode as the deformation gives an advance warning. Ductile fractures can be visually characterized by a reduction of the cross section area, so called necking. On a macroscopic level, the fracture surface can be characterized by voids called dimples. These are usually spherical, but can be elongated into a parabolic shape in the case of shear stress.

Metals that do not absorb much energy and undergo little to no deformation will have rapid crack propagation leading to a brittle fracture. This type of fracture will occur sudden and without warning. The fracture surface is visually characterized by a flat fracture surface that appears perpendicular to the stress direction. In cases of hard metals and fine grains, the surface will be smooth, whereas more coarse metals will show patterns of chevrons or ridges. Chevron patterns are V-shaped markings that point back to the crack

initiation site. Ridges will align like a fan and radiate from the crack initiation site.

Figure 6 below illustrates the differences between ductile and brittle fractures.
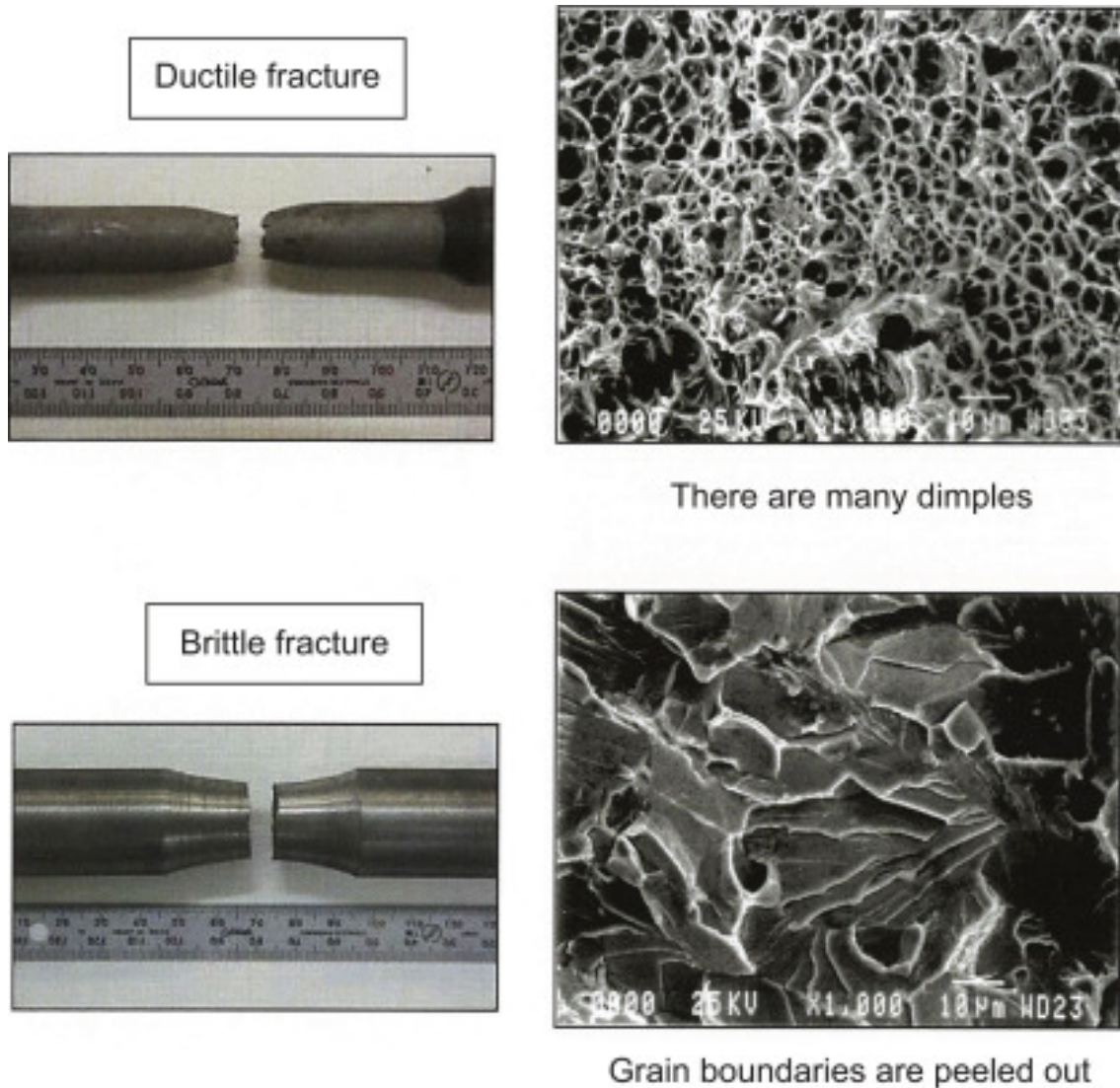

Figure 6: Ductile and brittle fracture characteristics [20]

In response to tensile stress, many metals are quite ductile, ceramics usually fracture in a brittle manner and polymers display a range of behaviours [63]. Fracture was the fifth most common cause for revision surgery of hip joint prostheses in Norway in 2019 [27].

The direction of the applied loads affect the way a fracture develops. There are three displacement modes defined as *Mode I*, *Mode II* and *Mode III*. These are shown below in Figure 7 and they can occur alone or in various combinations. Other names for *Mode I, 2 and 3* are the *opening mode*, *sliding mode* and *tearing mode*. The first mode is the most common type of fracture displacement and is caused by tension stress. *Mode II* and *Mode III* are caused by shear stresses in the material. [17][63]
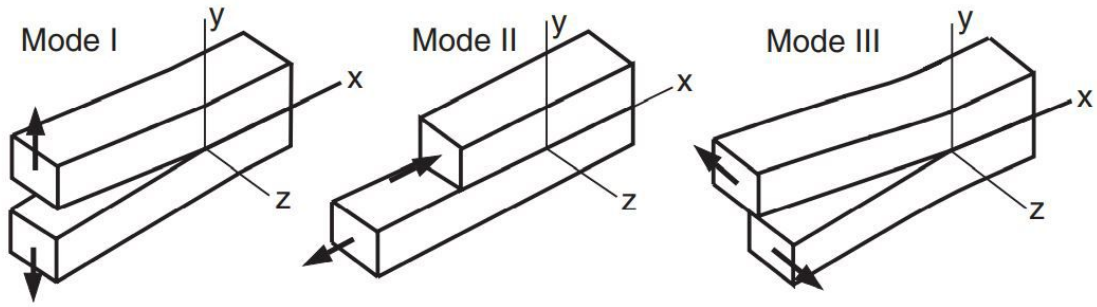
Figure 7: Fracture modes [17]

Fractures that propagate along the grain bounadries of a material are *intergranular* fractures. These can occur if the areas close to grain boundaries are weakened or embrittled. Fractures that propagate across grains are *transgranular* fractures. This breaks atomic bonds along specific crystallographic planes, which presents itself as cleavage in the material. Transgranular fractures are the most common, especially for brittle materials. [63][17]

Fatigue, as described in Section 3.6.2, can cause fracture. This happens in three stages: crack initiation, crack propagation connected to the cyclic stresses and then a rapid, final failure. Fatigue cracks tend to initiate at the surface of a component and any surface irregularity is especially prone to crack initiation. Some examples of this are surface scratches and dents along with geometrical changes with regards to the design of the component. The *notch sensitivity factor*, given by equation 6 below, indicates how sensitive a material is to notches in the surface with regards to fatigue. The value will be in between 0 and 1, where the material is fully notch sensitive at the value 1 and not notch sensitive at all at the value 0. k_t is the ratio of the local notch stress, σ, to the nominal stress, S. k_f is the fatigue notch factor, which relates the fatigue strength of a notched member to the fatigue strength of an unnotched member from the same material. [17]

$$q = \frac{k_f - 1}{k_t - 1} \qquad (6)$$

Surrounding the initiation point of a fatigue crack are circular or semi circular lines that indicate how the fracture developed. When the stress on the component ceases, a crack will stop propagating. This process causes a line, called a beach mark, that is large enough to be seen with the naked eye. Beach marks are typically seen in components that are utilized regularly, but with breaks in between, for example machines being operated only during normal work hours and not during the night. Temperature and chemical environment may also affect crack propagation velocity and hence beach marks. At a microscopic level there are smaller lines called striations. In the case of fatigue, the stress is cyclic. Each decrease in stress causes the crack to stop propagating or drastically reduce its velocity, creating a striation with each cycle. Once the fatigue fracture reaches stage three and rapid failure begins, there are no more striations or beach marks created. Figure 8 below illustrates the fracture surface of a typical fatigue fracture. [63][17]
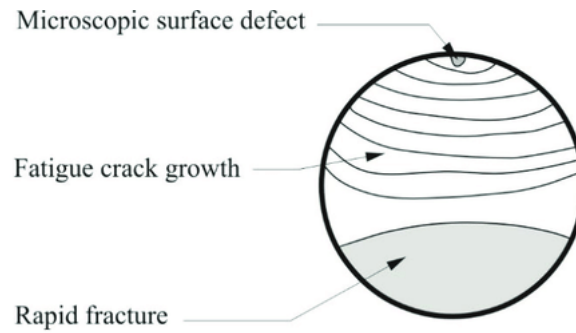
Figure 8: The fracture surface of a typical fatigue fracture [16]

3.7 Grain structure

Metals and ceramics used in engineering are usually *polycrystalline* materials, which means they consist of crystalline grains separated by grain boundaries. The size and shape of the grains can give valuable information about the properties and history of the material, especially regarding physical deformation. For instance, cold rolling or pressing a metal during manufacture will typically lead to elongated grains in the affected areas. Grains within a cast component will usually have uneven edges of the grains, whilst forged components will have sharper boundaries.

Grains that have been subjected to plastic deformation at a relatively low temperature, for instance through cold rolling of the material, can be restored through heat treatment. The heat treatment process is called annealing and consists of heating the material for a certain period of time before cooling it down at a slow, controlled rate. When heating, new grains will appear. This is called recrystallization. These new grains are strain free and have approximately the same diameter in all directions. The new grains grow until they eventually consume the original, deformed grains. If the grains are kept for an even longer time period at this temperature, the grains will keep growing. Heat treatment can also be used to enlarge the average grain size, at the expense of smaller grains, of any metal regardless of previous deformations. [63]

Materials with smaller grains are typically harder, stronger and more resistant to fatigue. The *Hall-Petch* equation below, Equation 7, shows the relation between the average grain size diameter, d, and the yield strength, σ_y, for a material. This equation is valid for most materials, σ_0 and k_y being material constants, but will not be valid for grains that are very large or very small.

$$\sigma_y = \sigma_0 + k_y d^{-1/2} \tag{7}$$

Grain boundaries will present a barrier for crack propagation. This means that a given area of material will have more resistance to crack propagation and consequent failure the more grain boundaries that are present. Smaller grains provide more grain boundaries, strengthening the material. This is due to two neighbouring grains having different orientations, forcing the dislocation to change the direction of motion when reaching the grain boundary. Also, atomic disorder in the grain boundary area discontinues slip planes

13

between the neighbouring grains. [63] [17]

Because the grain boundaries act as obstacles for moving dislocations, dislocations will pile up next to grain boundaries and cause stresses in the material. When a critical stress value is reached due to this pile up, the dislocations can surpass the grain boundaries and the material yields. Larger grains will have a large number of dislocations piled up near the grain boundaries, making them more susceptible to brittle fracture. This is because edge dislocations are accompanied by a partially open atomic structure as shown in Figure 9 below. A group of edge dislocations can create a microscopic crack that lowers the stress level required to initiate brittle fracture. [63] [23] [57]
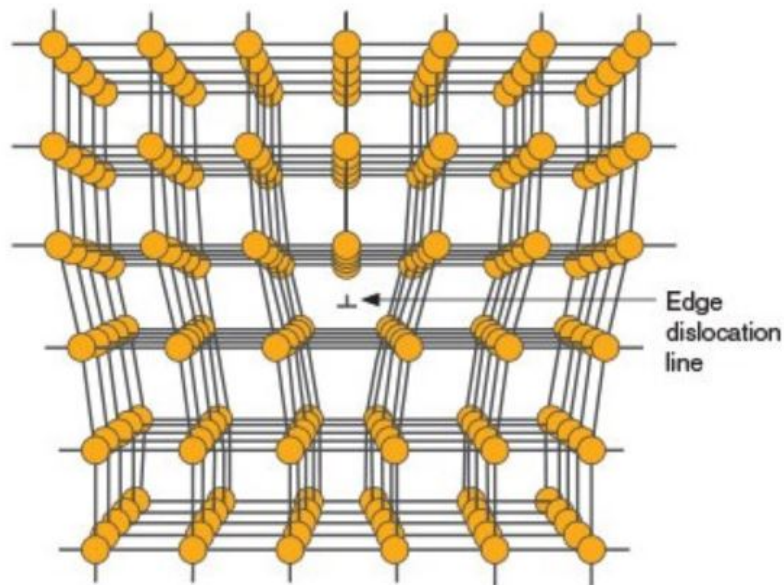
Figure 9: Illustration of an edge dislocation [33]

If a material has experienced mechanical shear forces or deformation followed by annealing, *twins* can arise in the grain structure. These are visible as straight lines running across grains, illustrated in Figure 10 below. Atoms located at one side of a twin boundary will have mirrored positions of the atoms located at the other side. [63][17]
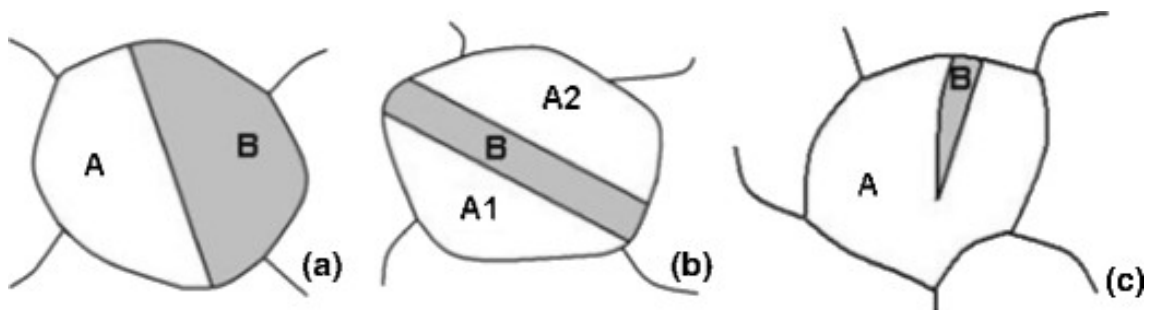
Figure 10: (a), (b) and (c) illustrate three variations of twins [13]

4 The materials

The materials examined in this thesis were used hip joint prostheses. The materials were three metal components made from two CoCrMo alloys and one stainless steel alloy. The prosthesis made from stainless steel will be referred to as *prosthesis SS*. The alloys made from CoCrMo will be referred to as *prosthesis Co* and *prosthesis Co-o*, where *-o* represents the spheres on the stem. All prostheses can be seen in Figure 11 below. The deviation in length seen for prosthesis Co-o is due to a fracture at the stem.

Figure 11: The prostheses examined in this thesis

The element content of these prostheses was extracted from the X-Ray Fluorescence (XRF) results in Section 6.2.1 of this thesis and is presented in Table 2 below.

Table 2: The average XRF results for the stem sections of the prostheses.
The uncertainty is given with two standard deviations, assuming the machine provides one standard deviation in its measurements.

Element content			
Element	Prosthesis SS [wt%]	Prosthesis Co [wt%]	Prosthesis Co-o [wt%]
Fe	63.3 ± 0.1	-	-
Cr	19.8 ± 0.1	28.0 ± 0.1	28.2 ± 0.1
Ni	9.91 ± 0.05	-	2.28 ± 0.02
Mn	4.15 ± 0.03	-	-
Mo	2.28 ± 0.01	7.01 ± 0.02	5.63 ± 0.02
Co	-	64.3 ± 0.1	62.5 ± 0.1

5 Methods

5.1 Background information

When receiving the prostheses, the provider was asked for any known background information about the use and handling of these prostheses. The goal was to gather information about how long the prostheses had been in use, why and when they were retrieved from the patient and how they had been handled in the time between retrieval and present time. This could help interpret later results.

The gathering of background information also continued throughout the project work, as serial numbers and other visual cues could reveal the exact model of each prosthesis. If the model is known, one can find information about how properties such as surface roughness, hardness and tensile stress originally were and compare them to measured values later on.

5.2 Visual inspection

Each prosthesis was examined with both the human eye and with the macroscope *Wild photomakroskop*. The goal was to reveal irregularities such as fractures, cracks, discoloration, surface layers, scratches or other features that could indicate deterioration of the prosthesis. The software *Zen 2 core v2.4* in the free examination mode was used to document findings.

5.3 XRF - X-ray fluorescence

In order to know the element composition of the prostheses, the *XSort* handheld XRF device from *Spectro* was used. The device was situated below a chamber in which a sample was put. A hole in the bottom of the chamber allowed for a measurement to be made from the material situated above. The setup is shown in Figure 12 below.
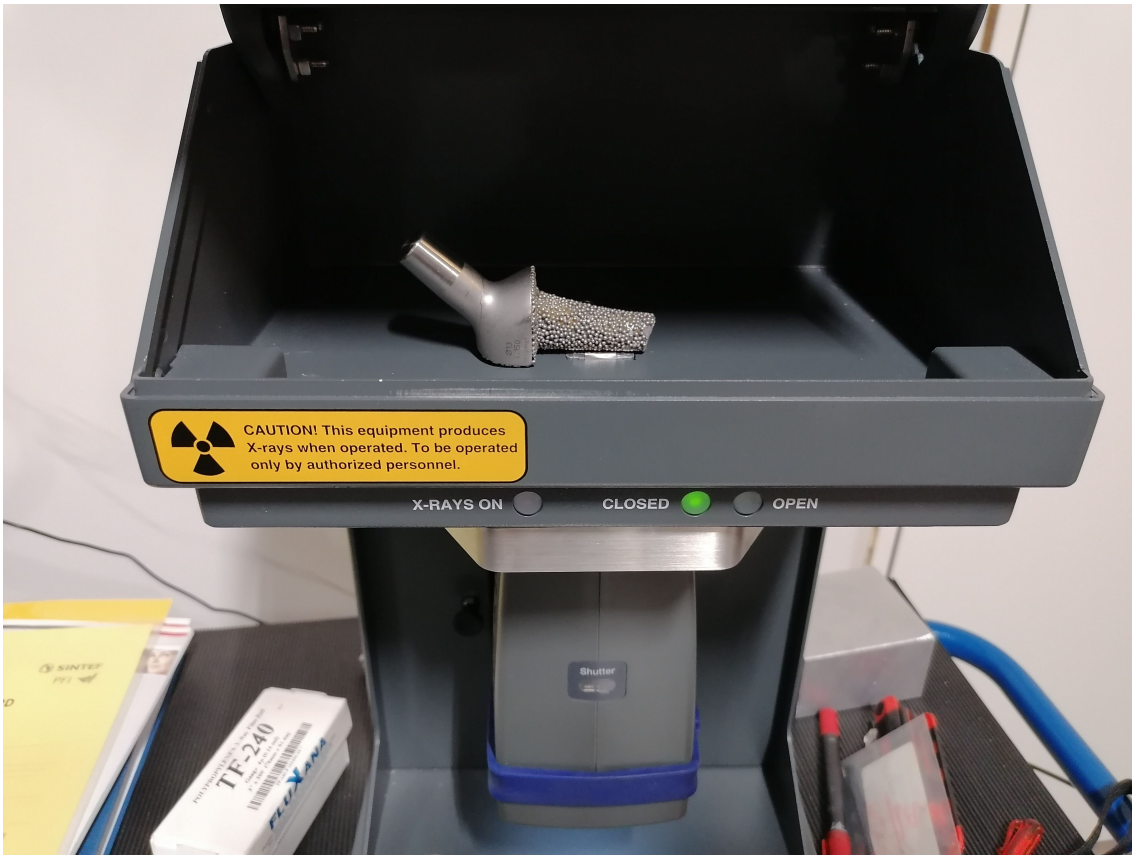
Figure 12: The XRF setup. The XRF device was situated below the chamber in which the prosthesis was placed

This was repeated for each of the prostheses. Measured points included femoral heads, necks and stems. For prosthesis Co-o, both the outer layer on the stem and the stem cross section were measured points. Three measurements were made at each area for each prosthesis.

5.4 SE - Secondary electron imaging

Prostheses Co and SS were too large to fit into the scanning electron microscope (SEM) chamber. The first step was therefore to cut the samples as shown in Figure 13 below. This was done using the cut-off wheel 60A25 and the cutting machine *Labotom-5* from *Struers*. The locations of the cuts were strategically placed to facilitate planned sample preparations at later stages of the project work.

Figure 13: The cuts made prior to SEM

Prior to the examinations in SEM, the samples were cleansed and degassed. Thin paper tissues with acetone, $(CH_3)_2CO$, were used to cleanse the samples. For degassing, the samples were put into an oven from *Memmert* keeping $60°$C for 15 minutes.

Secondary electron imaging was then used to examine the surfaces of the prostheses. The goal was to expose irregularities in the surface such as cracks, scratches and oxide layers. The scanning electron microscope *Zeiss Ultra, 55 Limited Edition* on high current mode was used for this purpose. The aperture size was set to 120 micrometer.

5.5   Optical microscopy

Deterioration of a joint prosthesis may affect the surface roughness. The optical microscope *InfiniteFocus G5 plus* from *Alicona* was used to measure the surface roughness of the three hip joint prostheses. Measured points for prostheses Co and SS were the femoral heads and necks along with the top and bottom of the stems. For prosthesis Co-o, measured points were the top and bottom of the slim part of the neck, the bust of the neck and the stem. The setup is shown in Figure 14 below.
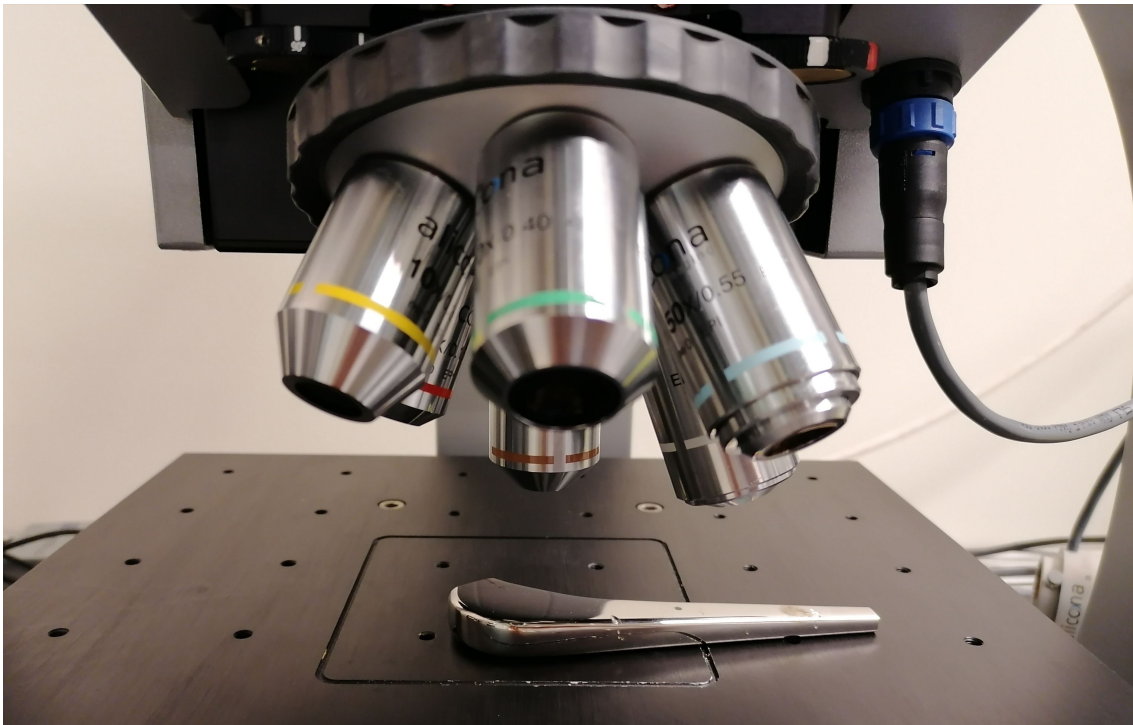
Figure 14: The setup for surface roughness measurements using an optical microscope

The surface roughness determined the choice of magnification, the maximum vertical resolution and the minimum total profile length required to provide accurate results. Guidelines for these parameters were found in the user manual of the microscope.

The approximate surface roughness was first found by performing a test measurement at a magnification of 20 times and a vertical resolution of 100 nm for each measuring point. The result was used to select the correct parameters and measurements were then made at each point until the total profile length exceeded the minimum requirement. Table 3 below lists the chosen magnifications, vertical resolutions and the required profile lengths.

Table 3: The magnifications and profile lengths for surface roughness measurements

Sample	Magnification	Vertical resolution	Minimum profile length
Neck of prosthesis SS Stem (top) of prosthesis SS Stem (bottom) of prosthesis SS	100x	20 nm	4.00 mm
Head of prosthesis Co Head of prosthesis SS	50x	100 nm	4.00 mm
Stem of prosthesis Co-o	5x	1 µm	40.00 mm
All other measured points	20x	100 nm	4.00 mm

A ring light with polarized light was used for the measurement of the femoral head of prosthesis Co. This option was chosen because the surface was highly reflective, giving

poor results with regular lighting. According to the user manual of the microscope, a magnification of 100 times should have been used for this measurement, but the size of the ring light device would have caused the lens to crash into the sample.

5.6 Sample preparation

5.6.1 Cutting

In order to further examine the prostheses, a number of samples were prepared. Figure 15 and Figure 16 below show how the prostheses were cut. The light blue colored lines represent the cuts that were previously made in Section 5.4. The dark blue and red cuts were made at this stage in the process.
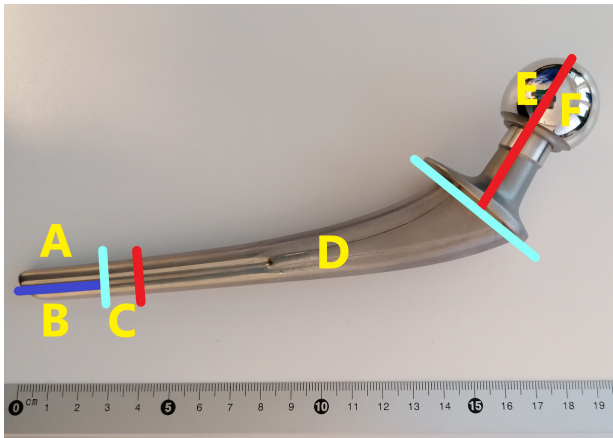
Figure 15: The cuts made for prostheses Co and SS
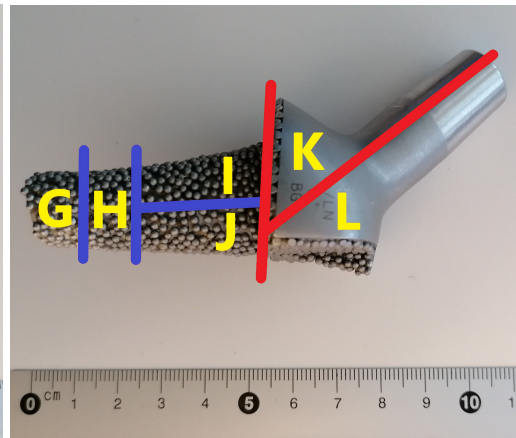
Figure 16: The cuts made for prosthesis Co-o

The red cuts in Figures 15 and 16 were made using the cutting wheel 60A25 and the cutting machine *Labotom-5* from *Struers*. The cutting machine *Accutom-5* from *Struers* was used for the dark blue lines. This machine was used due to the small sizes of sections *A*, *B*, *G*, *H*, *I* and *J* in Figure 15 and Figure 16. The cuts represented by the dark blue lines were executed using the diamond cut-off wheel BOD13 from *Struers*. The speed was set to 0.05 mm/second and 3000 rpm. The force limit was set to medium. The cuts made parallel to the stem length intentionally deviated from the center. The purpose of this was to account for material loss during polishing at a later stage. After each cut, each sample was cleaned using water and ethanol, C_2H_5OH. The sample was first rinsed in water, then covered in ethanol and dried with a hairdryer.

Section *G* in Figure 16 was covered during cutting in order to protect the fracture surface of prosthesis Co-o from the cooling water. A small plastic bag was cut with scissors and wrapped around the fracture tip. The plastic bag was secured using a small elastic band. Figure 17 below displays the protection used during the cut with *Labotom-5*. As the cut between section *G* and section *H* in Figure 16 was made, a smaller piece of plastic was used.
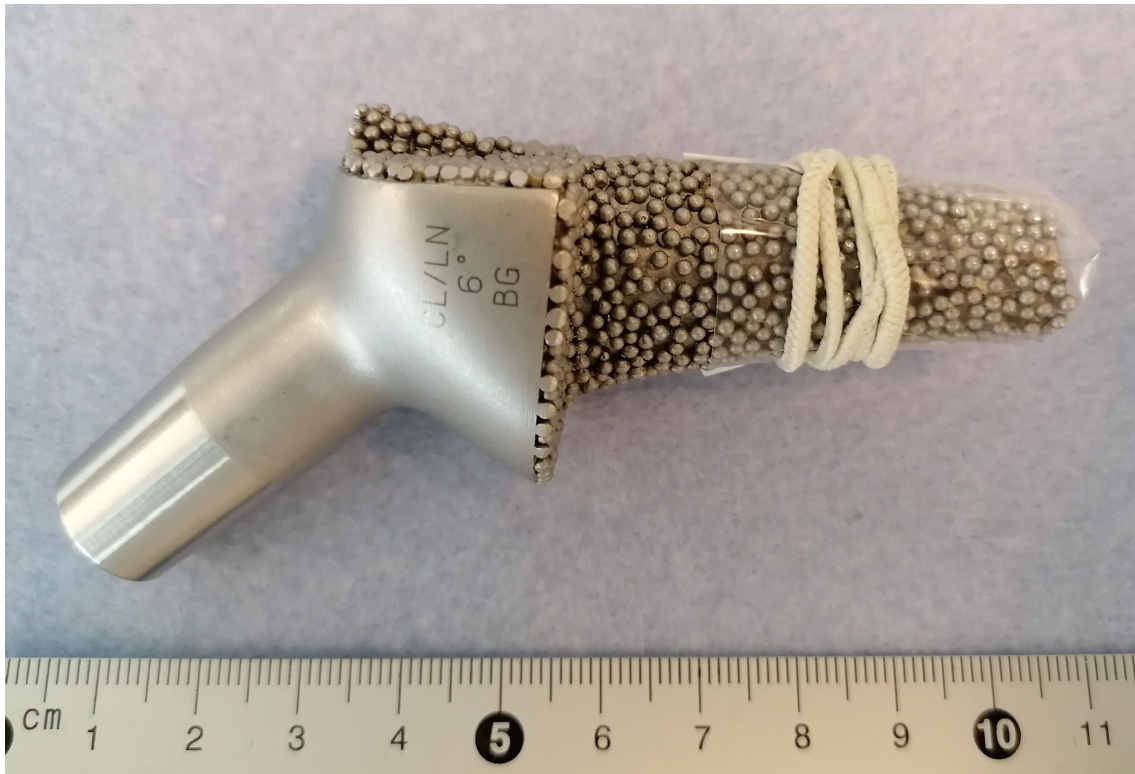
Figure 17: Protection of section *G* with a piece of plastic

5.6.2 Casting

The sections labelled *A*, *C*, *F*, *H*, *I* and *L* from section 5.6.1 were cast in epoxy to ease the polishing process. The samples were placed into plastic cups whose walls were covered with a thin layer of Korasilon-Paste from *Kurt Obermeier GmbH & Co. KG*. The samples were placed with the side that was to be polished facing down. The cups were subsequently filled with an epoxy mixture. The mixture consisted of 25 parts *Epofix* resin and 3 parts *Epofix* hardener that had been mixed for two minutes. A small sticker labelling each sample was placed close to the surface of the epoxy mixture on each sample to keep them organized. The cups were subsequently placed in the vacuum machine *CitoVac* from *Struers* to remove air from the epoxy mixture. The samples were kept in the vacuum machine at 0.1 bar for 2 minutes and 30 seconds. The samples were subsequently left to cure for 15 hours and then removed from the cups. Figure 18 below shows some of the final samples and the cups used.
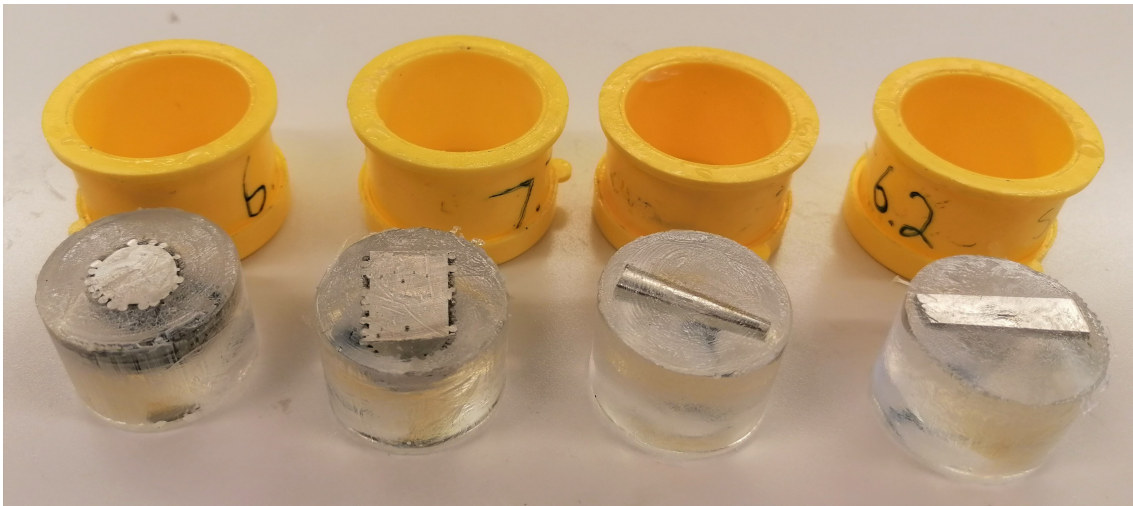
Figure 18: Cups and some of the final samples

5.6.3 Polishing

The samples cast in Section 5.6.2 were polished using the polishing machine *Tegramin-30* from *Struers*. Table 4 below lists the performed polishing steps for the samples originally from prosthesis SS.

Table 4: The polishing steps for prosthesis SS

Resource	Step 1	Step 2	Step 3	Step 4	Step 5
Surface	SiC Foil ♯ 220	MD-Largo	MD-Dac	MD-Nap	MD-Chem
Abrasive type	-	DiaPro Allegro/ Largo 9 μm	DiaPro Dac 3 μm	DiaProNap-B1	OP-S NonDry, 0.25 μm
Lubricant type	Water	-	-	-	-
Speed [rpm]	300	150	150	150	150
Force [N]	25	40	20	20	15
Holder direction	»	»	»	»	»
Time [min]	1	5	4	1	2

Table 5 below lists the performed polishing steps for the samples originally from prostheses Co and Co-o.

Table 5: The polishing steps for prostheses Co and Co-o

Resource	Step 1	Step 2	Step 3	Step 4	Step 5
Surface	SiC Foil ♯ 220	MD-Largo	MD-Dac	MD-Nap	MD-Chem
Abrasive type	-	DiaPro Allegro/ Largo 9 μm	DiaPro Dac 3 μm	DiaProNap-B1	OP-U NonDry, 0.04 μm
Lubricant type	Water	-	-	-	-
Speed [rpm]	300	150	150	150	150
Force [N]	40	30	30	20	15
Holder direction	»	»	»	»	><
Time [min]	2	3	3	1	2

Between each step for both processes, the samples were rinsed in water and then cleansed for five minutes using the ultrasound bath *VWR ultrasonic cleaner*. The ultrasound bath contained water, H_2O, and a beaker containing ethanol, C_2H_5OH. The samples were placed into this beaker of ethanol before starting the machine. The samples from the head and neck areas, labelled *F* and *L* in Section 5.6.2, did not fit into the ultrasound bath. These were consequently cleaned by hand using *Zalo* soap, water and a piece of cotton.

When the samples had undergone all five polishing steps and the subsequent cleansing, they were rinsed in water, covered in ethanol and dried with a hairdrier.

5.7 Light microscopy

In order to examine the microstructures of the samples cast in Section 5.6.2, the light microscope *Axio Vert.A1* from *Zeiss* was used. The free examination mode of the software *ZEN 2 core* was used to capture images. This was done both before and after the etching performed in Section 5.11.

5.8 BSE - Backscatter electron imaging

In order to clearly see the microstructures of the samples, they were examined using backscatter electrons in a scanning electron microscope.

To get a clear image, the polishing steps in Section 5.6.3 were repeated, except for the last step. This step was replaced with vibration polishing for 16 hours using the *Vibromet 2* vibration polishing machine from *Buehler*. The samples were placed in holders that each weighed 400 grams, but no extra weight was added. When the vibration polishing was complete, the samples were rinsed in water, H_2O, covered in ethanol, C_2H_5OH, and dried with a hairdryer.

Prior to the BSE analysis, the samples were made electronically conductive by wrapping them in aluminium foil as shown in Figure 19 below. To ensure electrical conductivity in the junction between the samples and the foil, a carbon sticker touching both surfaces was attached.
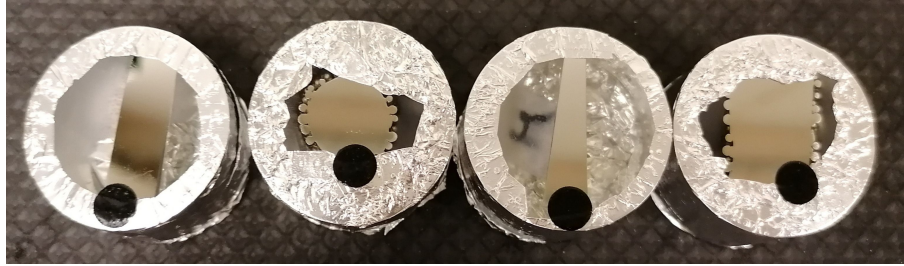
Figure 19: Samples made electrically conductive using aluminium foil and carbon stickers

Following the sample preparation, the samples were degassed in an oven from *Memmert* at 60°C for 48 hours. The samples were then examined using the *Zeiss Supra, 55 VP* scanning electron microscope on high current mode using backscatter electrons. The aperture size was set to 120 micrometer.

5.9 EDS - Energy dispersive x-ray spectroscopy

EDS was used to examine the element content of the cast samples along with their irregularities. Prior to the EDS analysis, the samples were cleansed with acetone, $(CH_3)_2CO$, using a paper tissue. They were then made electronically conductive by the same method used in Section 5.8 for the BSE analysis.

Following the sample preparation, the samples were degassed in an oven from *Memmert* at 60°C for 48 hours. The samples were then examined using EDS with the *Zeiss Supra, 55 VP* scanning electron microscope on high current mode. The aperture size was set to 120 micrometer.

5.10 EBSD - Electron backscatter diffraction

EBSD was used to examine the samples that originated from the stems of the prostheses. This was done to get a clear image of the grain structure and to see which phases were present. Vibration polishing, electrically conductive wrapping and degassing were performed as described in Section 5.8 prior to the EBSD analysis.

Using the scanning electron microscope *Zeiss Ultra, 55 Limited Edition*, each sample was tilted 70°. An accelerating voltage of 20 kV and the high current mode was used, along with an aperture size of 300 micrometer. The EBSD scan was then performed with 5 calibration points using the software *NORDIF 3*. The selected settings can be seen in Table 6 below. This software was also used to generate orientation contrast images of the samples. An image of the grain structure was then produced from the generated EBSD

pattern using the software *TSL OIM Data Collection 7*. For the stainless steel samples, iron in the alpha and gamma phases were used for indexing, along with chromium iron carbide. For the cobalt based samples, the unit cells FCC, BCC and HCP were used for indexing.

Table 6: The EBSD scannning settings for the stems of all prostheses. *PE* and *PA* refer to a perpendicular or parallel cut direction with regards to the stem length when making the sample.

Microscope settings						
	Prosthesis SS		Prosthesis Co		Prosthesis Co-o	
	PE	PA	PE	PA	PE	PA
Magnification	1000	2000	100	40	60	65
Accelerating voltage [kV]	20	20	20	20	20	20
Working distance [mm]	25.2	25.5	25.6	20.8	25.1	25.3
Tilt angle [°]	70	70	70	70	70	70
Calibration factor [μm/V]	10763.1	10763.1	10763.1	10763.1	10763.1	10763.1
Acquisition settings						
	Prosthesis SS		Prosthesis Co		Prosthesis Co-o	
	PE	PA	PE	PA	PE	PA
Frame rate [fps]	170	220	200	180	200	200
Resolution [px]	120x120	120x120	120x120	120x120	120x120	120x120
Exposure time [μs]	5832	4495	4950	5505	4950	4950
Gain	10	10	10	10	10	10
Calibration settings						
	Prosthesis SS		Prosthesis Co		Prosthesis Co-o	
	PE	PA	PE	PA	PE	PA
Frame rate [fps]	60	80	70	60	70	60
Resolution [px]	160x160	160x160	160x160	160x160	160x160	160x160
Exposure time [μs]	16616	12450	14235	16616	14235	14235
Gain	5	5	5	5	5	5
Step size [μm]	0.38	0.25	4.00	11.00	7.00	7.00

5.11   Etching

In order to get a better view of the microstructures in the light microscope, the samples were polished as described in Section 5.6.3 and subsequently etched.

The samples from prostheses Co and Co-o were etched using Murakami's etchant. 300 mL of distilled water, H_2O, was poured into a glass beaker. This beaker was placed onto a magnetic stirrer with a heat plate and put into a fume cupboard. A magnet was used to stir the distilled water at 500 rpm whilst gradually adding potassium hydroxide, *KOH*. No extra heat was added during this process. Once all the potassium hydroxide was added and the mixture was clear, potassium ferricyanide, $K_3Fe(CN)_6$, was gradually

added whilst raising the temperature of the mixture to 90°C. The mixture was stirred at 500 rpm throughout this procedure. A thermometer was held into the mixture using a retort stand with a burette clamp. Figure 20 below shows the setup.
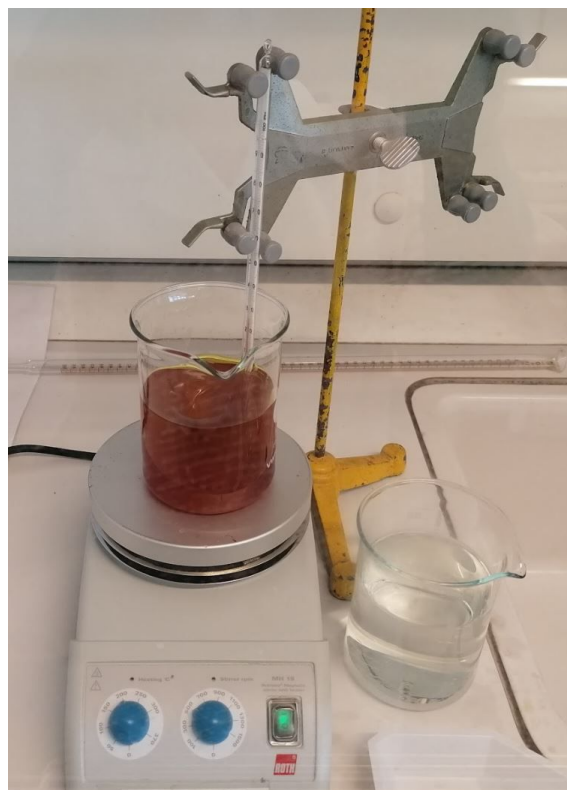
Figure 20: The setup for mixing Murakami's etchant as described above. The left beaker contained the etchant and the right beaker contained water, H_2O, to dip the samples into post etching

Once the mixture was thoroughly mixed and had reached the desired temperature, the stir was set to 0 and one sample at a time was put into the mixture using crucible tongs. Table 7 below lists the time each sample was submerged in the etchant, as the ideal time frame varied among them.

Table 7: The time frame for etching each sample. *Perpendicular* and *parallel* cut refer to a perpendicular or a parallel cut direction with regards to the stem length when making the sample.

Sample	Time etched
Head of prosthesis Co	(45 + 35 + 10) s
Neck of prosthesis Co	20 s
Stem of prosthesis Co, perpendicular cut	35 s
Stem of prosthesis Co, parallel cut	35 s
Neck of prosthesis Co-o	(45 + 9x5) s
Stem of prosthesis Co-o, perpendicular cut	(35 + 10 + 8x5) s
Stem of prosthesis Co-o, parallel cut	35 s + 8 min

After each sample was etched, the sample was dipped into another beaker containing water, H_2O. The sample was then rinsed in water and cleaned using *Zalo* soap. It was then drenched in ethanol, C_2H_5OH, and dried with a hairdryer.

Multiple etchants were tried to attempt finding the microstructure of prosthesis SS. Prior to each attempt, the samples were polished as described in Section 5.6.3. At each attempt, the samples were immersed into the etchant using crucible tongs for a variety of time periods. The samples were immersed in the etchant for 5, 10, 20 and 30 seconds, then 1, 2, 5, 10, 15 and 30 minutes, cleaning the samples in between each round of etching. The cleaning was done using *Zalo* soap and water, before drenching the samples in ethanol and drying them with a hairdryer. The following etchants were tried:

- **Murakami's etchant**: The approach was the same as described above for the Cobalt based samples.

- **2 % Nital**: 69 % nitric acid, HNO_3, was mixed with 96 % ethanol, C_2H_5OH, at a volumetric ratio of 50:1.

- **Marble's etchant**: 50 mL distilled water, H_2O, was mixed with 10 g copper sulfate, $CuSO_4$. 50 mL hydrochloric acid, HCl, was then added. Right before use, a few drops of sulfuric acid, H_2SO_4, was also added.

- **Adler's etchant**: 75 mL distilled water, H_2O, was mixed with 150 mL hydrochloric acid, HCl, 45 g ferric chloride, $FeCl_3$, and 9 g copper ammonium chloride, Cl_3CuH_4N. This was only tested for five and (5+10) seconds as it created a brown layer across the sample surfaces.

After etching, all samples were examined and photographed using a light microscope as described in Section 5.7.

5.12 Hardness tests

Hardness tests were performed to see if there were differences between the prostheses, between samples from the same prosthesis and if they differed from expected values.

Five measurements were taken from each sample using the *Innovatest* hardness testing machine. The force was set to 5 kg and the dwell time was at 10 seconds. Hardness was measured using the unit Hardness Vickers (HV).

5.13   Tensile tests

Tensile tests were performed to see how ductile the prostheses were and if the results differed from expected values. Due to strict requirements for dimensions and the need for special equipment, the tensile test samples were made by *Finmekanisk verksted* at NTNU. For prostheses Co and SS, the section labelled *D* in Figure 15 was used to make samples for tensile testing. For prosthesis Co-o, the section labelled *K* in Figure 16 was used. Figure 21 below shows the specimen dimensions and Figure 22 displays the test setup.
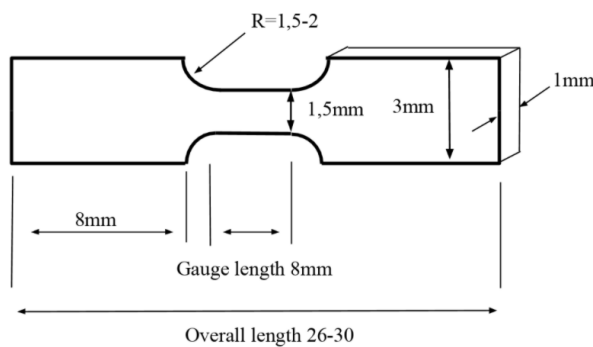
Figure 21: The dimensions of the tensile test samples
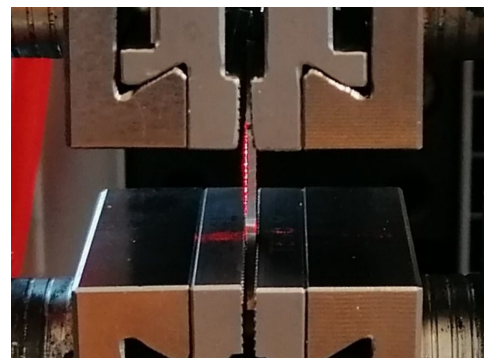
Figure 22: The tensile test setup

For the testing of these samples, the tensile testing machine *Zwick/Roell* was used along with the software *testXpert III*. Three samples from each prosthesis were elongated at a pace of 2 mm/min until failure. The elongation was first measured in percentage by a laser video extensometer, but the results were notably inaccurate. Therefore, the elongation was measured in millimeters using the grip separation of the tensile test machine. This deviation was then used to determine the engineering strain using Equation 8 below. Δl was the deviation in millimeters and l was the original gauge length of 8 millimeters.

$$Strain = (\frac{\Delta l}{l}) \cdot 100 \qquad (8)$$

After the tensile tests were completed, the fracture surfaces of the test samples were examined in the scanning electron microscope *Zeiss Ultra, 55 Limited Edition*, using secondary electron imaging on high current mode. Prior to this the samples had been degassed in an oven from *Memmert* keeping 60°C for 15 minutes. The goal of this examination was to gain information about the ductility and grain structures of the materials.

6 Results

To describe the results as accurately as possible, the two sides of the prostheses were defined as *Side 1* and *Side 2*. These definitions are shown in Figure 23 and Figure 24 below.
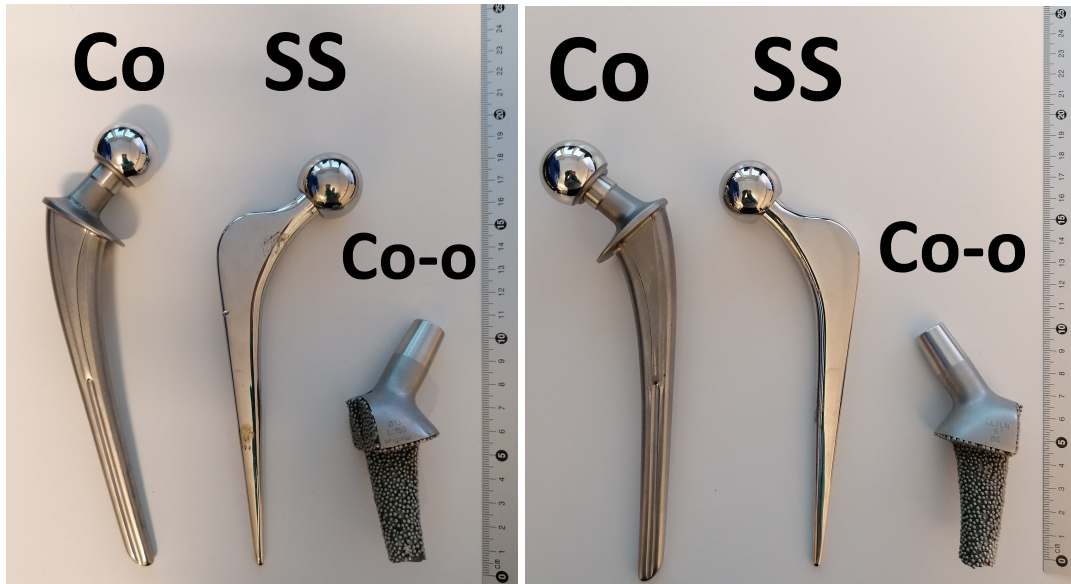
Figure 23: The definition of *Side 1*   Figure 24: The definition of *Side 2*

The femoral head, femoral neck and femoral stem will in this chapter be referred to as head, neck and stem.

6.1 Background information

The prostheses were delivered in two clear plastic bags. Prostheses SS and Co-o were in the same bag. All three prostheses were hip joint prostheses according to the provider, but no further information was known prior to the examinations performed in this thesis.

Prosthesis SS had an *Exeter* femoral stem from the company *Stryker*. This was the second most frequently inserted femoral stem for primary surgeries in Norway in the years of 2015 to 2019 [27]. Identical symbols on both sides of the top of the stem were there to help position the prosthesis during insertion [25]. The prosthesis was forged and consisted of Orthinox stainless steel [58]. A study from 2013 measured two Exeter stems prior to use and found the average surface roughness to be 22-29 nm [50].

Prosthesis Co had a *Lubinus SP II* femoral stem from the German company *Link*. This stem was made from CoCrMo and was the third most frequently inserted femoral stem for primary surgeries in Norway in the years of 2015 to 2019 [27][37]. This stem was developed in 1978 and has been available as a modular system since 1984 [37].

Prosthesis Co-o was a *Lord* stem from the company *Stryker*. A known issue for this kind of prosthesis is for the spheres of the porous stem coating to loosen [25].

6.2 Element content

This section presents the element content of the prostheses from x-ray fluorescence and energy dispersive x-ray spectroscopy results.

6.2.1 XRF - X-ray fluorescence

The XRF results show which elements were measured at the surfaces of the prostheses. Included in this section are average values for XRF results that rose above 1 wt% in at least one of the measurements of a given point. The full results along with uncertainty for each measurement can be read in Appendix A.

XRF revealed that all parts of prosthesis SS were made from a stainless steel alloy. Table 8 below lists the average XRF results for prosthesis SS.

Table 8: The average XRF results for prosthesis SS. The uncertainty is given with two standard deviations, assuming the machine provides one standard deviation in its measurements.

	Prosthesis SS		
Element	Head [wt%]	Neck [wt%]	Stem [wt%]
Fe	63.4 ± 0.1	33.1 ± 0.1	63.3 ± 0.1
Cr	20.1 ± 0.1	15.5 ± 0.1	19.8 ± 0.1
Ni	9.57 ± 0.05	4.38 ± 0.02	9.91 ± 0.05
Mn	4.22 ± 0.03	2.31 ± 0.02	4.15 ± 0.03
Mo	2.24 ± 0.01	-	2.28 ± 0.01

All parts of prosthesis Co and prosthesis Co-o were made from a CoCrMo alloy. The element content was similar for all measured points for prosthesis Co, but varied between measured points for prosthesis Co-o. Table 9 below lists the average XRF results for prosthesis Co and prosthesis Co-o.

Table 9: The average XRF results for prosthesis Co and Co-o. *Ext.* and *Int.* abbreviate *External* and *Internal*. The uncertainty of the measurements is given with two standard deviations, assuming the machine provides one standard deviation in its measurements.

	Prosthesis Co			Prosthesis Co-o			
Element	Head [wt%]	Neck [wt%]	Stem [wt%]	Neck(Top) [wt%]	Neck(Bottom) [wt%]	Stem(Ext.) [wt%]	Stem(Int.) [wt%]
Co	64.0 ± 0.1	64.1 ± 0.1	64.3 ± 0.1	35.0 ± 0.1	62.5 ± 0.1	23.6 ± 0.1	62.5 ± 0.1
Cr	28.1 ± 0.1	27.9 ± 0.1	28.0 ± 0.1	18.6 ± 0.1	28.1 ± 0.1	13.9 ± 0.1	28.2 ± 0.1
Mo	6.63 ± 0.02	7.54 ± 0.03	7.01 ± 0.02	3.61 ± 0.01	5.87 ± 0.02	1.97 ± 0.01	5.63 ± 0.02
Ni	-	-	-	0.99 ± 0.02	2.31 ± 0.02	-	2.28 ± 0.02

6.2.2 EDS - Energy dispersive x-ray spectroscopy

Table 10 below lists some representative EDS results for the bulk, discolorations, pores and particles for each prosthesis. The uncertainty for all values is ±0.01 wt%. Appendix B lists the full results along with the error range for the determination of the correct element.

Table 10: The EDS results for all prostheses. The uncertainty for all values is ±0.01 wt%. *Column, spot* refers to the column and spot location in Appendix B.

	Prosthesis SS			Prosthesis Co				Prosthesis Co-o				
Column, Spot	D,4	C,1	A, 4	E,4	F,3	H,3	G,2	I,4	K,3	I,2	I,1	L,2
Description	Bulk	Pore	Particle	Bulk	Pore	Spots, in BSE	Particle	Bulk	Pore	Pattern, dark	Pattern, light	Particle
Fe [wt%]	51.66	-	60.26	-	-	-	10.50	-	-	-	-	-
Cr [wt%]	31.93	-	21.53	36.57	9.33	26.41	-	33.77	4.10	70.17	26.74	33.25
Ni [wt%]	4.10	-	8.35	-	-	-	-	-	-	-	-	-
Mn [wt%]	3.51	-	4.13	-	-	-	-	-	12.47	-	-	-
C [wt%]	1.00	-	5.74	0.93	-	-	88.16	0.98	-	4.78	-	1.01
Al [wt%]	0.30	45.30	-	-	7.30	2.29	-	-	13.51	-	-	1.47
O [wt%]	-	42.24	-	1.47	42.26	12.31	-	1.57	43.06	3.04	-	3.50
Ca [wt%]	-	11.68	-	-	-	-	-	-	6.30	-	-	-
Si [wt%]	-	-	-	1.27	31.23	8.96	1.34	1.59	20.56	-	4.47	1.90
Co [wt%]	-	-	-	53.95	-	46.35	-	54.95	-	9.83	25.84	54.04
Mo [wt%]	-	-	-	5.82	-	3.68	-	7.15	-	12.17	42.95	4.82

6.3 Visual inspection

This section presents the visual inspection of the prostheses using the human eye and a macroscope.

6.3.1 Prosthesis SS

Prosthesis SS had serial numbers *BG S 0580-0-442* and *U251179-01/96 44 ♯2* on the neck. Figure 25 below shows these. In addition to the serial numbers, there were identical symbols on both sides of the top of the stem. The symbols are shown in Figure 26 below. All horizontal lines were about 9 mm long and the distances between the vertical lines and the edge of the prosthesis were about 3.1, 7.3 and 11.4 mm on both sides of the prosthesis.
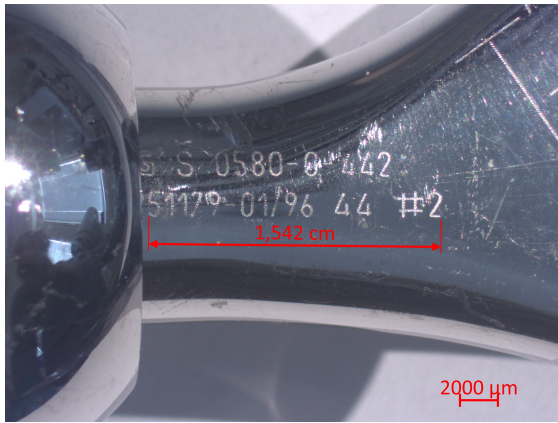
Figure 25: Prosthesis SS
Markings on side 1 of the neck
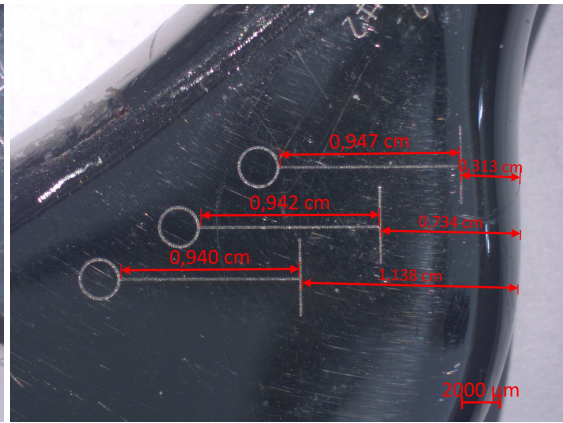
Figure 26: Prosthesis SS
Symbols on side 2 of the stem

Further visual inspection revealed there were light surface scratches across the whole prosthesis. The scratches on the back of the neck area had a greater depth and are shown in Figure 27 below. The head had some light grey discolorations in addition to the general surface scratches. Such gray discolorations were also found on the neck and stem. An example of this can be seen in Figure 27 as well. Orange discoloration was found on several spots on the prosthesis. On the front part of the stem there were such discolorations both at the curve and on the lower section. Side 1 of the stem had two spots of discoloration, one near the neck and one at the lower section. Figure 28 below shows one of these discolorations.
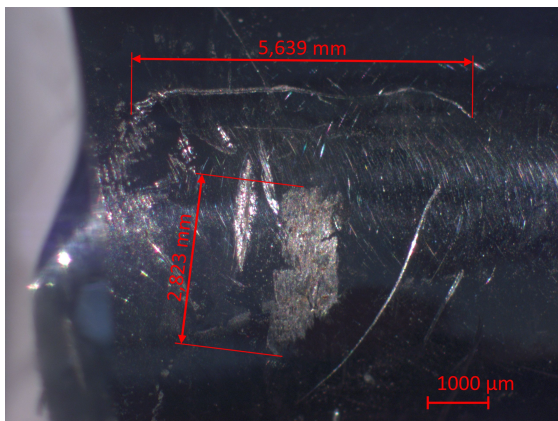
Figure 27: Prosthesis SS
Scratches and discoloration on the neck
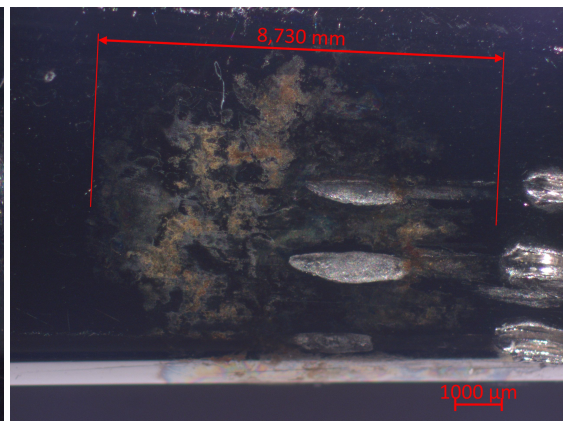
Figure 28: Prosthesis SS
Discoloration on side 1 of the stem

Deep notches were also found on side 1 of the neck close to the head, on the back of the stem and on side 1 of the stem. Figure 29 and Figure 30 below show some of these notches.
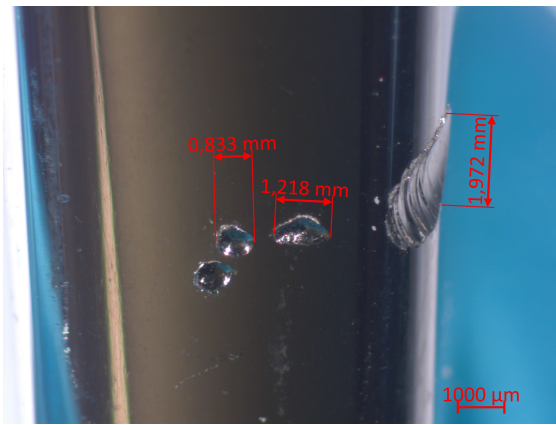
Figure 29: Prosthesis SS
Notches on the back of the stem
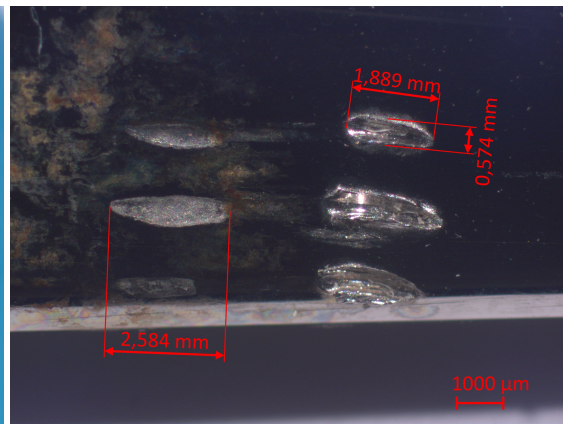
Figure 30: Prosthesis SS
Notches on side 1 of the stem

6.3.2 Prosthesis Co

Prosthesis Co had *ɸ28 49.5mm LINK 128-747* and *081295/640* printed on the underside of the edge of the head. This is shown in Figure 31 below. Side 1 of the neck had *071195/354* printed on it, shown in Figure 32, and the area of the neck between side 1 and side 2 was marked with *126○* and *L3*. The upper part of side 1 of the stem was marked with *CE 0047 LINK 127-727/26⋆* and *150 links stark*.
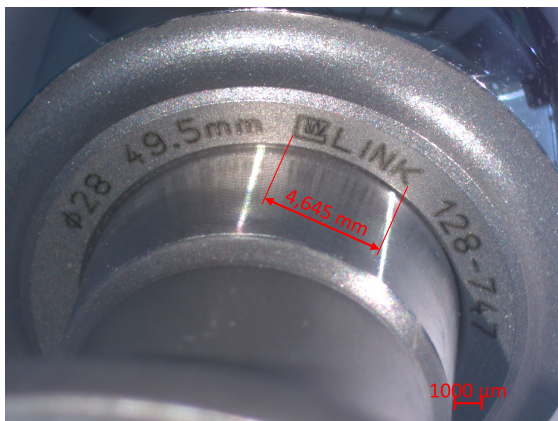
Figure 31: Prosthesis Co
Markings on the head

Figure 32: Prosthesis Co
Markings on side 1 of the neck

Prosthesis Co did not have obvious signs of damage or deterioration. The front and back of the stem, the head and the underside of the neck had superficial scratch marks, as shown in Figure 33 below. There were discolorations in various shades of gray on both sides of the head, side 1 of the neck and both sides of the stem. Most of these were in a light gray color and hardly noticeable, like the one in Figure 34 below.

33
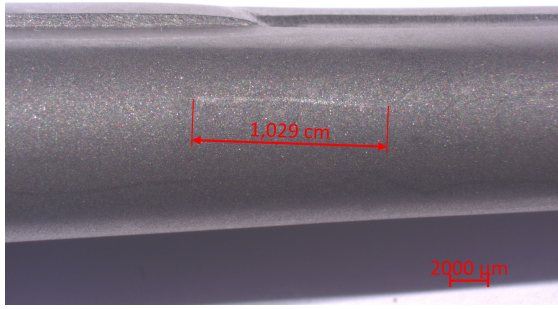
Figure 33: Prosthesis Co
Scratch on the front of the stem
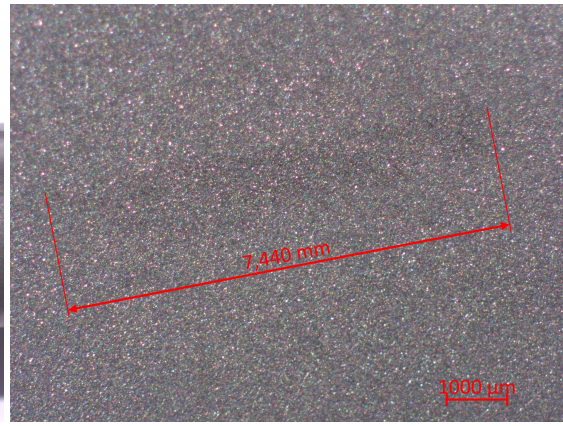
Figure 34: Prosthesis Co
Discoloration on side 2 of the stem

6.3.3 Prosthesis Co-o

The neck of prosthesis Co-o was marked with *Ø13*, *L.150* and *original* on side 1. Side 2 of the neck was marked with *CL/LN*, *6○* and *BG*. Figure 35 and Figure 36 below show these.

Figure 35: Prosthesis Co-o
Markings on side 1 of the neck

Figure 36: Prosthesis Co-o
Markings on side 2 of the neck

For prosthesis Co-o, the femoral head was not part of the provided sample. The area where the head used to be had a more shiny appearance, which can be seen in Figure 37 below. The same image displays some of the superficial scratch marks on the neck section of the prosthesis. Some discoloration could be found on the top of the neck and on side 1 of the neck, close to the bottom of the more shiny part. This is shown in Figure 38 below.

34
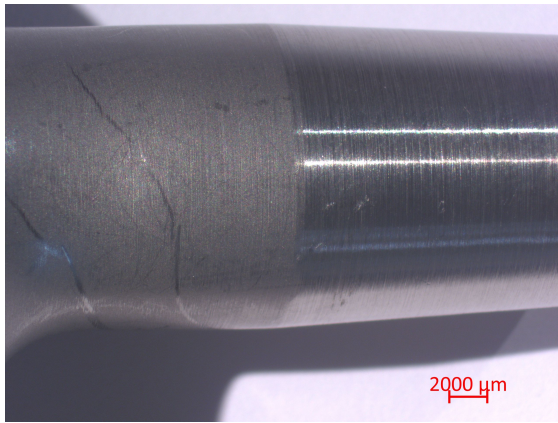
Figure 37: Prosthesis Co-o
Difference in surface reflection
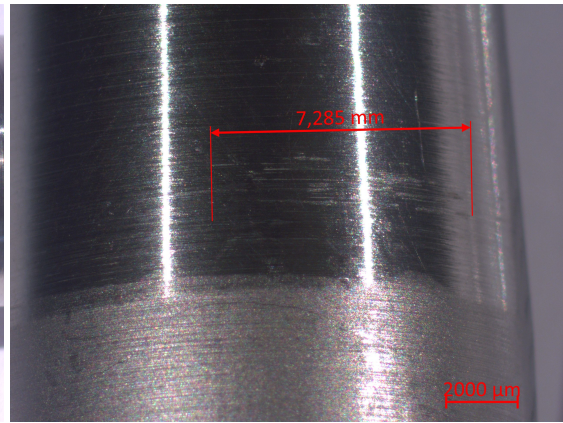
Figure 38: Prosthesis Co-o
Discoloration on side 1 of the neck

The stem of prosthesis Co-o had a porous surface with spheres. The individual spheres had a diameter of approximately 1.5 mm. Between these spheres were two types of thick layers. One layer was brown and and is shown in Figure 39 and Figure 40 below. This type of layer covered large sections of the underside of the neck and the front part of the stem. The layer was also found on both sides and the back of the stem.
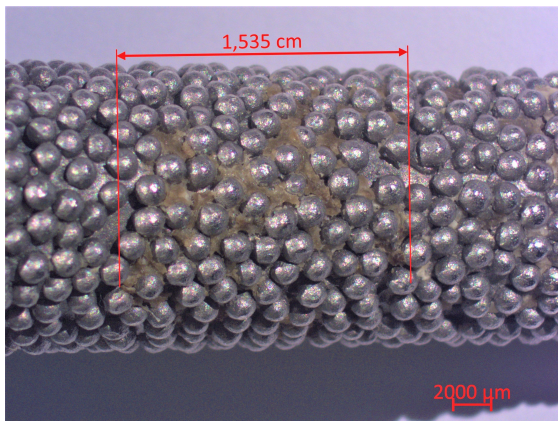
Figure 39: Prosthesis Co-o
Brown layer on the back of the stem
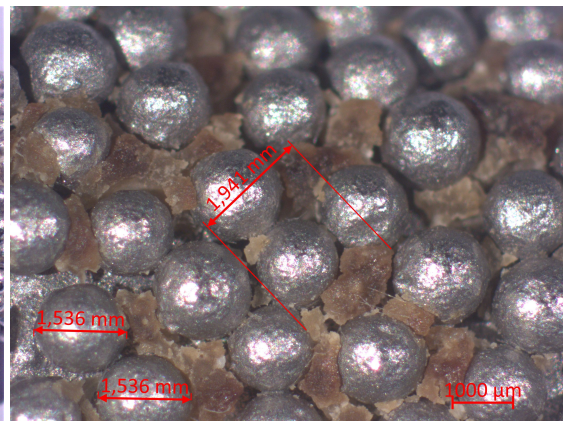
Figure 40: Prosthesis Co-o
Closeup of the brown layer

The other layer was white and is shown in Figure 41 and Figure 42 below. This layer was found near the fracture on the backside and both sides of the stem, covering the end close to the fracture. There was also white layer at the front of the stem, close to the neck area.
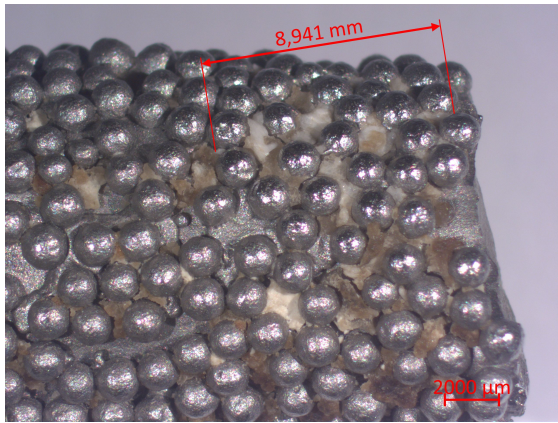
Figure 41: Prosthesis Co-o
White layer on the back of the stem
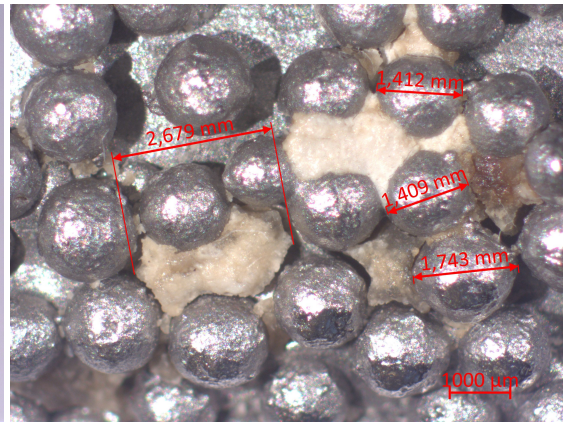
Figure 42: Prosthesis Co-o
Closeup of the white layer

The most prominent damage for prosthesis Co-o was a fracture to the stem. This can be seen in Section 6.4.

6.4 Fracture analyses

Neither prosthesis Co nor prosthesis SS displayed any external fractures. Prosthesis Co-o had a fracture about 4 cm from the edge of the neck. The fracture occurred at an angle of about 21 degrees and is shown in Figure 43 below. On side 1 of the prosthesis, the fracture had chipped off a piece from the stem edge. This is shown in Figure 44 below. Figures 43 and 44 are macroscope images.
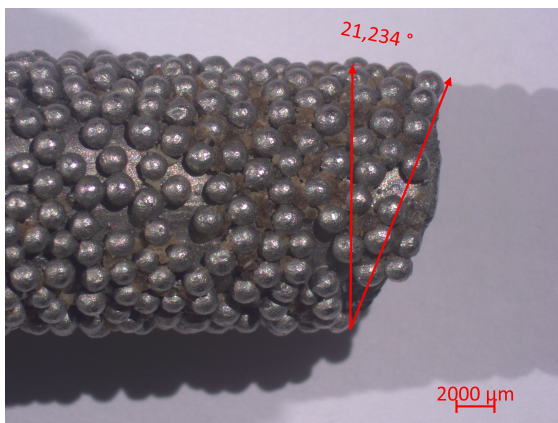
Figure 43: Prosthesis Co-o
The fracture from the front part of the stem
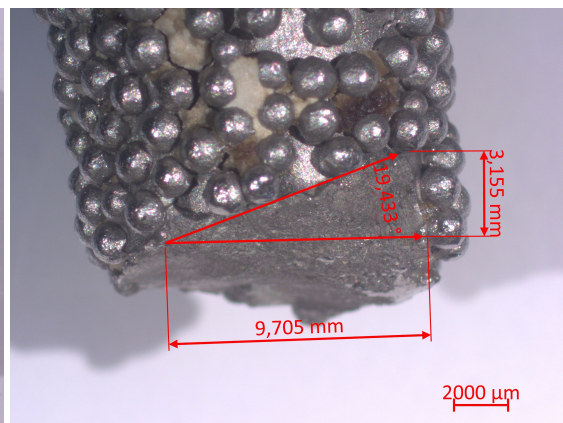
Figure 44: Prosthesis Co-o
The fracture from side 1 of the stem

The cross section of the fracture of prosthesis Co-o can be been in Figure 45, a macroscope image, below. The prominent initiation point was situated at 12 o'clock, marked with a red arrow, accompanied by clear beach marks below. The initiation point was situated in the interface between the bulk material and the spheres on the stem. There were also some white spots in the cross section, which can be seen at about 4 o'clock in Figure 45. The fracture surface was otherwise rather smooth and the chipped off piece seen in in

36

Figure 44 above was situated at the opposite end of the initiation site. The red square in Figure 45 indicates where the SEM images in Figure 46 and Figure 47 later in this section were taken.
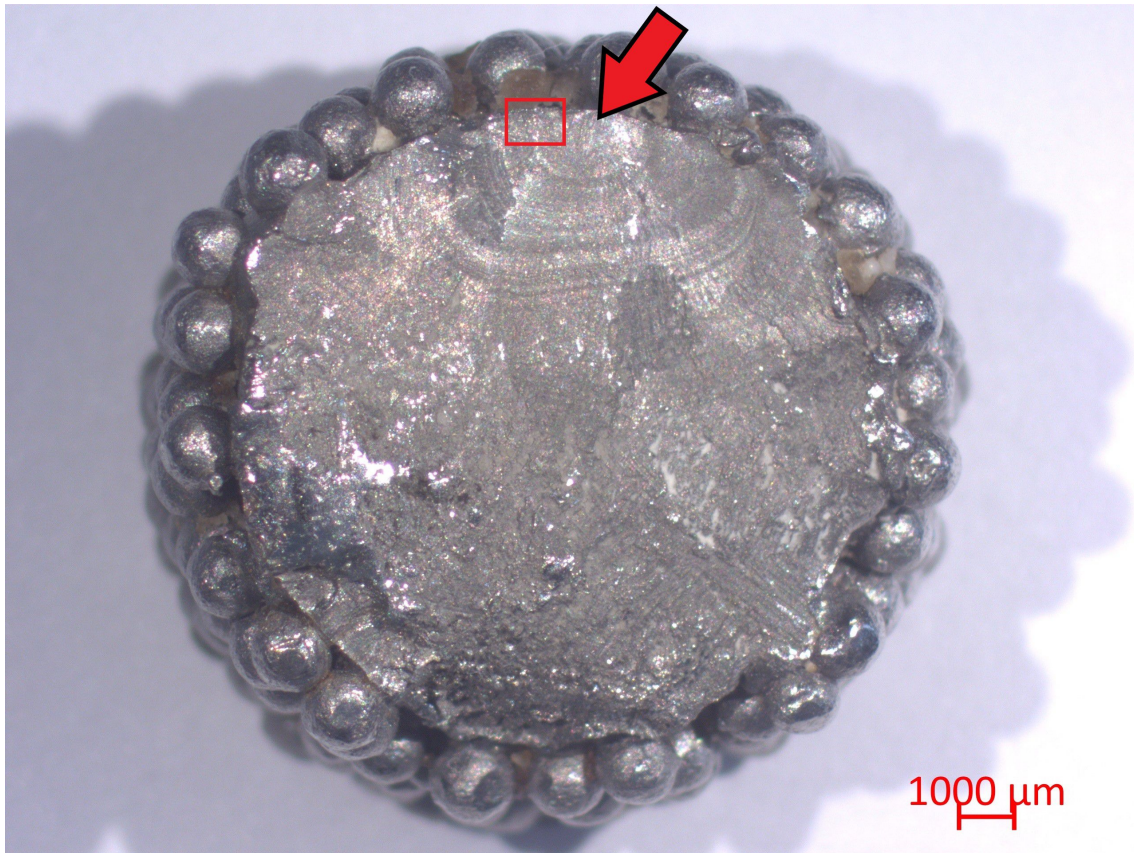
Figure 45: The fracture surface of prosthesis Co-o

By looking at the fracture surface using secondary electrons in a scanning electron microscope, vertical lines were revealed within the beach marks surrounding the initiation point. Beach marks are shown in Figure 46 and the vertical lines are shown in Figure 47. The red square in Figure 45 indicates where on the surface these images were taken.
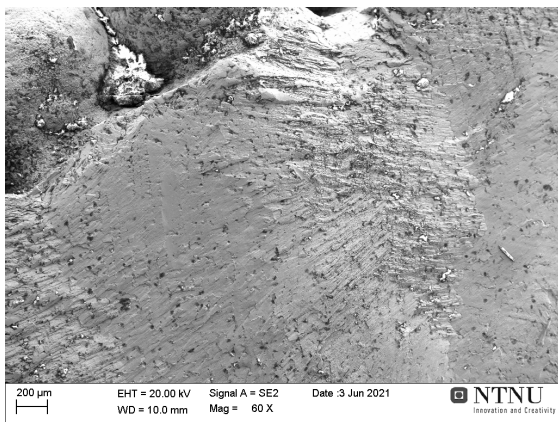
Figure 46: Prosthesis Co-o
Beach marks
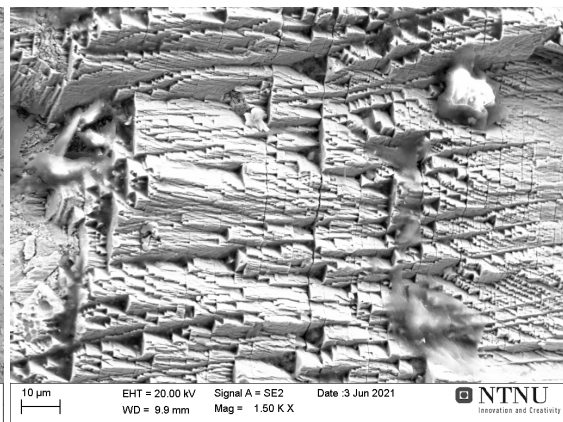
Figure 47: Prosthesis Co-o
Vertical lines

The center of the initiation point is shown in Figure 48 below. The opposite end of the fracture surface is shown in Figure 49. Both surfaces were flat and without dimples.
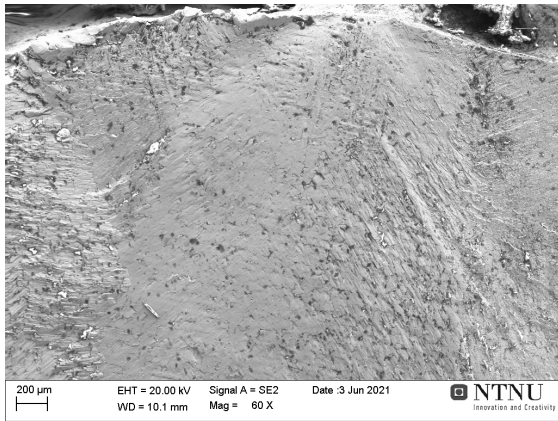
Figure 48: Prosthesis Co-o
The initiation site
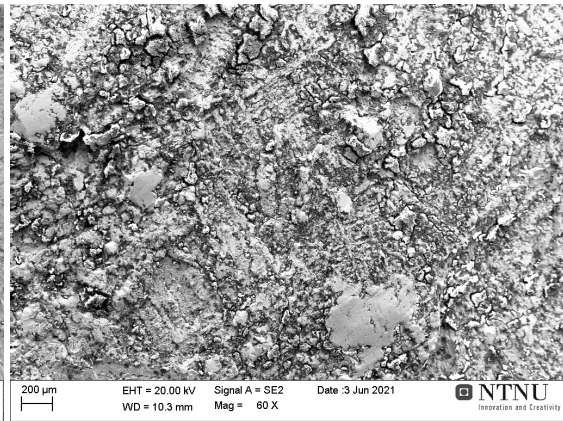
Figure 49: Prosthesis Co-o
Opposite side from the initiation site

The fracture surfaces from the tensile tests were also examined. A representative fracture surface photographed in SEM can be seen for prosthesis SS in Figures 50 below. The tensile fracture surface of prosthesis SS was fairly smooth with only a few ridges. At a closer view, shown in Figure 51 below, dimples were clearly visible in the surface.
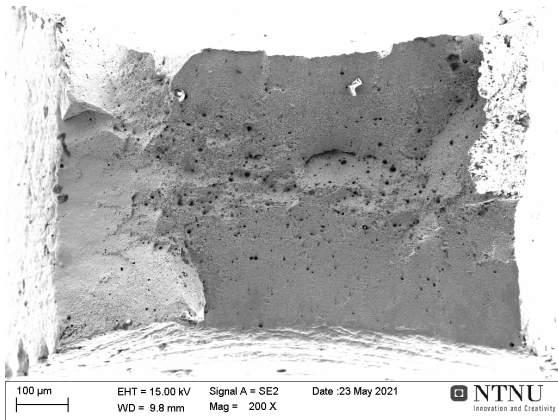
Figure 50: Prosthesis SS
Tensile fracture surface
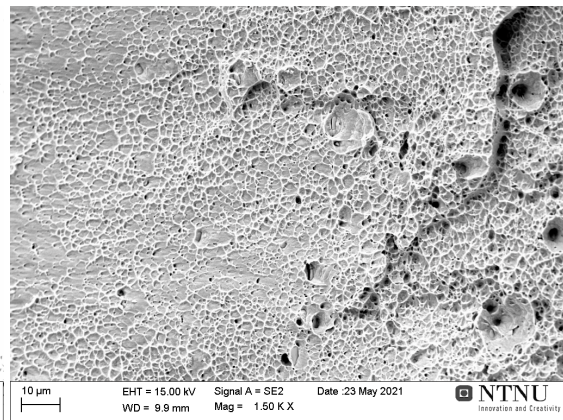
Figure 51: Prosthesis SS
Closeup of the tensile fracture surface

The tensile fracture surface of prosthesis Co had large facets, around half a millimeter in size, and several variations in surface height. Figure 52 and Figure 53 below show this fracture surface.
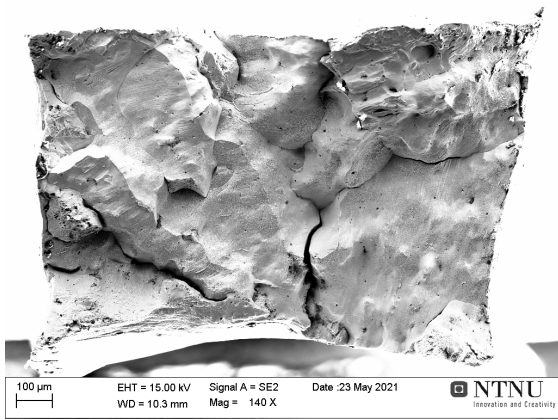
Figure 52: Prosthesis Co
Tensile fracture surface
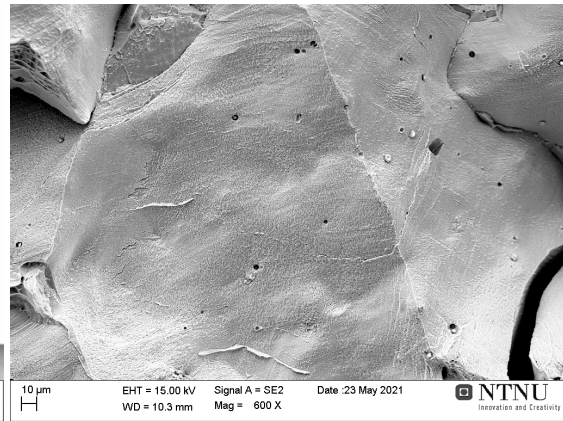
Figure 53: Prosthesis Co
Closeup of the tensile fracture surface

The tensile fracture surface area of prosthesis Co was mainly quite flat like the example seen in Figure 54 below, but also had some areas with shallow dimples. This can be seen in Figure 55 below.
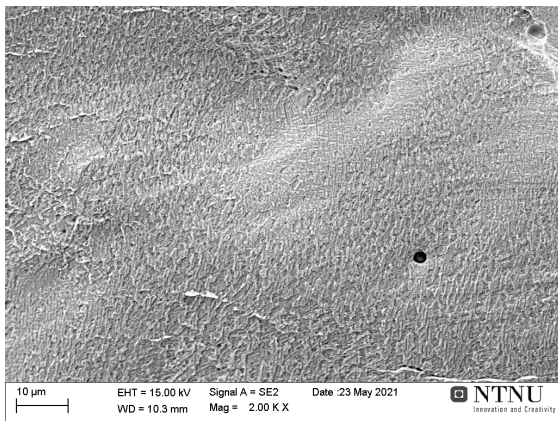
Figure 54: Prosthesis Co
Fracture surface without dimples
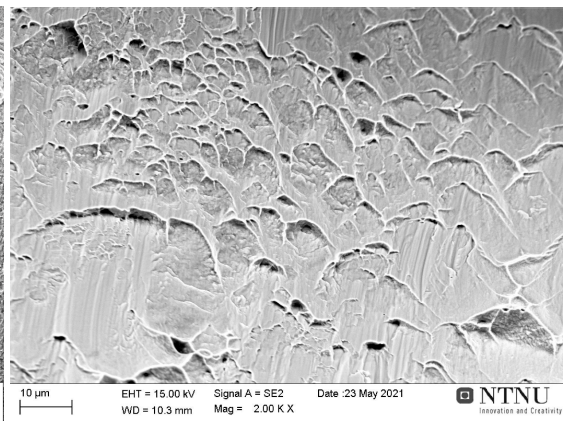
Figure 55: Prosthesis Co
Fracture surface with dimples

The tensile fracture surface of prosthesis Co-o had many facets of a smaller size, around 100 micrometer, and some variations in surface height. Figure 56 and Figure 57 below show this fracture surface. The majority of the surface area was smooth, but there were also areas with dimples. Slip lines or deformation bands are visible in Figure 57.
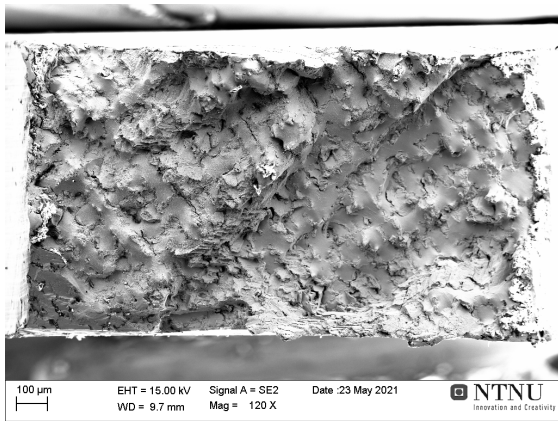
Figure 56: Prosthesis Co-o
Tensile fracture surface
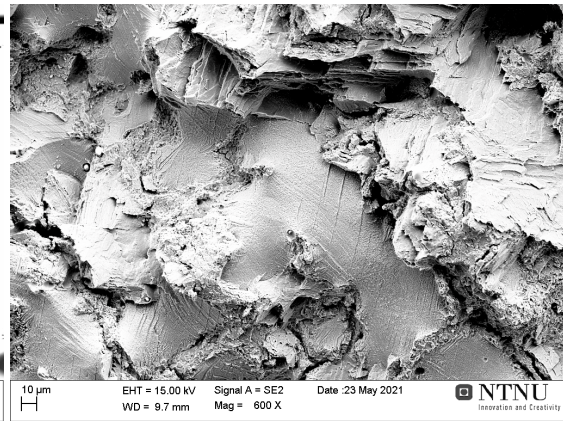
Figure 57: Prosthesis Co-o
Closeup of the tensile fracture surface

6.5 SE - Secondary electron imaging

This section presents the external examination of the prostheses through secondary electron imaging results.

6.5.1 Prosthesis SS

Prominent features of prosthesis SS were sets of circular discolorations. These were found at both sides of the neck and stem along with side 2 of the head. They were more frequent towards the end of the neck and down throughout the stem. This type of circular discoloration frequently contained dark spots that, upon closer inspection, had a dendrite shape. These dark, crystalline growths were always connected to such a discoloration at the stem, but appeared independently on the neck. Figure 58 below shows a circular discolor and Figure 59 below shows an independent crystalline growth.
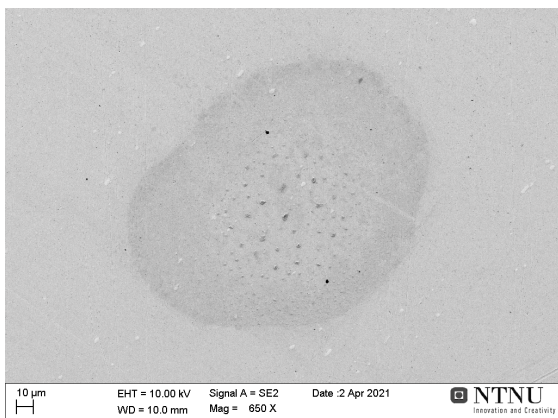
Figure 58: Prosthesis SS
Circular discoloration on the stem
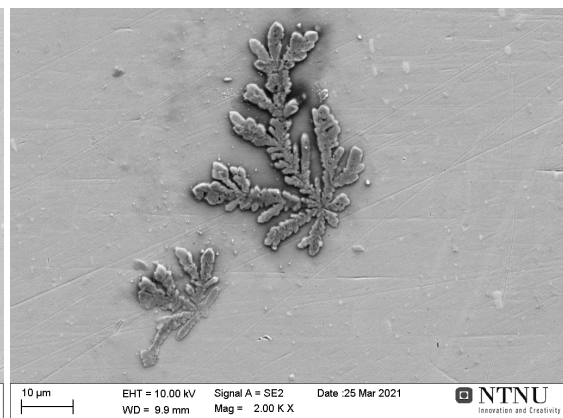
Figure 59: Prosthesis SS
Closeup of a crystalline growth on the neck

At a few locations were also circular discolorations, but these differed through having layers atop the discoloration and a significant increase in the surface roughness within. These

were found on the top right section of side 2 of the neck and the upper part of the stem. They did not contain dendrite shaped spots. Examples of such circular discolorations with layers can be seen in Figure 60 and Figure 61 below.
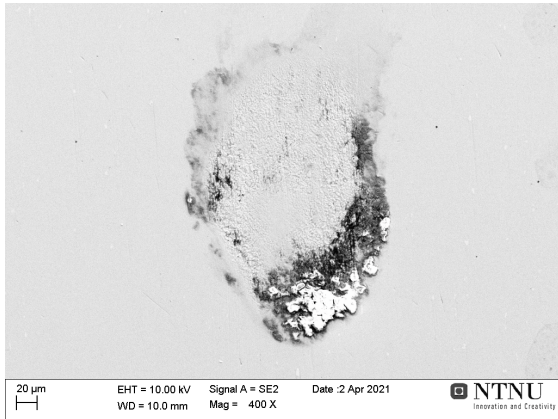
Figure 60: Prosthesis SS
Circular area with a rough surface along with layer
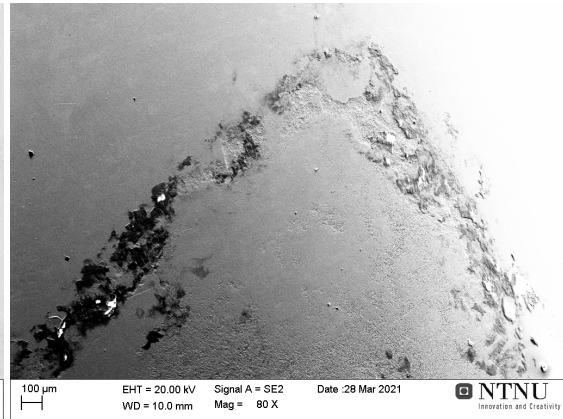
Figure 61: Prosthesis SS
Circular area with a rough surface along with layer

The surface of the prosthesis had systematic pits at a few locations. Figure 62 and Figure 63 below show two examples.
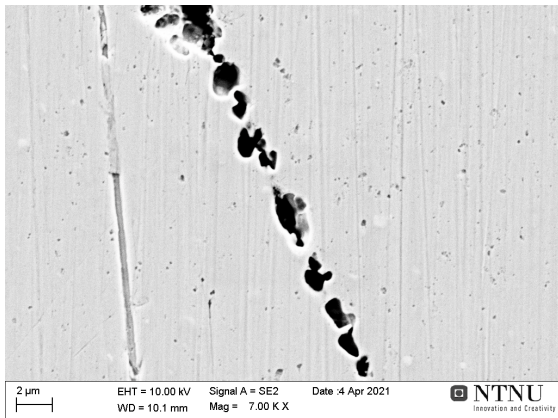
Figure 62: Prosthesis SS
Pits on side 2 of the stem
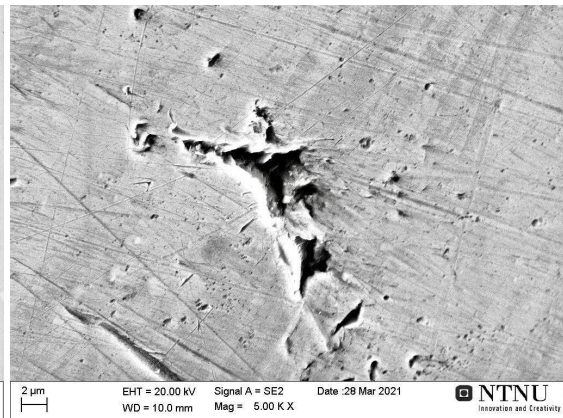
Figure 63: Prosthesis SS
Pits on the head

All parts of the prosthesis had areas of dark discolor. Both sides on the neck and stem had areas covered in large amounts of such discolor combined with a thick layer. This can be seen in Figure 64 and Figure 65 below.
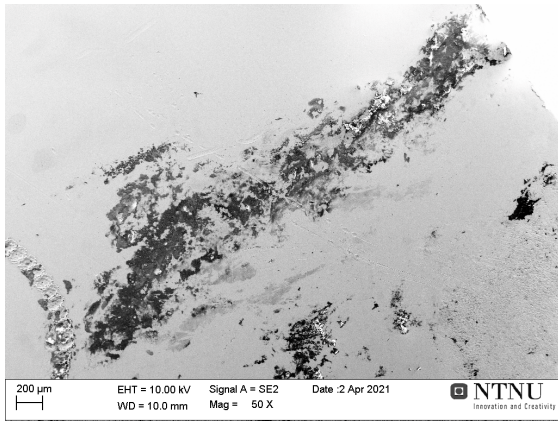
Figure 64: Prosthesis SS
Layer on the stem
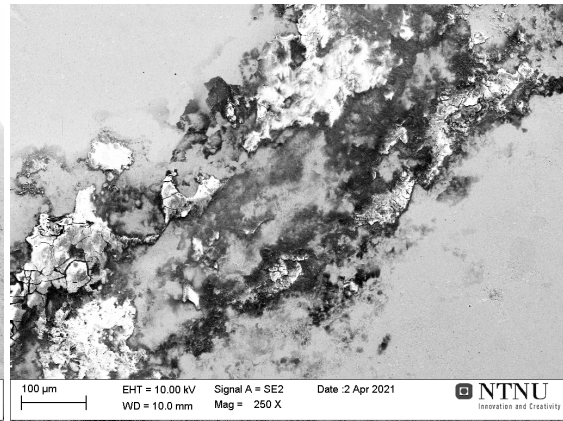
Figure 65: Prosthesis SS
Closeup of the layer

The entire prosthesis had superficial scratch marks all over. These can be seen in the background of other images in this section. Some scratches ran deeper, and some of these contained discolor, particles, a layer or a combination of these. An example is shown in Figure 66 below. The material also contained pores, one of which is shown in Figure 67 below.

Figure 66: Prosthesis SS
Scratch on the neck

Figure 67: Prosthesis SS
Pore on the stem

At side 1 of the neck and towards the tip of both sides of the stem were crater like indents in the surface. Figure 68 shows one example. Figure 69 below shows a closer image, displaying how the indents were layered.
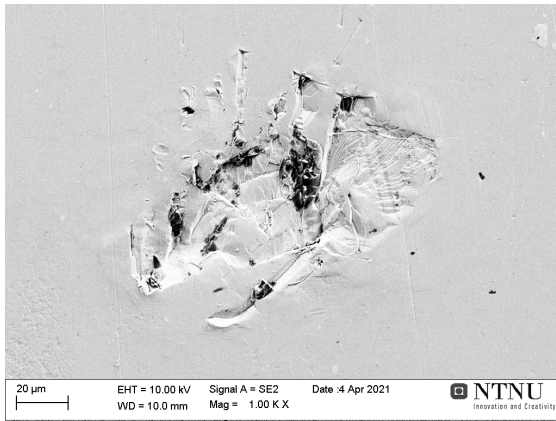
Figure 68: Prosthesis SS
Example of a crater on the stem
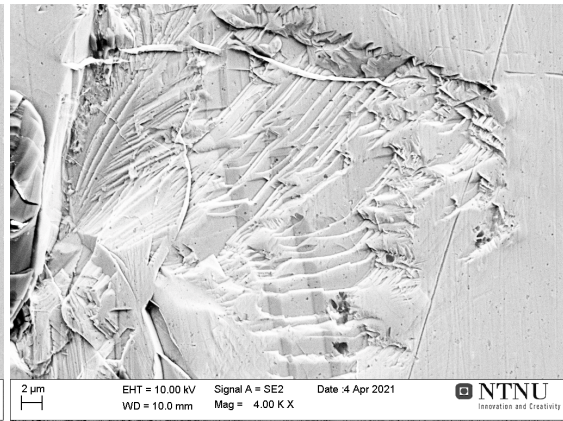
Figure 69: Prosthesis SS
Closeup of the crater on the stem

6.5.2 Prosthesis Co

The very top of the neck of prosthesis Co had a ridged section. The majority of this had clear ridges with some dark discoloration in between them. This is shown in Figure 70 below. On the section closest to the head, shown in Figure 71 below, these ridges were far more flat and the amount of discoloration was larger. This covered side 1 and the left area of side 2.
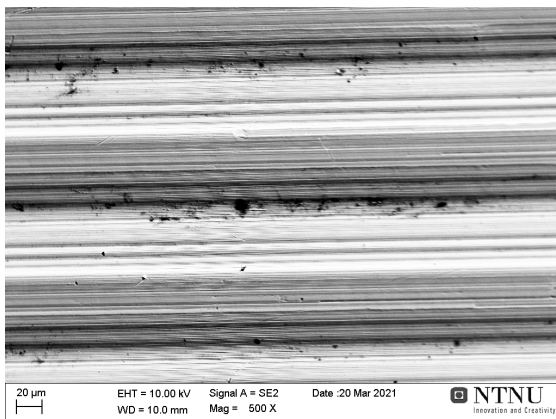

Figure 70: Prosthesis Co
Ridges with discoloration

Figure 71: Prosthesis Co
Flatter ridges with discoloration

The head of the prosthesis had areas of dark discoloration. The stem also had dark spots of discoloration, many of which had a surface layer on top. An example is shown in Figure 72 below. On side 1 of the stem, this occurred mainly on the top of the stem, whilst side 2 had spots like these across the whole length. Also, the general surface structure of the stem had craters with discoloration. Some of these contained layers or particles as displayed in Figure 73 below.
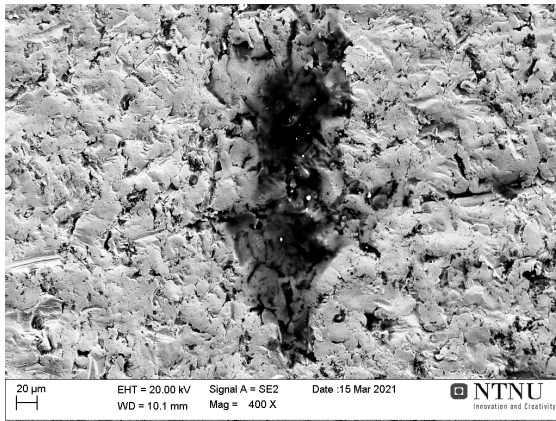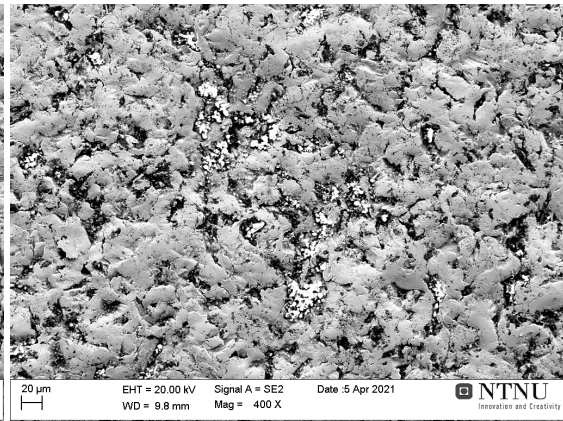
Figure 72: Prosthesis Co
Layer on the stem

Figure 73: Prosthesis Co
Layer on the stem

The surface of the head had a structure as shown in Figure 74 and Figure 75 below. Figure 74 illustrates how the surface also contained pores in some areas.
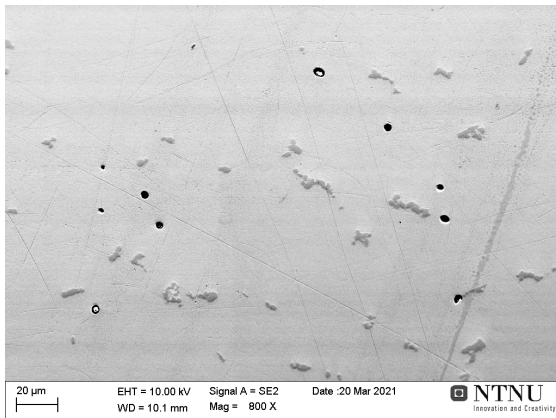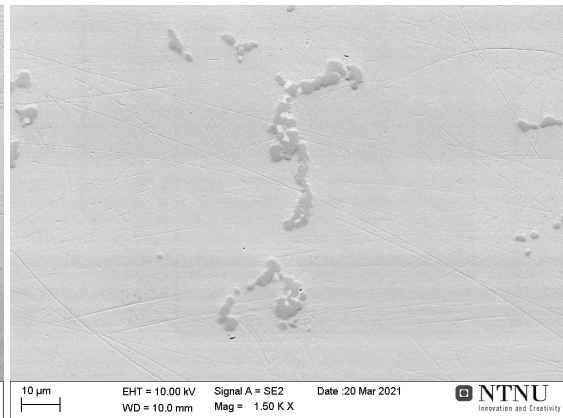

Figure 74: Prosthesis Co
General structure

Figure 75: Prosthesis Co
Closeup of the general structure

The head and neck were covered in general, superficial scratches. Throughout the entire prosthesis, there were some deeper scratches, such as the ones shown in Figure 76 and Figure 77 below.
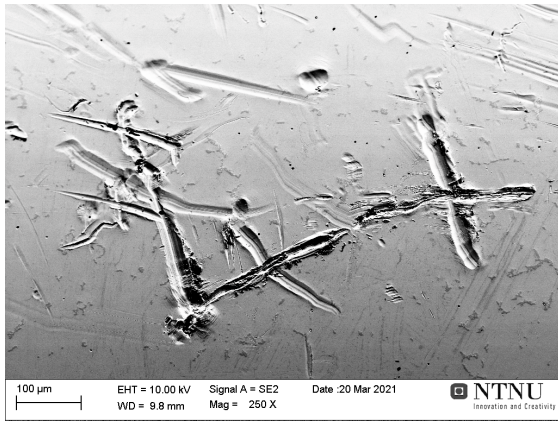
Figure 76: Prosthesis Co
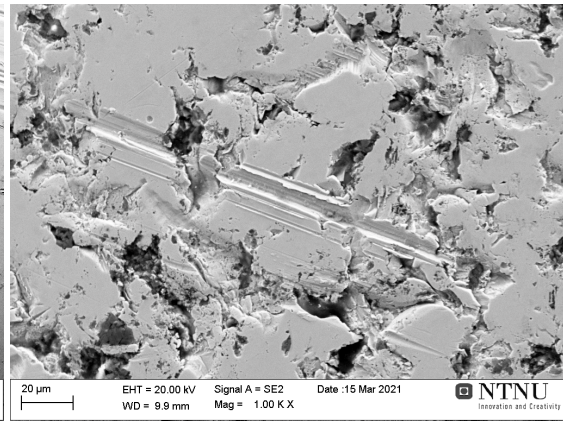Scratches on the head

Figure 77: Prosthesis Co
Scratch on the stem

6.5.3 Prosthesis Co-o

The neck of prosthesis Co-o had a ridged surface. At the shiniest, top part of the neck, this was clearly visible, whilst the lower part of the neck did not display this pattern as clearly. The lower area also had a more course surface with regular craters. The difference is shown in Figure 78 and 79 below.
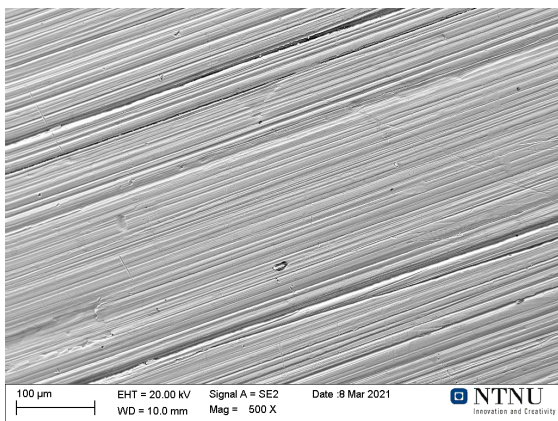

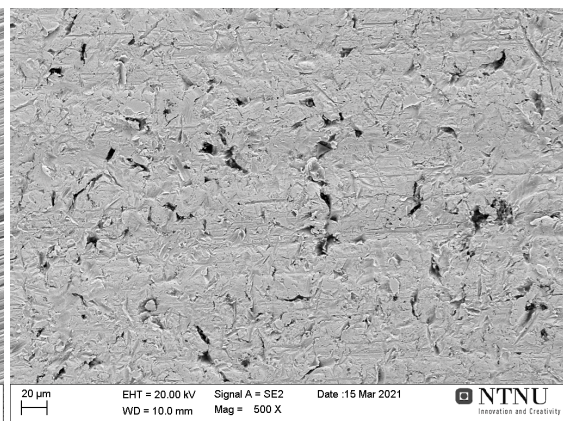Figure 78: Prosthesis Co-o
Top, shiny part of the neck

Figure 79: Prosthesis Co-o
Bottom, less shiny part of the neck

The ridges of the neck, shown in Figure 78 above, stopped abruptly at several locations. This is shown in Figure 80 below. The neck of the prosthesis also had a few sub surface particles, one of which is shown in Figure 81 below.
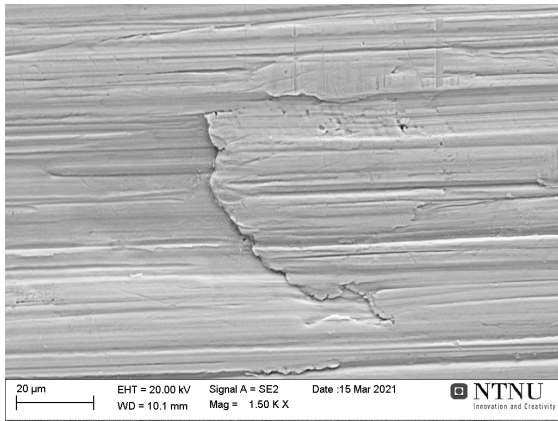
45

Figure 80: Prosthesis Co-o
Ridge stops

Figure 81: Prosthesis Co-o
Sub surface particle

In between some of these ridges were discolorations. Some of these discolorations, mainly the ones located at the less shiny part of the neck, were similar to deep scratches in appearance, as shown in Figure 82 below. Other discolorations, located mainly on the more shiny part of the neck, were cracked, dark surface layers. These are shown in Figure 83 below.
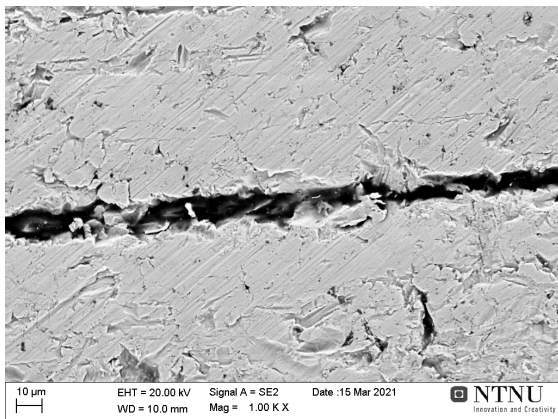

Figure 82: Prosthesis Co-o
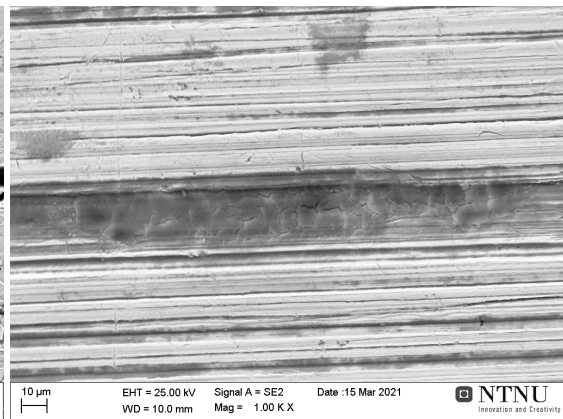Closeup of a discolored line

Figure 83: Prosthesis Co-o
Closeup of another discolored line

All over the neck of the prosthesis were also superficial surface scratches. This can be seen in Figure 84 below. A thick layer covered large parts of the stem in between the particles. This type of layer covered large sections of the front part of the stem, and could also be found frequently on side 1, side 2 and the back. Parts of these layers were cracked. An example of such a layer can be seen in Figure 85 below.
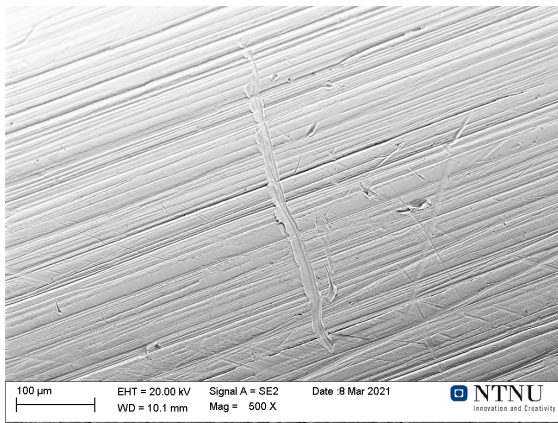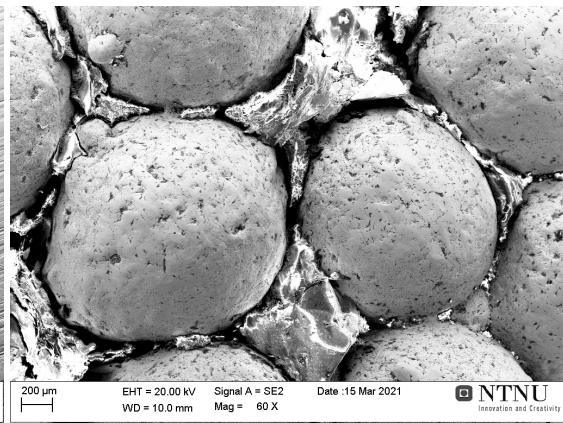
Figure 84: Prosthesis Co-o
Scratches

Figure 85: Prosthesis Co-o
Thick layer

The area in between the particles on the stem, that were not covered in the thick layer described above, had spots of dark discoloration. The only exception was the very top part of the stem, towards the neck. On many of these spots were thin layers, some of which were cracked. This can be seen in Figure 86 below. Side 2 of the neck also had such areas of dark discoloration with layers. The spheres on the stem surface had patches of dark discoloration as well. Many of these areas had layers on top, as seen in Figure 87 below. Some of those layers were cracked.
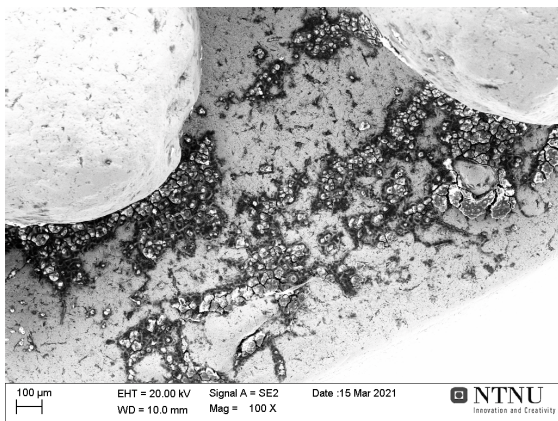

Figure 86: Prosthesis Co-o
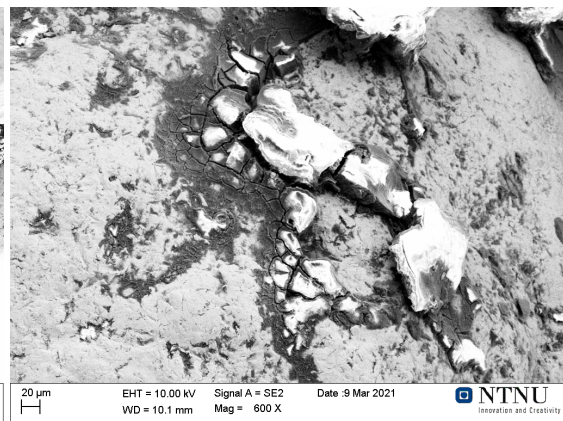Discoloration and layer between the spheres

Figure 87: Prosthesis Co-o
Discoloration and layer on the spheres

Figure 88 below shows the discoloration on the spheres at a lower magnification. Some areas of dark discolorations were located within shallow craters, as seen in Figure 89.
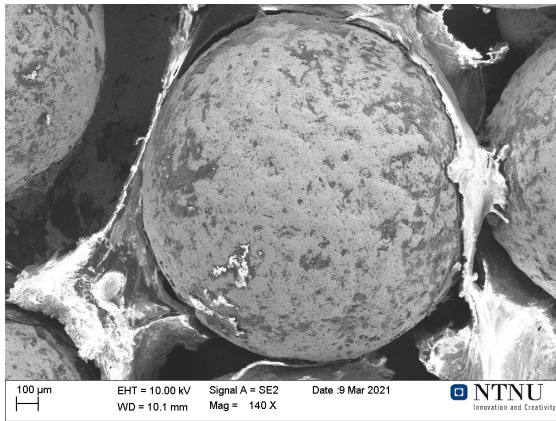
Figure 88: Prosthesis Co-o
Discolor
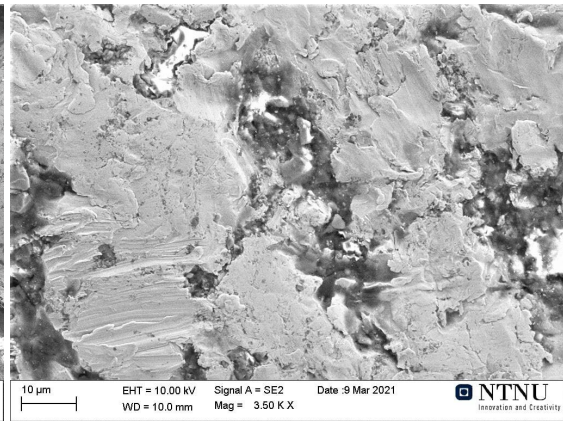
Figure 89: Prosthesis Co-o
Crater

At the root of some spheres on the stem, on side 1 and the back, were deep pits. Examples of this can be seen in Figure 90 and Figure 91 below.
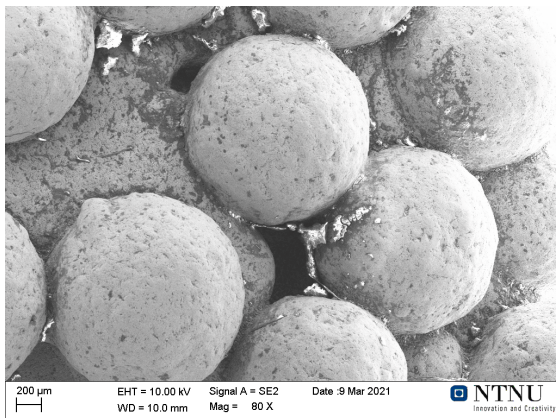
Figure 90: Prosthesis Co-o
Pits surrounding a particle
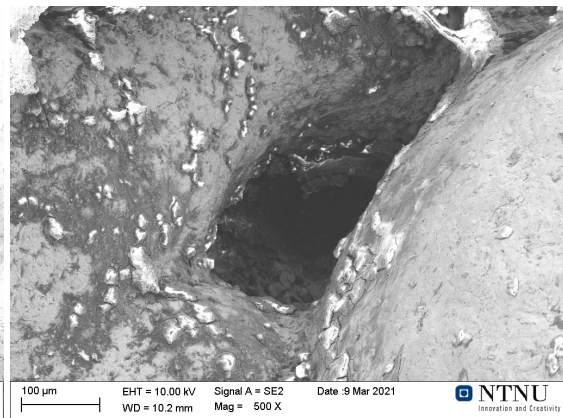
Figure 91: Prosthesis Co-o
Closeup of one of the pits

6.6 Surface roughness

The surface roughness was measured in three different ways. The software uses the following definitions:

- R_a: *Average roughness of profile*

- R_q: *Root-Mean-Square roughness of profile*

- R_z: *Mean peak to valley height of roughness profile*

Table 11 below lists the average results from the surface roughness measurements. The full results can be read in Appendix C.

Table 11: The average surface roughness results from all prostheses. The uncertainties are based on a continuous uniform distribution and given with two standard deviations.

Placement	R_a	R_q	R_z	Profile length
Prosthesis SS				
Head	420 ± 30 nm	550 ± 50 nm	2.4 ± 0.2 μm	9.20 mm
Neck	100 ± 8 nm	140 ± 10 nm	600 ± 200 nm	4.38 mm
Stem (Top)	126 ± 9 nm	190 ± 30 nm	700 ± 200 nm	4.83 mm
Stem (Bottom)	120 ± 20 nm	170 ± 20 nm	700 ± 200 nm	4.81 mm
Prosthesis Co				
Head	130 ± 20 nm	190 ± 30 nm	850 ± 90 nm	4.55 mm
Neck	500 ± 90 nm	700 ± 100 nm	2.7 ± 0.5 μm	4.62 mm
Stem (Top)	360 ± 60 nm	460 ± 70 nm	1.8 ± 0.3 μm	4.44 mm
Stem (Bottom)	500 ± 100 nm	600 ± 200 nm	2.5 ± 0.7 μm	4.11 mm
Prosthesis Co-o				
Neck (Top)	310 ± 50 nm	380 ± 70 nm	1.6 ± 0.3 μm	4.44 mm
Neck (Bottom)	310 ± 40 nm	400 ± 80 nm	1.5 ± 0.4 μm	4.58 mm
Neck (Bust)	310 ± 30 nm	390 ± 40 nm	1.5 ± 0.3 μm	4.45 mm
Stem	260 ± 30 μm	320 ± 50 μm	900 ± 200 μm	71.14 mm

6.7   Microstructures

This section presents the microstructures of the prostheses using results from backscatter electron imaging, electron backscatter diffraction, orientation contrast imaging and light microscope imaging.

6.8   Prosthesis SS

The grain structures for prosthesis SS, found by BSE analysis, are presented in Figure 92 below. The grain size was larger for the neck, section b) in Figure 92, than for the stem sections. There was no clear difference in grain size between the perpendicularly and parallel cut stem sections. Lines indicative of twins can be seen in all sections of Figure 92.
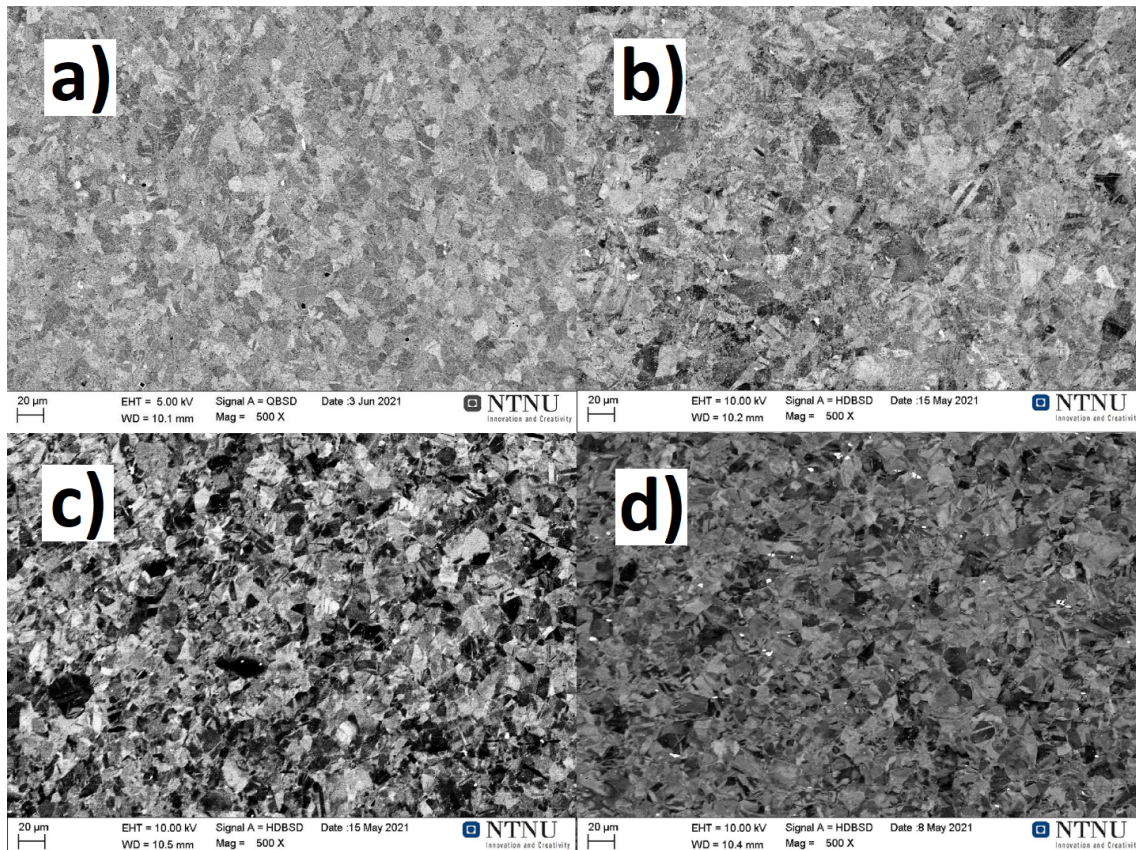
Figure 92: BSE images of Prosthesis SS
a) Head b) Neck c) Stem, perpendicularly cut d) Stem, parallel cut

Figure 93 and Figure 94 below show the EBSD scan for the perpendicularly and parallel cut stem sections. The grain size was larger for the perpendicularly cut sample. A manual estimate of the grain size along the diagonal of the image, not counting noise as grains, gave an approximate grain size of 6.1 microns for the perpendicularly cut sample and 2.4 microns for the parallel cut sample. The largest grains in the perpendicular direction of the stem spun up to 30 micrometers, and the parallel direction had grains up to 14 micrometers. Lines indicative of twins can be seen in both figures.
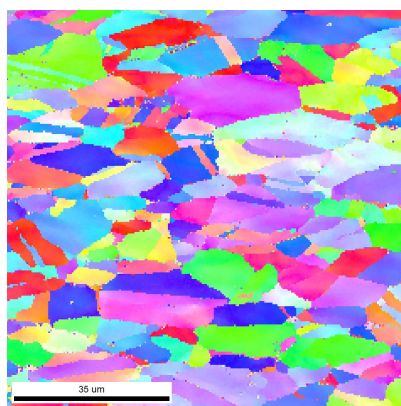

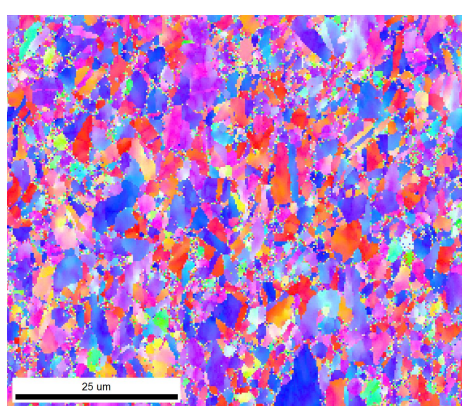Figure 93: Prosthesis SS Stem, perpendicularly cut

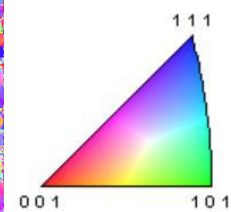Figure 94: Prosthesis SS Stem, parallel cut

Figure 95: Inverse pole figure

Phases included in the figures above were mainly iron in the gamma phase. Table 12 below lists the exact phase distribution. Phase maps can be seen in Appendix D.

Table 12: The phase distribution for prosthesis SS. *Perpendicular* and *parallel* cut refer to a perpendicular or a parallel cut direction with regards to the stem length when making the sample.

Phase	Perpendicular cut [%]	Parallel cut [%]
Iron (Alpha)	1.0 ± 0.1	4.7 ± 0.1
Iron (Gamma)	98.1 ± 0.1	86.7 ± 0.1
Chromium iron carbide	1.0 ± 0.1	8.6 ± 0.1

The images from the light microscopy did not provide any significant information, but can be seen in Appendix E.

6.9 Prosthesis Co

The grain structures for prosthesis Co, found by BSE analysis, are presented in Figure 96 below. The grain sizes were overall quite large, with most grains approaching or exceeding a millimeter each in their longest direction. The grains of the neck had a more rounded shape than the grains of sections a), c) and d) in Figure 96.
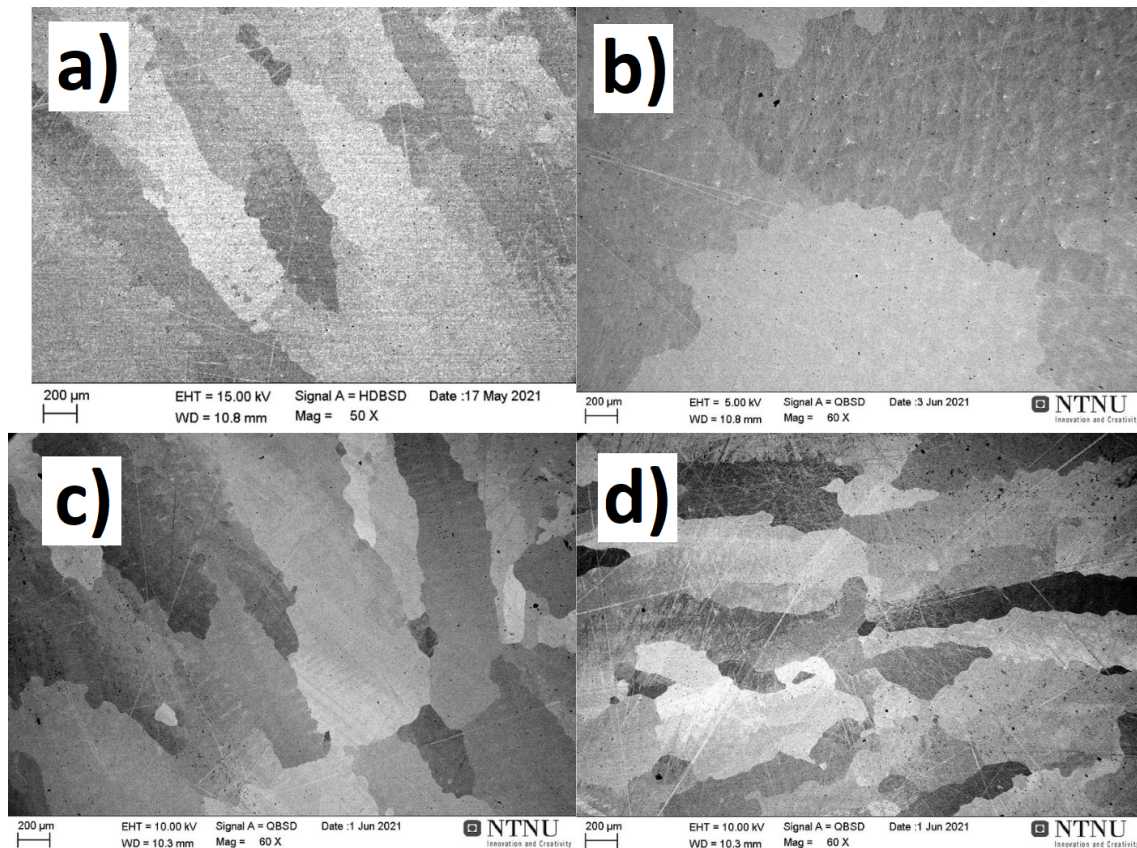

Figure 96: BSE images of Prosthesis Co
a) Head b) Neck c) Stem, perpendicularly cut d) Stem, parallel cut

Section a) in Figure 96 above represents the side of the head, with elongated grains lying perpendicular compared to the prosthesis length. The top of the prosthesis had more rounded grains. The difference can be seen in Figure 97 and Figure 98 below. The black area surrounding the images is due to a low magnification compared to the aperture size. The dark, misplaced spots in Figure 97 are residue from the cleansing process.
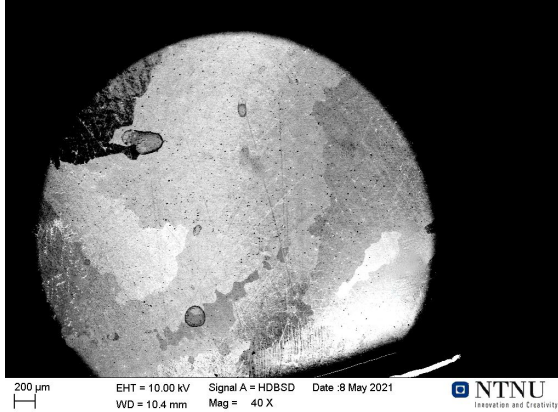

Figure 97: Prosthesis Co
The top of the head
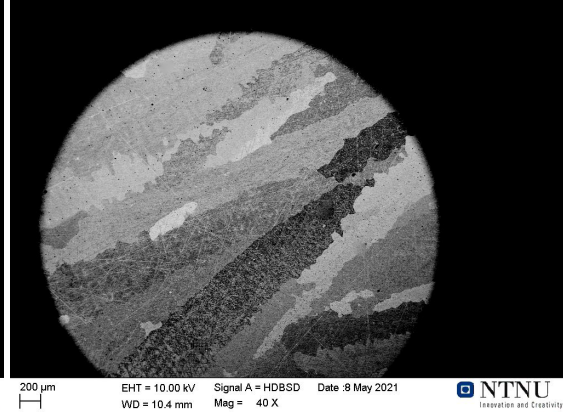
Figure 98: Prosthesis Co
The side of the head

Figure 99 and Figure 100 below show the EBSD scan for the perpendicularly and parallel cut stem sections. The EBSD images also showed grains that approached or exceeded 1 mm in their longest direction. Phases included in the figures below were almost entirely based on FCC unit cells. Some HCP unit cells were located at the grain boundaries and made up less than half a percentage of the phases. Phase maps can be seen in Appendix D.
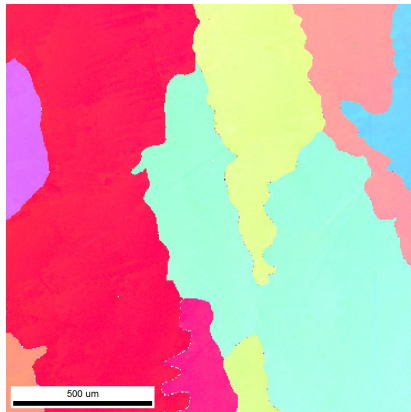
Figure 99: Prosthesis Co
Stem, perpendicularly cut
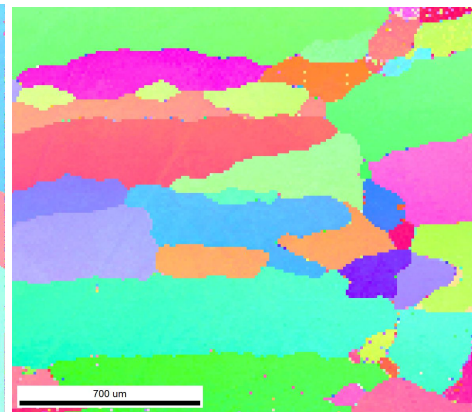
Figure 100: Prosthesis Co
Stem, parallel cut
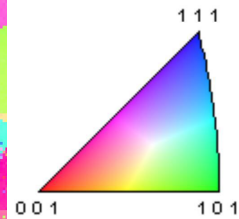
Figure 101:
Inverse
pole figure

The orientation contrast images from the EBSD scanning process also showed the grain structure of the stem sections clearly. These images are shown in Figure 102 and Figure 103 below. A manual estimate of the grain size along the diagonal of the image gave an approximate grain size of 0.8 mm for the perpendicularly cut sample and 0.2 mm for the parallel cut sample.

Figure 102: Prosthesis Co
Stem, perpendicularly cut

Figure 103: Prosthesis Co
Stem, parallel cut

The Murakami etchant revealed the structure of the samples. For the neck of prosthesis Co, a pattern was clear towards the top, but scarce towards the bottom. This can be seen in Figure 104 and Figure 105 below.
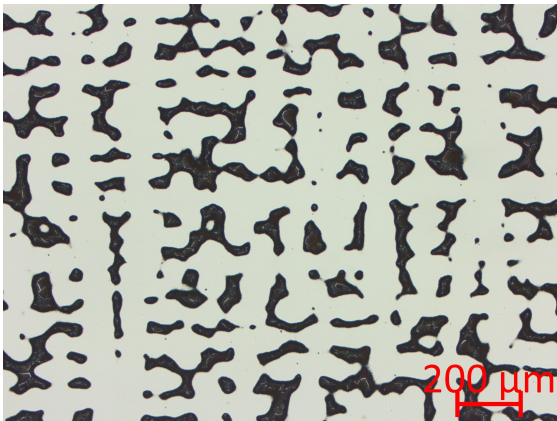
Figure 104: Prosthesis Co
The top of the neck
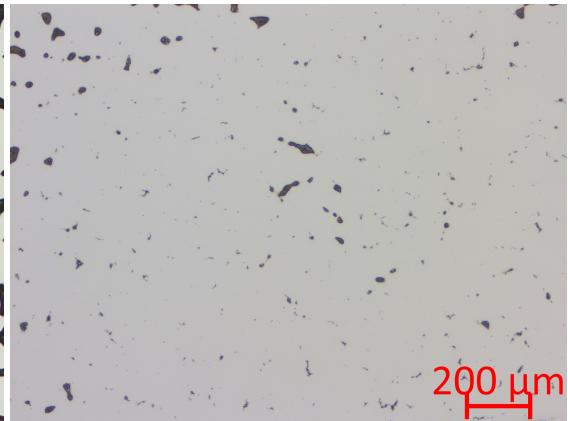
Figure 105: Prosthesis Co
The bottom of the neck

The parallel cut cross section of the stem also had variations in pattern. The pattern was clear in the middle of the sample, as seen in Figure 106 below, but faded towards the edges as seen in Figure 107.
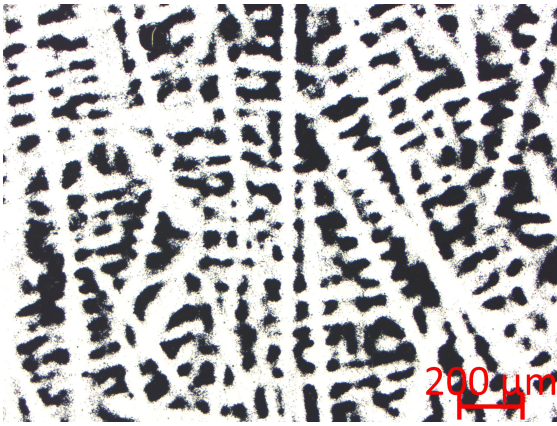
Figure 106: Prosthesis Co
The middle of the parallel cut stem
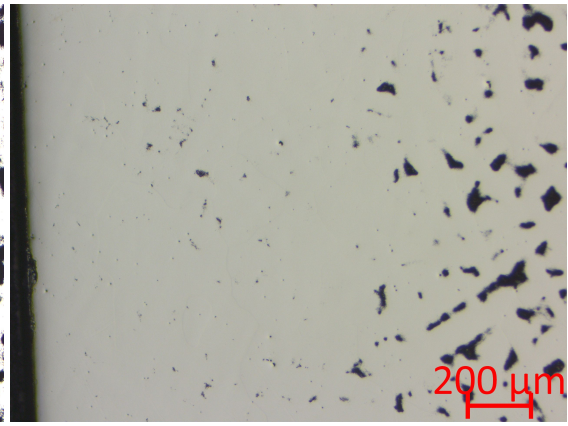
Figure 107: Prosthesis Co
The edge of the parallel cut stem

The perpendicularly cut stem and the head of prosthesis Co had even patterns. These are shown in Figure 108 and Figure 109 below.
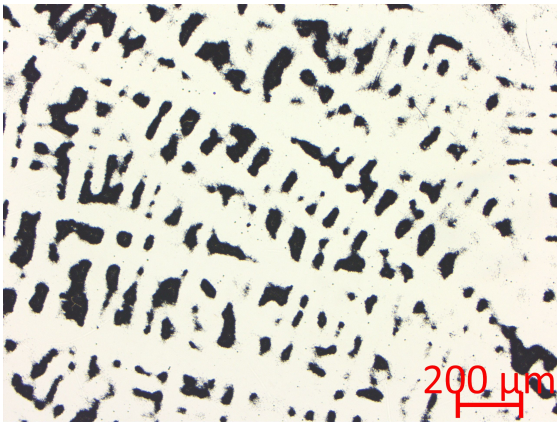
Figure 108: Prosthesis Co
The perpendicularly cut stem
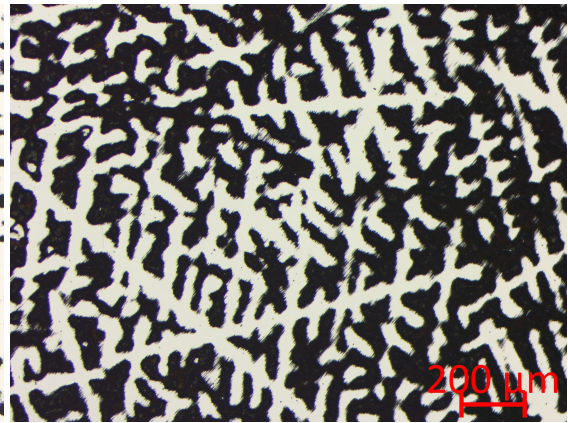
Figure 109: Prosthesis Co
The head

6.10   Prosthesis Co-o

The grain structures for prosthesis Co-o, found by BSE analysis, are presented in Figure 110 below. Section b) in Figure 110 clearly demonstrates that the spheres on the stem were in fact part of the bulk material, as the grains continued uninterrupted in the transition. Grains were large in all sections, exceeding a millimeter in their longest directions.
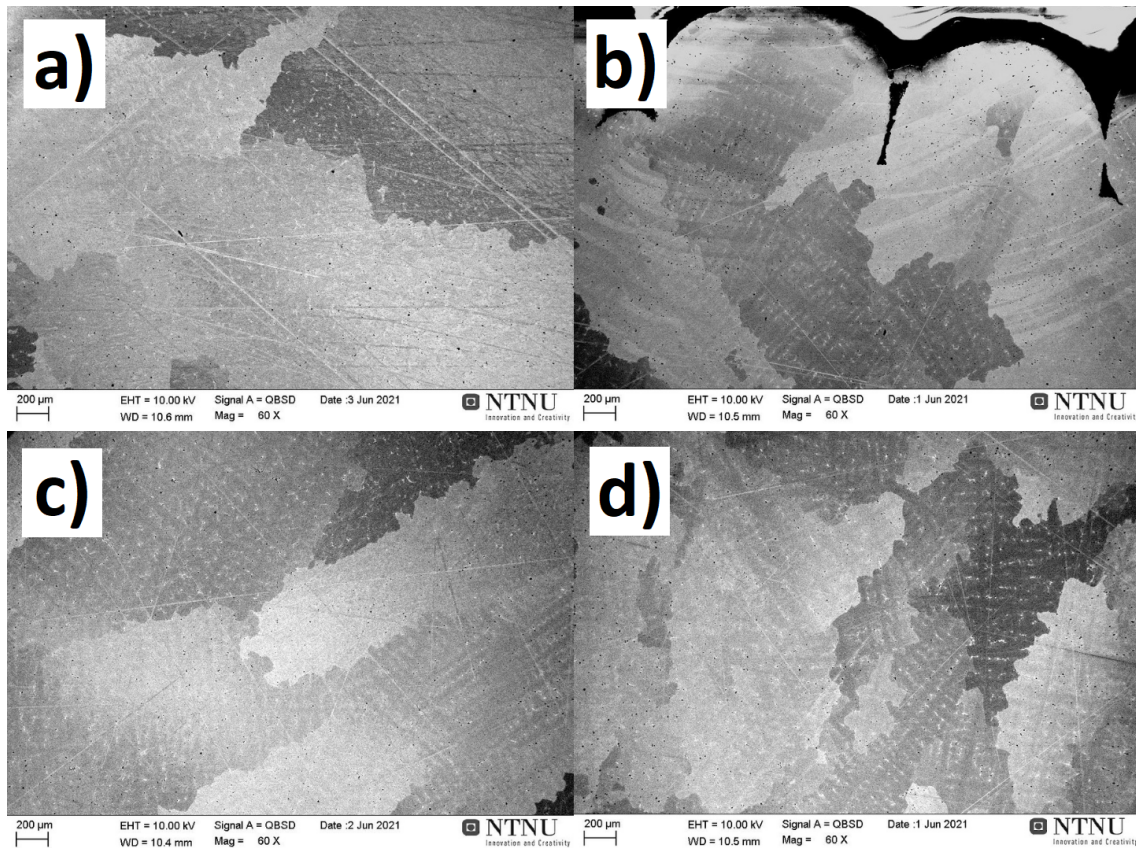
Figure 110: BSE images of Prosthesis Co-o
a) Neck b) Porous coating, from parallel cut stem c) Stem, perpendicularly cut d) Stem, parallel cut

Figure 111 and Figure 112 below show the EBSD scan for the perpendicularly and parallel cut stem sections. The images confirm large grains exceeding a millimeter. Phases included in the figures below were almost entirely based on FCC unit cells. Some HCP unit cells were located at the grain boundaries and made up half a percentage of the phases or less. Phase maps can be seen in Appendix D.
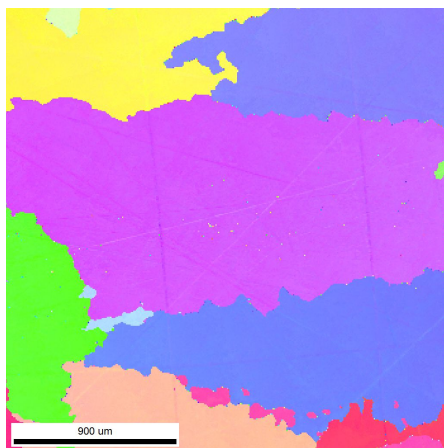
Figure 111: Prosthesis Co-o
Stem, perpendicularly cut
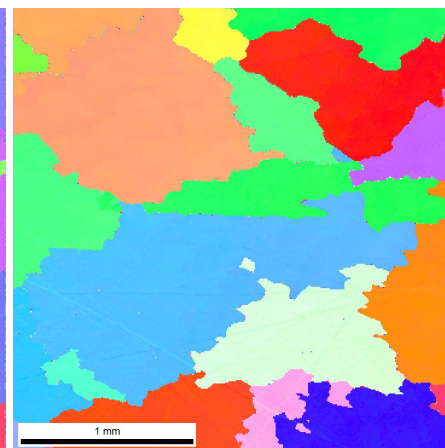
Figure 112: Prosthesis Co-o
Stem, parallel cut
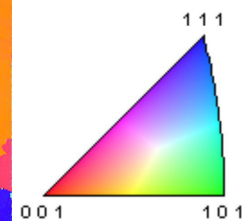
Figure 113:
Inverse
pole figure

The orientation contrast images from the EBSD scanning process also showed the grain structure of the stem sections clearly. These images are shown in Figure 114 and Figure 115 below. A manual estimate of the grain size along the diagonal of the image gave an approximate grain size of 1.1 mm for the perpendicularly cut sample and 0.8 mm for the parallel cut sample.
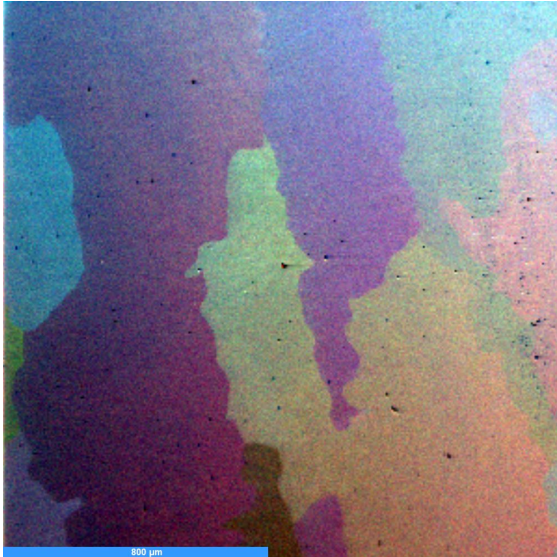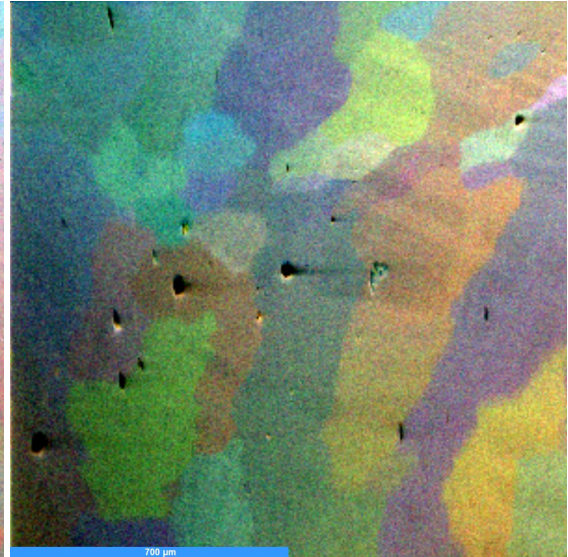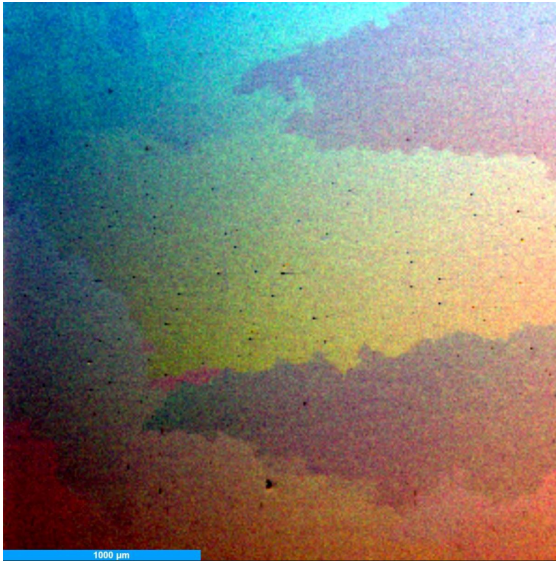

Figure 114: Prosthesis Co-o
Stem, perpendicularly cut
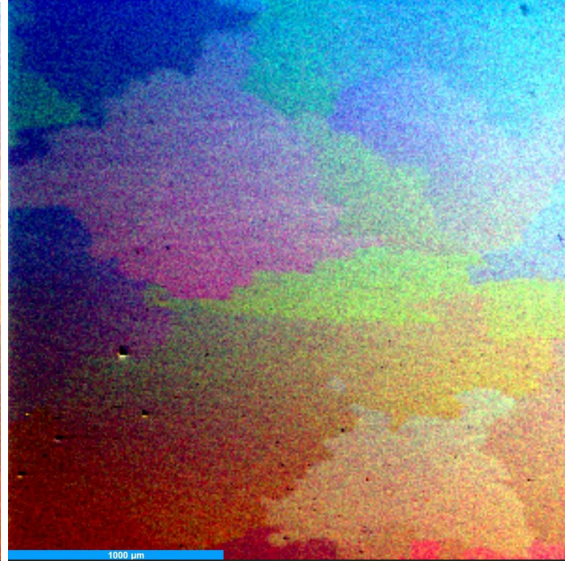
Figure 115: Prosthesis Co-o
Stem, parallel cut

The Murakami etchant revealed the structure of the samples from prosthesis Co-o as well. For the neck of the prosthesis, most of the surface was as shown in Figure 116 below. There were a few patches with a larger pattern, such as the one seen in Figure 117.
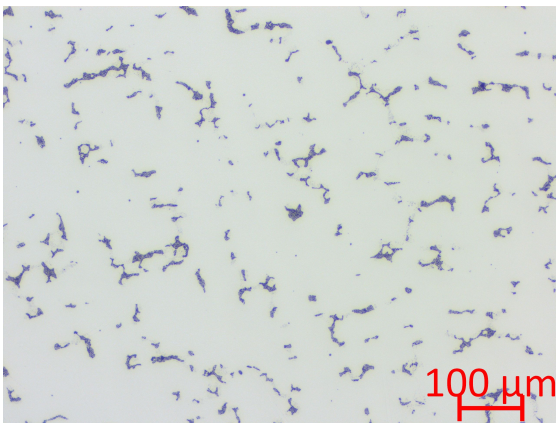
Figure 116: Prosthesis Co-o
Smaller pattern
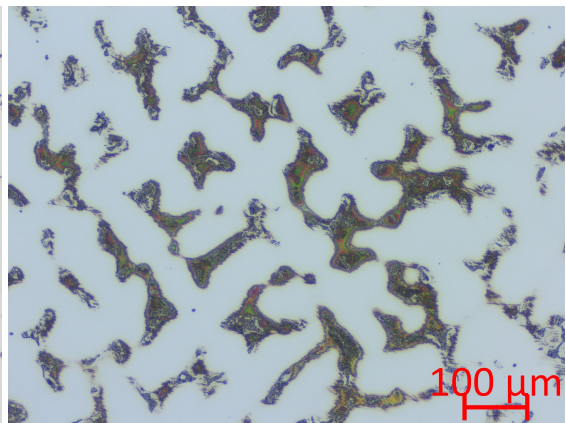
Figure 117: Prosthesis Co-o
Larger pattern

The surfaces of both the perpendicularly and parallel cut stem had even patterns in the areas that were not part of the external spheres. This can be seen in Figure 118 and Figure 119 below.
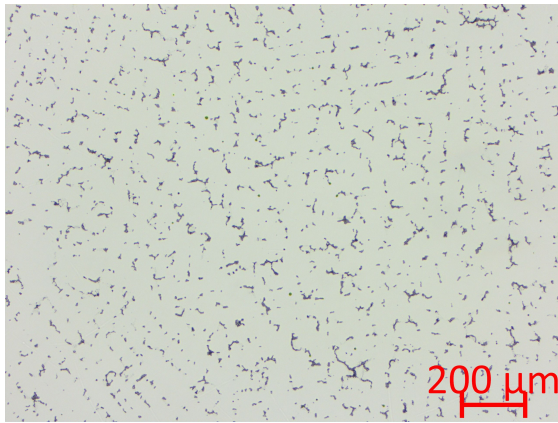
Figure 118: Prosthesis Co-o
Perpendicularly cut stem
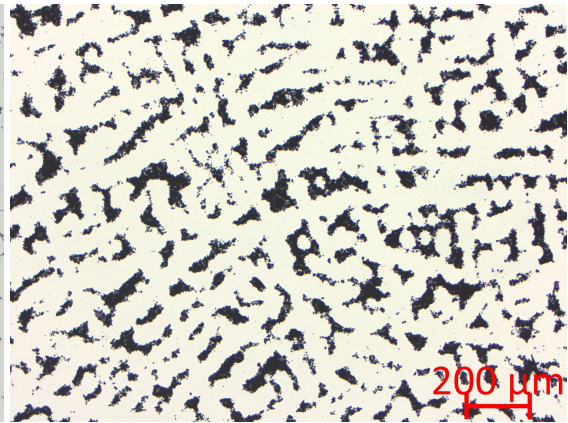
Figure 119: Prosthesis Co-o
Parallel cut stem

The external spheres had patterns similar to the parallel cross section of the stem. On this particular sample, this pattern developed earlier than the bulk material in terms of time. When the bulk pattern of the parallel cut stem had fully developed, the spheres were typically over etched with a brown and yellow appearance. Figure 120 below shows the pattern of the spheres, which was the same for all samples. Figure 121 below shows the transition between the sphere pattern and the bulk pattern of the neck sample.
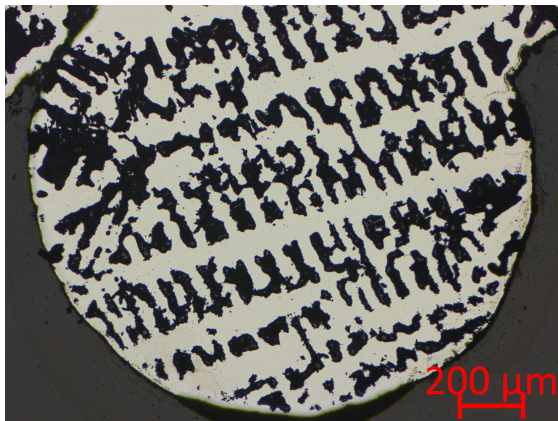
Figure 120: Prosthesis Co-o
Sphere pattern on the neck
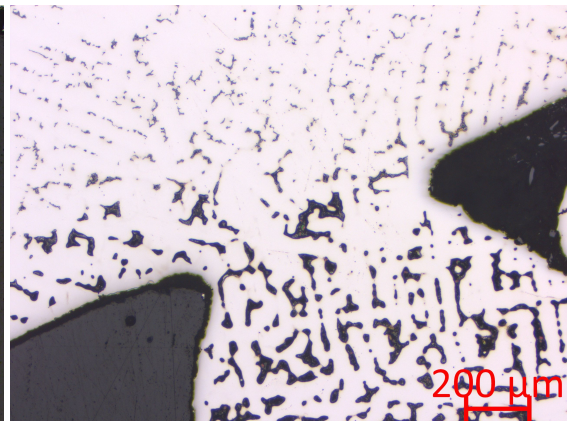
Figure 121: Prosthesis Co-o
Transition between patterns on the stem

6.10.1 All prostheses

Figure 122 below shows the image quality maps for the EBSD scans of all prostheses. A light color represents a good quality for the electron diffraction pattern, so it can clearly be seen that the pattern quality was low at the grain boundaries for all EBSD scans.

57
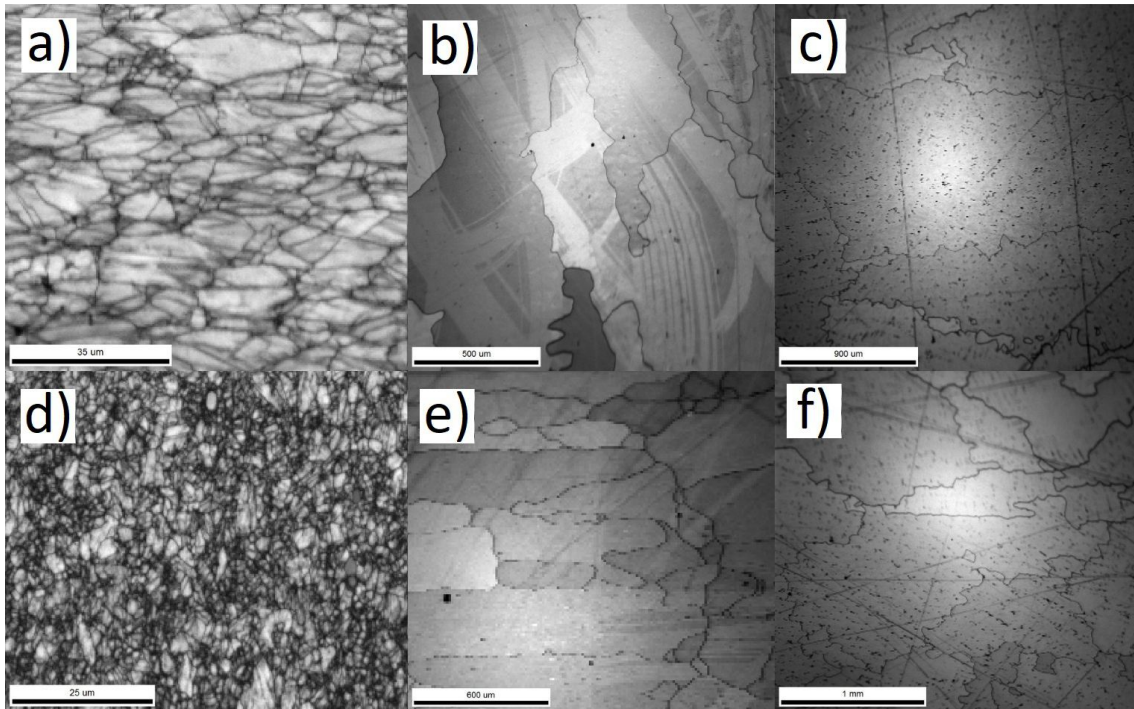
Figure 122: Top row shows the perpendicular cut and bottom row shows the parallel cut
a) and d) are from prosthesis SS, b) and e) are from prosthesis Co, c) and f) are from
prosthesis Co-o

6.11 Hardness properties

Table 13 below lists the results from the hardness measurements by average values. Full
results can be seen in Appendix F.

Table 13: The average hardness values for prostheses SS, Co and Co-o. The uncertainties
are based on a continuous uniform distribution and given with two standard deviations.
Perpendicular and *parallel* cut refer to a perpendicular or a parallel cut direction with
regards to the stem length when making the sample.

Prosthesis SS					
Position	Head	Neck	(Parallel cut) Stem	(Perpendicular cut) Stem	-
Hardness [HV]	265 ± 3	344 ± 5	350 ± 10	380 ± 10	-
Prosthesis Co					
Position	Head	Neck	(Parallel cut) Stem	(Perpendicular cut) Stem	-
Hardness [HV]	320 ± 10	310 ± 10	290 ± 20	300 ± 10	-
Prosthesis Co-o					
Position	(Top) Neck	(Bottom) Neck	Bust	(Parallel cut) Stem	(Perpendicular cut) Stem
Hardness [HV]	340 ± 10	330 ± 10	320 ± 10	320 ± 10	310 ± 10

6.12   Tensile properties

Figure 123 below shows engineering stress-strain curves where results from all prostheses are included. The elongation in percentage is based on the grip separation in the tensile test machine and the original gauge length. The results are presented this way because the stress-strain curves from the laser video extensometer displayed a negative elongation in parts of the curves. The cause for this is discussed in Section 7.5. Stress-strain curves for each individual prosthesis, including the measurements with the laser video extensometer, can be seen in Appendix G.
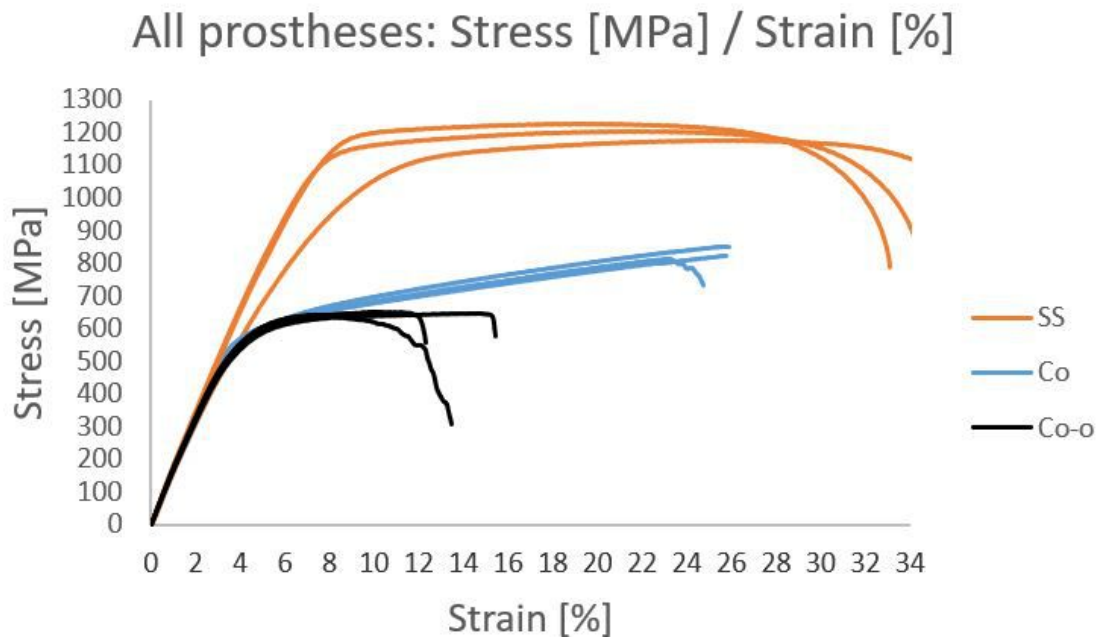
Figure 123: Engineering stress versus engineering strain in percentage

Table 14 below lists the average values of the tensile properties measured from Figure 123 above. The yield strength values are estimated based on the Young's moduli seen in this table. It can clearly be seen that prosthesis SS had both the highest ultimate tensile strength and the highest yield strength of the three prostheses. Full results can be seen in Appendix G.

Table 14: The average tensile properties for the three prostheses. The uncertainties are based on a continuous uniform distribution and given with two standard deviations.

Value	Prosthesis SS	Prosthesis Co	Prosthesis Co-o
Ultimate tensile strength [MPa]	1200 ± 30	830 ± 20	647 ± 5
Young's modulus [GPa]	15.9 ± 0.9	15.9 ± 0.7	16.0 ± 0.5
Yield strength at 0.2% elongation [MPa]	800 ± 200	500 ± 40	482 ± 3

7 Discussion

The samples were identified as two CoCrMo alloys and one stainless steel alloy. The two CoCrMo alloys were similar in element content, except for prosthesis Co-o having a slightly higher content of nickel. Prostheis SS had an Exeter type stem, prosthesis Co had a Lubinus SP II type stem and prosthesis Co-o was a Lord type stem.

7.1 Fracture of prosthesis Co-o

Prosthesis Co-o was the only prosthesis with a fracture. It differed from the other prostheses through its porous surface, making it a cementless prosthesis meant to grow into the femoral bone of the patient. This type of prosthesis takes some time to settle in securely, and during this time it is difficult to avoid all movement. The shape of this stem may have been rotationally unstable, making it possible for the prosthesis to have properly secured towards the bottom of the stem and not at the top[25]. This would make the prosthesis unstable and much more prone to fatigue fracture. The surface spheres had wear craters, shown in Figure 89. This suggests that there has either been some movement in the interface between the stem and the bone or the surface has been damaged by corrosion. Furthermore, the white layer seen in Figure 42 was mainly located close to the fracture of the stem. The rest of the remaining stem had no such layer, except for a small area close to the front of the neck. The element content of this white layer is not known, due to XRF being unable to isolate such small areas and EDS requiring a polished surface. However, if this was in fact bone growth, it could confirm that the prosthesis was only secured properly at the lower half of the stem.

Prostheses are exposed to cyclic stresses through everyday use, so the design of the prostheses should take this into account. An important part of this is to avoid stress raisers in the surface of the prosthesis, as explained in Section 3.6.7. The porous surface covering the stem presented numerous potential stress raisers that could initiate a crack. In addition, it is known from Section 6.1 that the spheres on this stem type could loosen from the surface. Spheres that fall off the stem are likely to leave geometrical changes, such as dents in the surface, that will act as stress raisers. Figure 90 shows examples of stress raisers.

If a crack was to initiate in the surface of this stem, which it did, the material used for this prosthesis was not very resistant to crack propagation. Figures 110, 111 and 114, among others, display a huge overall grain size surpassing a millimeter in the longest directions. With grain sizes this big, there was little resistance to crack propagation. Smaller grains would have presented more grain boundaries and hence more resistance to crack propagation as described in Section 3.7. An initiated crack would therefore propagate fast in this material. Also, as described in Section 3.7, the large grains made the material more susceptible to brittle fracture. With a grain size this large, the stress level required for initiation of brittle fracture was lowered.

Section b) in Figure 110 shows that the porous coating on the stem was in fact part of the bulk material. This means that there was no boundary between the bulk material and the spheres, so any crack that developed due to stress raisers around these spheres could easily propagate into the material.

Figure 45 of the fracture surface clearly states that this was a fatigue fracture. The semi circular lines that surrounded the crack initiation point were beach marks that indicated the slower crack propagation following the cyclic stresses that the prosthesis was exposed to. The outer area represented a rapid crack propagation in the final failure of the prosthesis stem. This area, seen in Figure 49, was fairly smooth and without dimples, indicating that the material was brittle. Figure 47, showing vertical lines in a closeup next to the crack initiation site, displays cleavage of the material. This is also indicative of a brittle material.

Comparing the fracture of the stem to the one found when looking at the tensile test fracture, seen in Figure 56, the stem fracture appeared more brittle. In the tensile fracture, there were a few sections of ductile areas with dimples and such areas were not found in the stem fracture. Brittle materials tend to be hard, but the hardness measurements did not show that the stem was harder than the rest of the prosthesis. It would be interesting to dedicate future work to finding out whether an environmental factor could have made this particular section of the stem more brittle than the rest.

The main causes of this fracture were fatigue through cyclic stresses combined with surface stress raisers and a material with a large grain size.

7.2   External damages

All of the prostheses had larger damages that were visible to the human eye. Examples of such damages are Figure 29 for prosthesis SS, Figure 33 for prosthesis Co and Figure 84 for prosthesis Co-o. It is reasonable to believe that these damages did not occur during use, but rather during extraction and later transportation and storage. Because two of the prostheses were provided within the same bag, with no protective means, it is assumed that few or no measures were taken to avoid causing post use damages.

Systematic, small pits, such as the ones seen in Figures 62 and 63 for prosthesis SS, can likely be connected to the manufacturing process. The prosthesis was forged, causing particles to be lined up when the material was formed. This could potentially leave pits like these. Regular, rounded pores as seen in Figures 67 and 74 were either originally part of the material or exposed as embedded particles fell out from the surface during manufacture or wear. This was confirmed by EDS, which showed that the pore content was either bulk material or oxides.

Discoloration and surface layers could be seen both with the naked eye and in SEM examinations of all three prostheses. Examples can be seen in Figures 28 and 65 for prosthesis

SS, Figure 72 and 73 for prosthesis Co and Figures 39 and 85 for prosthesis Co-o. These were likely oxide layers caused by corrosion. Their contents are not known, as the XRF does not isolate areas that small and EDS requires a polished surface to be accurate. Particles similar to the ones seen at the oxide layers were either similar to the bulk material or carbon based according to the EDS analysis. The crystalline growth within circular discoloration for prosthesis SS, seen in Figure 59, could be due to localised corrosion of alloy elements and subsequent crystalline growth of the corrosion product. Further, it is unknown how the prostheses were cleansed after extraction. It is possible that some of the discoloration and corrosion layers found on the prostheses are due to chemicals from the cleansing process reacting with the metal surfaces.

Uniform corrosion can explain the circles with a higher surface roughness found on prosthesis SS, seen in Figures 60 and 61. These circular areas were surrounded by surface layers. This indicates that there used to be larger surface layers there, covering these areas. These surface layers were likely scraped off of the surface, either by wear or through the extraction process. This would leave such rough surface areas behind. Wear could be a possible cause if the prosthesis had loosened, creating motion in the contact area between the stem and the bone cement. As seen in Section 3.1, loosening is a common cause for revision surgery for prostheses, but the extraction process is the more likely cause of the two. A loose prosthesis would have given a much larger surface roughness at the stem compared to the neck, assuming they were identical prior to use. Also, there were dents with cleavage on the stem, seen in Figures 68 and 69, indicating that the stem has been exposed to some force when extracting it. Layers, particles or bone cement posing resistance to the extraction could have ripped out some of the stem surface, leaving such cleavages in the surface.

Both prostheses Co and Co-o had ridged surfaces on the top of the neck. Both prostheses had sections with discolorations in between these ridges, seen in Figures 71 and 83. Wear can also be seen, especially when comparing Figure 70 to Figure 71. Since these damages were located at the top of the necks, there could have been unwanted movement between the femoral head and neck, causing wear. The discoloration was likely due to a chemical process, for instance crevice corrosion in between the femoral head and necks. The combination of wear and corrosion means that these damages were likely a result of tribocorrosion. The pore like sites at the neck of prosthesis Co-o, seen in Figure 81, were sub surface particles that emerged during the machining process. The machining process was likely also the cause of the abrupt endings to some of the ridges at the neck of prosthesis Co-o, seen in Figure 80.

Geometrical changes in a surface are known to be stress raisers, creating initiation sites for fatigue cracks. This is presented in Section 3.6.7. Serial numbers such as the ones seen in Figure 25 for prosthesis SS, Figure 32 for prosthesis Co and Figure 36 for prosthesis Co-o were carvings in the material that could potentially be such crack initiation sites. This should be kept in mind when deciding which location and which method to choose when adding script to the prostheses. The best option would be to avoid indents

to the material, and if this is the chosen option it should be added to a low stress location.

Overall, there were not many external damages that occurred during use, except for the stem fracture of prosthesis Co-o. Most damages occurred post use. Uniform corrosion, tribocorrosion and crevice corrosion were the most prominent damage mechanisms stemming from the use of these prostheses. The external damages found on the prostheses align well with the ones expected from Section 3.2.2.

7.3   Surface roughness

The surface roughness measurements showed that the average roughness was significantly larger at the head for prosthesis SS. This means that there has been a significant amount of wear at this location, indicating third body abrasive wear due to wear debris from the acetabular cup or liner. The rest of the prosthesis was worn quite evenly, assuming that the original surface roughness was the same at all parts of the prosthesis. An estimate of the original surface roughness was made in Section 6.1. If this estimate was correct, the surface roughness had increased from 22-29 nm to 100-120 nm, over four times as large. It would be highly interesting to have the exact numbers for the original surface roughness from the manufacturers of all prostheses.

The average surface roughness of prothesis Co was significantly lower at the head. This is due to the design of the prosthesis, where the goal was to create as little friction as possible between the head and liner or acetabular cup. The remaining components had similar average surface roughness. Since there was little to no difference in average surface roughness between the lower stem and the neck in prosthesis Co or SS, assuming these values were originally alike, it can be assumed that either none of these prostheses have been loose or they were only loose for a short time before extraction.

In general, increases in surface roughness for all prostheses were likely chemical, due to bone cement or human body environment interacting with the prosthesis surface. It could to some degree also have been due to the removal of bone cement post use or due to fatigue fretting by microscopic motions between the bone cement and the prostheses, but these cases would increase the surface roughness of the stem compared to the neck. Prosthesis Co-o was the only prosthesis where signs of physical wear were present, shown in Figure 89.

7.4   Microstructures

For prosthesis SS, twins could be seen in both BSE and EBSD images, Figures 92, 93 and 94, meaning that the material has been exposed to either mechanical shear forces or deformation followed by annealing. It is known from Section 6.1 that the prosthesis was forged, so the twins seen in prosthesis SS were from the deformation during this process. The images in Figures 92, 93 and 94 clearly show small grains with a relatively even grain size. This combined with the high strength shown in the tensile tests excludes annealing

and recrystallization as causes for the twins.

Prosthesis SS had average grain sizes around 2.4 microns in the parallel cut direction of the stem and about 6.1 microns in the perpendicularly cut direction when looking at the EBSD images of the stem, Figures 93 and 94. The perpendicular direction also had the largest grain sizes when looking only at the largest grains. This difference in grain size was not visible in the BSE images, but EBSD is more reliable of the two. Smaller sized grains are beneficial for slowing crack propagation, as seen in Section 3.7, but the structure of the grains was not beneficial. Prosthesis SS had grain sizes that were larger in the perpendicularly cut direction of the stem than the parallel cut direction, giving a structure as seen in section a) in Figure 124 below.
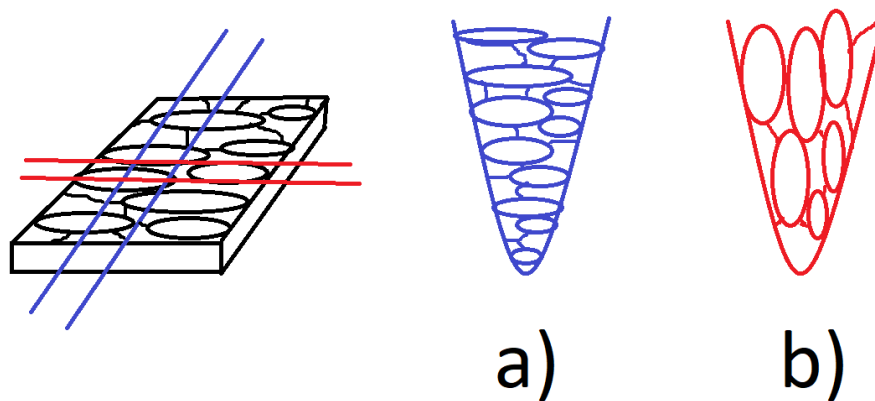
Figure 124: Illustration of resultant grain structures when cutting a material with elongated grains

This was a weakness for the component, because initiated cracks would propagate perpendicularly to the stem length or with an angle below 90 degrees compared to a horizontal line. Such components are mainly exposed to alternating tensile and compressive loads, which could cause pores within the material. If that happens, cracks could propagate from the edges of such a pore, giving fracture in the perpendicular direction with regards to the prosthesis length. In the case of a bending force, the perpendicular direction would also be preferred for crack propagation. This means that configuration b) in Figure 124 is superior to the configuration shown in section a). With a structure like the one seen in section a), fewer grain boundaries are there to impede crack propagation. Knowing that prosthesis SS was forged, it can be assumed that the original piece of bulk material was forged and then machined into the final shape. The bulk material would then have elongated grains prior to machining. By considering the grain orientation when machining the final shape - one could control the grain structure of the prosthesis. By cutting in the direction shown with red lines in Figure 124, one could deliberately create a stem with grains as shown in section b). This would give a stem that is more resistant to crack propagation. A superior solution is to forge the prosthesis into the desired shape straight away. This would give the desired grain structure and there would be less machining, which causes fewer potential crack initiation sites along the surface of the component.

Both prostheses Co and Co-o had grains of similar sizes in both directions within the stem, though the perpendicular direction of the stem appeared to have slightly bigger grains. It is difficult to determine the correct grain sizes in both directions due to the large size of the grains. More grains are needed in frame to make accurate estimates, but the sizes of prosthesis Co were around a millimeter in the longest direction, and the grains of Co-o measured up to a few millimeters. Having grains this large is not beneficial, as explained in Section 3.7, and the materials were therefore prone to rapid crack propagation and failure should a crack arise. The grains were more rounded at the top of the head than on the sides for prosthesis Co, and the grains of the stem were elongated for both prostheses Co and Co-o. The uneven grain boundaries and the dendritic microstructures suggest the materials have been cast, so the shape of the grains were likely a result of heat distribution and cooling rates for the prostheses. The phases found with EBSD were all built from FCC unit cells, which aligns well with the theory in Section 3.2.2. The few detected phases built from HCP or BCC unit cells were located at the grain boundaries. Due to the grains having individual orientations, some misorientation is to be expected at the grain boundaries. The image quality maps for EBSD, seen in Figure 122, show a low quality of the electron diffraction patterns at the grain boundaries. This made it difficult for the software to index these areas correctly. This confirms that the the HCP and BCC phases were likely indexed incorrectly and the material consisted entirely of FCC unit cells. For Prosthesis SS, the pattern quality was low at the grain boundaries and in the areas with noise, which was where the aplha and chromium iron carbide phases were detected. This leads to the conclusion that these phases were incorrecly indexed. The material in prosthesis SS was likely only gamma phase, and was therefore austenitic steel. This also aligns well with Section 3.2.2.

Prostheses Co and Co-o had similar microstructures obtained by etching with the Murakami etchant. The patterns were even - confirming that these prostheses were cast. The Murakami pattern showed that the surface pattern seen in the SEM examinations, shown in Figure 75, was obtaining a darker color that expanded with the use of this etchant. EDS showed that the lighter parts of this pattern, pre etching, consisted of cobalt, chromium and molybdenum, only the molybdenum content was far higher than in the bulk material. The darker parts of the pattern, pre etching, consisted mainly of chromium. The Murakami images from the light microscope showed that the frequency of these patterns varied with location. The parallel cut sample of the stem had stronger coloration, indicating that these patterns were possibly elongated and located similarly to the grains illustrated in section b) of Figure 124. The mid sections of the samples generally had stronger patterns than the edges, towards the prosthesis surface. This indicated that the segregation of alloy elements were more pronounced in the centre of the prosthesis. This aligns well with the prosthesis being manufactured through casting.

7.5   Hardness and tensile properties

The stainless steel alloy presented both the hardest and the most ductile material among the three prostheses. This was shown in hardness measurements, in the elongation within

the tensile testing, seen in Figure 123, and in the dimpled fracture surfaces of the tensile test specimens, seen in Figure 51. The hardness of the sample was about 30 HV higher at the perpendicular cross section of the stem than the parallel cross section, which was a beneficial distribution considering the loads a prosthesis stem is subjected to. The combination of ductility and overall high hardness benefited the material by allowing it to withstand large amounts of loads and stresses before fracturing.

Prosthesis Co and Co-o both had high hardness values as well, though not as high as prosthesis SS. There was no obvious difference in hardness within the stems in either direction. It is worth noting that the large grain size of these prostheses means that each hardness measurement only measured one or two grains, depending on the location. The diameters of the hardness measurement indentations for prostheses Co and Co-o did not exceed 190 micrometer, which means that a higher number of hardness measurements would be necessary to get an estimate that is fully representative of each material as a whole. This was also a challenge for the tensile tests.

Co-o was the most brittle of prosthesis Co and prosthesis Co-o based on the tensile test, though they both had mainly brittle fractures when examining the tensile test fracture surfaces. These can be seen in Figure 52 and 56. Though prostheses Co and Co-o started to plastically deform at approximately the same load and elongation, prosthesis Co-o had a much lower total elongation before fracture occurred compared to prosthesis Co. The slip lines seen in Figure 57 were also indicative of a brittle material. Looking at the fractures of the tensile samples, prosthesis Co and Co-o fractured very differently. Prosthesis Co fractured along the grain boundaries, an intergranular fracture, leaving large facets of about half a millimeter. Prosthesis Co-o had much smaller facets that did not align with grain boundaries. This was a brittle transgranular fracture.

The tensile tests reflected the *Hall-Petch* equation in the sense that prosthesis SS, that had the smaller grains, also had the highest yield strength of the prostheses. This equation can be seen in Equation 7. The yield strength for prostheses Co and Co-o were similar, even though prosthesis Co-o had larger grains than prosthesis Co. This could be because the Hall-Petch equation stops being valid for very coarse grains. Cast components typically have more pores, which aligns well with the forged stainless steel prosthesis having the highest ultimate tensile strength. However, prosthesis SS was from a different alloy than the other prostheses, so these results are not directly comparable.

The Young's modulus was incorrect for all three prostheses and was abnormally low. This was due to error sources tied to the samples and to the method in which the data was obtained. The listed Young's moduli were based on the stress-strain curves from the grip separation of the machine and not from the laser video extensometer. This does not take into account the stiffness of the sample and machine, which would give lower values for Young's moduli. The samples were also very small, causing large amounts of movement within the material. This movement was not just located around the fracture sites, but throughout the whole specimens. This is the reason that the laser video extensometer was

not able to measure correct values, and the large amounts of deformation in the samples could have affected the Young's modulus based on the grip separation as well. In addition to these factors, the grains of prostheses Co and Co-o were very large, which would mean that only a few grains were present in the cross section of the tensile test samples. This can clearly be seen in the large facets of Figure 52. Larger samples containing more grains would give more accurate measurements.

7.6 Further work

For further work, it would be valuable to examine multiple prostheses of the same kind in order to reveal patterns and flaws that could be improved within the individual designs. More background knowledge would strongly benefit this work. From the factory this includes methods and parameters for the production and properties prior to use. From the use of the prosthesis it would be beneficial to know how long the prosthesis was in place, how active the patient was during this time and the reason for removal.

Furthermore, it would be informative to examine the individual materials in more detail. For the stainless steel alloy, it would be beneficial to try several more etchants, for example the A3 etchant from *Struers*, which contains methanol and 2-Butoxyethanol, to examine the structure in a light microscope. For the CoCrMo alloys it would be of interest to find an etchant that revealed the grain structure in a light microscope. This would allow examinations to be made at a lower magnification, making it easier to see the grain structure as more grains would fit in each image.

For all alloys, x-ray diffraction could be used to obtain specific information about the crystallographic structures. This combined with EBSD can give valuable information about the phases in the material. Further, Charpy tests could be used to find the notch tougnesses for the prostheses. It would also be beneficial to look at how the materials interact with various environments, possibly combined with cyclic stresses as well. Corrosion tests could be performed by exposing material samples to various liquids or gases.

8 Conclusion

Two prostheses from CoCrMo and one prosthesis from stainless steel were investigated. Both prostheses from CoCrMo had unfavourably large grains that would not impede crack propagation well. One of these prostheses had a fatigue fracture caused by cyclic stresses during use. The stainless steel alloy had an unfavourable grain orientation with regards to expected potential crack propagation, and all prostheses had some corrosion. There were signs of tribocorrosion between the femoral heads and necks for the CoCrMo prostheses. Larger damages that likely occurred post use were found on all prostheses.

References

[1] Ortomedic via Anders Sundal. "Informasjon om gammel protese fra DePuy". In: *Message to Anette Johannessen* 04.01.21 (Email).

[2] Stefano Mischler Anna Igual Munoz Nuria Espallargas. *Triboorrosion*, pp. 2,35.

[3] Einar Bardal. *Corrosion and Protection*. Springer, 2003, pp. 94–110,345–353.

[4] Jo De Schepper Bart J.Vundelinckx Luk A.Verhelst. "Taper Corrosion in Modular Hip Prostheses: Analysis of Serum Metal Ions in 19 Patients". In: *The Journal of arthroplasty* 28.7 (2013), pp. 1218–1223.

[5] Teak-Rim Yoon Chang Yong Hu. "Recent updates for biomaterials used in total hip arthroplasty". In: *BMC* (2018).

[6] Harmen B. Ettema-Cees C. Verheyen Christiaan P.van Lingen Luigi M. Zagra. "Sequelae of large-head metal-on-metal hip arthroplasties: Current status and future prospects". In: *EFORT open reviews* 1.10 (2016), 345–353.

[7] Christoph Schweigel Olaf Keßler Rainer Bader Christian Schulze Markus Weinmann. "Mechanical Properties of a Newly Additive Manufactured Implant Material Based on Ti-42Nb". In: *Materials* Vol.11.1 (2018), p.124.

[8] Allalou A. Poichotte A. et al. Colas S. "Exchangeable Femoral Neck (Dual-Modular) THA Prostheses Have Poorer Survivorship Than Other Designs: A Nationwide Cohort of 324,108 Patients." In: *Clin. Orthop. Relat.* 475 (2017), pp. 2046–2059.

[9] European Commission. *Current Directives EU*. 2020. URL: https://ec.europa.eu/health/md_sector/current_directives_en(downloaded26.01.21at12.55).

[10] European Commission. *Medical Devices - New regulations*. URL: https://ec.europa.eu/health/md_newregulations/overview_en(downloaded26.01.21at12.55).

[11] European Commission. *New EU Rules to Ensure Safety of Medical Devices. DOI: 10.2873/51617*. 2018. URL: https://ec.europa.eu/docsroom/documents/30908(downloaded26.01.21at13.11).

[12] European Commission. *Regulation (EU) 2017/745 on Medical Devices*. URL: https://eur-lex.europa.eu/legal-content/EN/TXT/?uri=CELEX:02017R0745-20200424#tocId142(downloaded26.01.21at13.55).

[13] S. Cronjé et al. "Twinning in copper deformed at high strain rates". In: *Bulletin of Materials Science* 36 (Feb. 2013).

[14] Michael B. Cross. "Revision Total Hip Replacement". In: *OrthoInfo* (2017).

[15] Jens ; Turger Anke ; Helmecke Patrick ; Correa Tomas ; Hurschler Christof Denkena Berend ; Köhler. "Manufacturing Conditioned Wear of All-ceramic Knee Prostheses". In: *Procedia CIRP* 5 (2013), pp.179–184.

[16] Jelena Djokovic et al. "Estimate of the steel bridges fatigue life by application of the fracture mechanics". In: *IOP Conference Series: Materials Science and Engineering* 419 (Sept. 2018).

[17] N. Dowling. *Mechanical Behavior of Materials - Engineering Methods for Deformation, Fracture and Fatigue*. 4th edition. Pearson Prentice Hall, 2007.

[18] N. Dunne and J. Clements. *Joint replacement technology*. Chapter 8, 2nd edition. Woodhead Publishing, 2014, p. 212.

[19] O.K. Muratoglu E. Oral S.M. Kurtz. "Ultrahigh Molecular Weight Polyethylene Total Joint Implants". In: *Comprehensive Biomaterials II* ISBN 9780128051443 (2017), pp. 34–57.

[20] Y. Enomoto. "Steam turbine retrofitting for the life extension of power plants". In: *Advances in Steam Turbines for Modern Power Plants* 17 (2017), pp. 397–436.

[21] S.Aaron Catledge Michelle D. McClenny Jack Lemons K.David Moore Erick M. Santos Shikhar Vohra. "Examination of surface and material properties of explanted zirconia femoral heads". In: *The Journal of Arthroplasty* 19.7 (2004), pp. 30–34.

[22] Fehim Findik. "Latest progress on tribological properties of industrial materials". In: *Materials Design* Volume 57 (2014), pp. 218–244.

[23] Mohammadreza Yaghoobi George Z. Voyiadjis. *Size Effects in Plasticity: Chapter 1 - Introduction: Size effects in materials*. Academic Press, 2019, pp. 1–79.

[24] Carlos Vidal-Fernández Guillermo Sánchez-Inchausti Javier Vaquero-Martín. "Effect of Arthroscopy and Continuous Cryotherapy on the Intra-articular Temperature of the Knee". In: *Arthroscopy: The Journal of Arthroscopic Related Surgery* Volume 21.Issue 5 (2005), pp. 552–556.

[25] Dr. Åke Hamberg. "Re: Identifisere proteser". In: *Message to Anette Johannessen* 01.04.21 (Email).

[26] B P P N Siddappa Sampathkumar L Prashanth L Hanamantraygouda M Shivakumar. "Effect of Cold Forging on Microstructure and Mechanical Properties of Al/SiC Composites". In: *IOP Conference Series: Materials Science and Engineering* 310 (2018).

[27] Nasjonal kompetansetjeneste for leddproteser og hoftebrudd. *Rapport juni 2020*. 2020. URL: http://nrlweb.ihelse.net/Rapporter/Rapport2020.pdf(downloaded13.12.20at18.19).

[28] F. Heatley J. Walczak F. Shahgaldi. "In vivo corrosion of 316L stainless-steel hip implants: morphology and elemental compositions of corrosion products". In: *Biomaterials* 19 (1998), pp. 229–237.

[29] Wei W. Jin C. "Wear". In: *Narayan R. (eds) Biomedical Materials* Chapter 6.3.1 (2009).

[30] Michael D. Ries Richard W. McCalden Abraham Salehi David C. Kelman John L. Masonis Robert B. Bourne. "Zirconia femoral head fractures: A clinical and retrieval analysis". In: *The Journal of Arthroplasty* 19.7 (2004), pp. 898–905.

[31] Robert Whittaker Gordon Blunn John Skinner Alister Hart Kevin Ilo Emma Derby. "Fretting and Corrosion between a metal shell and metal liner may explain the high rate of failure of R3 modular metal on metal hips". In: *The Journal of arthroplasty* Vol.32.5 (2016), pp.1679–1683.

[32] Ludwig T. E. Liebisch G. Zhang R. Siebert H. Wilhelm J. Steinmeyer J Kosinska M. K. "Articular joint lubricants during osteoarthritis and rheumatoid arthritis display altered levels and molecular species". In: *PloS One* 10.5 (2015), p. 1.

[33] Lawrence Livermore National Laboratory. *Solving the mysteries of metal hardening*. 2018. URL: `https://str.llnl.gov/2018-09/bulatov(Downloaded20.06.21at16.34)`.

[34] Catherine Van Der Straeten Floris Wuyts Leen Maes Laura Leyssens Bart Vinck. "Cobalt toxicity in humans—A review of the potential sources and systemic health effects". In: *Toxicology* 387 (2017), pp. 43–56.

[35] A. Pramanikc L.C. Zhang E.C.S Kiat. "A Briefing on the Manufacture of Hip Joint Prostheses". In: *Advanced Materials Research* 76-78 (2009), pp. 212–216.

[36] Young Wook ; Kwon Soon Yong ; Kwon Soon Yong ; Sun Doo Hoon ; Sun Doo Hoon ; Kim Yong Sik ; Kim Yong Sik Lim Young Wook ; Lim. "The Otto Aufranc Award: Enhanced Biocompatibility of Stainless Steel Implants by Titanium Coating and Microarc Oxidation". In: *Clinical orthopaedics and related research* Vol.469.2 (2011), pp.330–338.

[37] Link. *Lubinus SP II® Anatomically Adapted Hip Prosthesis System*. URL: `https://www.linknederland.nl/_cache/link/media/xmjiw48674/Link_Nederland_SPII_Instrumenten-Implantaten-OK_techniek_08_2017_nieuw.pdf?hash=bce64ac0dd543b11(downloaded05.06.21at20.21)`.

[38] G. J. Roger M. J. Cross and J. Spycher. *Joint replacement technology*. 2nd edition. Woodhead Publishing, 2014. Chap. 7, pp. 186–195.

[39] The library of manufacturing. *Metal Forging*. URL: `https://thelibraryofmanufacturing.com/forging.html(downloaded16.02.21at14.00)`.

[40] Saverio Affatato Massimiliano Merola. "Materials for Hip Prostheses: A Review of Wear and Loading Considerations". In: *Materials (Basel, Switzerland)* 12(3).495 (2019).

[41] Vidmar J Kovač S Trebše R. Milošev I Levašič V. "pH and metal concentration of synovial fluid of osteoarthritic joints and joints with metal replacements." In: *J. Biomed. Mater. Res. B. Appl. Biomater.* 105.8 (2017), pp. 2507–2515.

[42] Icahn School of Medicine at Mount Sinai. *Cobalt poisoning*. 2021. URL: `https://www.mountsinai.org/health-library/poison/cobalt-poisoning(downloaded20.06.21at21.17)`.

[43] Mitsuo Niinomi. "Metallic biomaterials". In: *Journal of artificial organs : the official journal of the Japanese Society for Artificial Organs* 11 (Feb. 2008), pp. 105–10.

[44] Yoshimitsu Mori Okazaki. "Mechanical Performance of Artificial Hip Stems Manufactured by Hot Forging and Selective Laser Melting Using Biocompatible Ti-15Zr-4Nb Alloy". In: *Materials* 14(4) (2021), p.732.

[45] Steven M Kurtz;Kevin Ong. "Chapter 6 - Contemporary Total Hip Arthroplasty: Hard-on-Hard Bearings and Highly Crosslinked UHMWPE". In: *UHMWPE Biomaterials Handbook* (2009), pp.55–79.

[46] Volker Otten. *The Uncemented Cup in Total Hip Arthroplasty - Stability, Wear and Osteolysis*. Department of Surgical and Perioperative Sciences, Orthopaedics, Umeå, 2019, pp.13–15,19–23.

[47] Øyvind Palm. "Leddvæske". In: *Store medisinske leksikon* https://sml.snl.no/leddv%C3%A6ske(downloaded20.12.20at13.16) (2020).

[48] Lim S. J. Park Y. S. Park C. W. "Modular Stems: Advantages and Current Role in Primary Total Hip Arthroplasty". In: *Hip pelvis* 3.30 (2018), pp.147–155.

[49] Link via Per Kristian Knutsen. "Informasjon om gamle proteser fra Link". In: *Message to Anette Johannessen* 04.01.21 (Email).

[50] M; Joyce T J Serrano-Pedraza I Reed M R; Partington P F Petheram T G; Bone. "Surface finish of the Exeter Trauma Stem: a cause for concern?" In: *The bone joint journal* Vol.95-B.2 (2013), pp.173–176.

[51] G von Wieding H Speitling-A Procter P von Oldenburg. *Implant Alloys and Interfacial Engineering*. Springer Berlin Heidelberg, 2006, p. 70.

[52] I.M. Hutchings R.I. Trezona D.N. Allsopp. "Transitions between two-body and three-body abrasive wear: influence of test conditions in the microscale abrasive wear test". In: *Wear* vol.225–229.Part 1 (1999), pp. 205–214.

[53] Sorin Boicean Adrian Bratu Dan Birlutiu Victoria Rus Liviu Tantar Cristian Mitariu Sebastian Roman Mihai Fleaca. "Assesment of Synovial Fluid pH in Osteoarthritis of the Hip and Knee". In: *Revista de Chimie* vol.68, 1st edition (2017), pp. 1340–1342.

[54] Mouhanad M ; Tzeng Tony H ; Mihalko William M ; Chambers Monique C ; Grupp Thomas M Saleh Khaled J ; El Othmani. "Acrylic bone cement in total joint arthroplasty: A review". In: *Journal of orthopaedic research* Vol.34.5 (2016), pp.737–744.

[55] Pierre D. Seeman Delmas. "MECHANISMS OF DISEASE: Bone Quality - The Material and Structural Basis of Bone Strength and Fragility". In: *The New England Journal of Medicine* 354(21) (2006), pp. 2250–61.

[56] Bandar AlMangour Dariusz Grzesiak Kee-Ahn Lee So-Yeon Park Kyu-Sik Kim. "Effect of unit cell topology on the tensile loading responses of additive manufactured CoCrMo triply periodic minimal surface sheet lattices". In: *Materials Design* Volume 206 (2021).

[57] Jan Ketil Solberg. *Kompendium: Teknologiske metaller og legeringer*. NTNU, 2017, pp. 67–69.

[58] Stryker. *Exeter Femoral Hip Stem*. 2021. URL: `https://www.stryker.com/us/en/joint-replacement/products/exeter.html(downloaded05.06.21at20.09)`.

[59] themechanicalgeek.blogspot.com. *What is galvanic corrosion*. 2014. URL: `http://themechanicalgeek.blogspot.com/2014/07/what-is-galvanic-corrosion.html(Downloaded15.06.21at20.26)`.

[60] Van Aken-D.C. Qing J. et al. Wan J. "A Comparison of Adhesive Wear with Three-Body Abrasive Wear Characteristics of Graphitic White Irons Designed for Metal-to-Metal Wear Systems". In: *Inter Metalcast* (2020).

[61] Paul K. Chu Weihong Jin. "Orthopedic Implants". In: *Encyclopedia of Biomedical Engineering* ISBN 9780128051443 (2019), pp. 425–439.

[62] WHO. *WHO Global Model Regulatory Framework for Medical Devices including in vitro diagnostic medical devices*. 2017. URL: `https://apps.who.int/iris/bitstream/handle/10665/255177/9789241512350-eng.pdf;jsessionid=5A65F777021E7410EF1BF0B29385C365?sequence=1(downloaded26.01.21at12.58)`.

[63] David G. Rethwisch William D. Callister. *Materials Science and Engineering*. 9th edition. John Wiley and sons, 2015, pp.163–164,266–312.

[64] E M Wooley P H ; Schwarz. "Aseptic loosening". In: *Gene therapy* Vol.11.4 (2004), pp.402–407.

[65] R. Trebše R. van der Linden-J. Pieper T. Sillat S. Virtanen V-M. Tiainen Y. T. Konttinen I. Milošev. *Joint replacement technology*. 2nd edition. Woodhead Publishing, 2014. Chap. 4, pp.84,131–134.

[66] Yanjing Su Lijie Qiao Yang Wang Yu Yan. "Release of metal ions from nano CoCrMo wear debris generated from tribo-corrosion processes in artificial hip implants". In: *Journal of the mechanical behavior of biomedical materials* 68.04 (2017), pp.124–133.

[67] Xiaoqing et al. Zhang. "Corrosion behaviour of CoCrMo alloys in 2 wt% sulphuric acid solution." In: *Electrochimica acta* 125 (2014), pp.543–555.

APPENDIX A - XRF measurements

Table A: The table below lists the full results from the XRF analysis. The yellow color represents prosthesis SS, blue color represents prosthesis Co and the green color represents prosthesis Co-o. It is assumed that the apparatus provides uncertainty with one standard deviation.

FEMORAL HEAD OF PROSTHESIS SS				FEMORAL NECK OF PROSTHESIS SS			
Element	Measurement 1 [wt%]	Measurement 2 [wt%]	Measurement 3 [wt%]	Element	Measurement 1 [wt%]	Measurement 2 [wt%]	Measurement 3 [wt%]
Mn	4.23 ± 0.03	4.21 ± 0.03	4.23 ± 0.03	Mn	2.31 ± 0.02	2.31 ± 0.02	2.30 ± 0.02
Cr	20.1 ± 0.1	20.1 ± 0.1	20.1 ± 0.1	Zn	0.005 ± 0.001	0.008 ± 0.001	0.008 ± 0.001
Mo	2.24 ± 0.01	2.24 ± 0.01	2.23 ± 0.01	Fe	33.1 ± 0.1	33.2 ± 0.1	33.1 ± 0.1
Ni	9.59 ± 0.04	9.58 ± 0.04	9.55 ± 0.04	Ni	4.38 ± 0.02	4.38 ± 0.02	4.39 ± 0.02
Cu	0.045 ± 0.007	0.053 ± 0.007	0.053 ± 0.007	Pb	0.009 ± 0.003	0.008 ± 0.002	0.010 ± 0.003
Nb	0.31 ± 0.01	0.31 ± 0.01	0.31 ± 0.01	Sn	0.011 ± 0.003	0.014 ± 0.004	0.012 ± 0.004
V	0.083 ± 0.006	0.085 ± 0.006	0.084 ± 0.006	Cr	15.5 ± 0.1	15.5 ± 0.1	15.5 ± 0.1
W	0.010 ± 0.010	-	-	V	0.059 ± 0.005	0.053 ± 0.005	0.057 ± 0.005
Zr	0.002 ± 0.002	0.004 ± 0.002	0.002 ± 0.002	Bi	0.014 ± 0.003	0.011 ± 0.003	0.011 ± 0.003
Fe	63.4 ± 0.1	63.4 ± 0.1	63.4 ± 0.1	Ga	0.013 ± 0.002	0.015 ± 0.002	0.013 ± 0.002
				Mo	0.86 ± 0.01	0.86 ± 0.01	0.86 ± 0.01
				Nb	0.18 ± 0.01	0.18 ± 0.01	0.18 ± 0.01
				As	0.003 ± 0.002	0.004 ± 0.001	0.003 ± 0.002
				Se	0.003 ± 0.001	0.007 ± 0.001	0.007 ± 0.001
				Pd	0.012 ± 0.003	0.014 ± 0.003	0.013 ± 0.003
				In	0.023 ± 0.004	0.023 ± 0.003	0.026 ± 0.004

FEMORAL STEM OF PROSTHESIS SS				FEMORAL HEAD OF PROSTHESIS Co			
Element	Measurement 1 [wt%]	Measurement 2 [wt%]	Measurement 3 [wt%]	Element	Measurement 1 [wt%]	Measurement 2 [wt%]	Measurement 3 [wt%]
Mn	4.16 ± 0.03	4.15 ± 0.03	4.15 ± 0.03	Mn	0.40 ± 0.02	0.40 ± 0.02	0.39 ± 0.02
Cr	19.8 ± 0.1	19.8 ± 0.1	19.8 ± 0.1	Cr	28.1 ± 0.1	28.1 ± 0.1	28.1 ± 0.1
Mo	2.27 ± 0.01	2.28 ± 0.01	2.29 ± 0.01	Ni	0.35 ± 0.02	0.32 ± 0.02	0.33 ± 0.02
Ni	9.91 ± 0.04	9.93 ± 0.04	9.90 ± 0.04	Mo	6.64 ± 0.02	6.63 ± 0.02	6.63 ± 0.02
Cu	0.061 ± 0.008	0.065 ± 0.008	0.062 ± 0.007	Fe	0.43 ± 0.01	0.45 ± 0.01	0.45 ± 0.01
Nb	0.35 ± 0.01	0.34 ± 0.01	0.34 ± 0.01	Ta	0.024 ± 0.011	-	-
V	0.086 ± 0.006	0.086 ± 0.006	0.084 ± 0.006	Nb	-	0.004 ± 0.003	0.003 ± 0.003
W	-	0.015 ± 0.009	0.015 ± 0.010	Co	64.0 ± 0.1	64.1 ± 0.1	64.0 ± 0.1
Zr	0.002 ± 0.002	0.002 ± 0.002	0.004 ± 0.002				
As	0.015 ± 0.003	0.014 ± 0.003	0.016 ± 0.003				
Fe	63.4 ± 0.1	63.3 ± 0.1	63.3 ± 0.1				

FEMORAL NECK OF PROSTHESIS Co				FEMORAL STEM OF PROSTHESIS Co			
Element	Measurement 1 [wt%]	Measurement 2 [wt%]	Measurement 3 [wt%]	Element	Measurement 1 [wt%]	Measurement 2 [wt%]	Measurement 3 [wt%]
Mn	0.13 ± 0.03	0.12 ± 0.03	0.086 ± 0.024	Mn	0.084 ± 0.021	0.091 ± 0.021	0.23 ± 0.02
Cr	27.9 ± 0.1	27.9 ± 0.1	27.9 ± 0.1	Cr	28.0 ± 0.1	28.0 ± 0.1	27.9 ± 0.1
Mo	7.54 ± 0.02	7.58 ± 0.02	7.51 ± 0.03	Ni	-	-	0.23 ± 0.02
Fe	0.27 ± 0.01	0.27 ± 0.01	0.28 ± 0.01	Mo	7.27 ± 0.02	7.28 ± 0.02	6.47 ± 0.02
Ti	0.014 ± 0.008	0.014 ± 0.008	0.014 ± 0.008	Fe	0.32 ± 0.01	0.33 ± 0.01	0.85 ± 0.02
Co	64.1 ± 0.1	64.1 ± 0.1	64.2 ± 0.1	V	0.008 ± 0.006	0.010 ± 0.006	-
				Ti	0.017 ± 0.007	0.018 ± 0.007	-
				Zr	0.007 ± 0.003	0.004 ± 0.003	0.004 ± 0.002
				Co	64.3 ± 0.1	64.3 ± 0.1	64.3 ± 0.1

FEMORAL NECK (TOP) OF PROSTHESIS Co-o				FEMORAL NECK (BOTTOM) OF PROSTHESIS Co-o			
Element	Measurement 1 [wt%]	Measurement 2 [wt%]	Measurement 3 [wt%]	Element	Measurement 1 [wt%]	Measurement 2 [wt%]	Measurement 3 [wt%]
Mn	0.33 ± 0.02	0.33 ± 0.02	0.32 ± 0.02	Mn	0.64 ± 0.02	0.62 ± 0.02	0.65 ± 0.02
Fe	0.15 ± 0.01	0.16 ± 0.01	0.14 ± 0.01	Cr	28.0 ± 0.1	28.1 ± 0.1	28.2 ± 0.1
Ni	1.01 ± 0.02	1.01 ± 0.02	0.94 ± 0.02	Ni	2.31 ± 0.02	2.31 ± 0.02	2.30 ± 0.02
Cr	18.8 ± 0.1	18.8 ± 0.1	18.3 ± 0.1	W	0.14 ± 0.02	0.15 ± 0.02	0.051 ± 0.013
Co	35.6 ± 0.1	35.6 ± 0.1	33.9 ± 0.1	Mo	5.90 ± 0.02	5.89 ± 0.02	5.82 ± 0.02
Mo	3.69 ± 0.01	3.70 ± 0.01	3.44 ± 0.01	Fe	0.39 ± 0.01	0.39 ± 0.01	0.39 ± 0.01
Nb	0.002 ± 0.002	0.003 ± 0.002	0.003 ± 0.002	V	0.010 ± 0.005	0.008 ± 0.005	-
Rh	-	0.018 ± 0.009	-	Ti	0.037 ± 0.007	0.038 ± 0.007	0.007 ± 0.007
				Co	62.5 ± 0.1	62.5 ± 0.1	62.6 ± 0.1

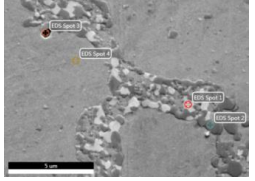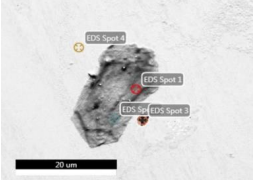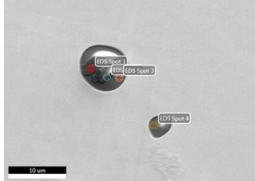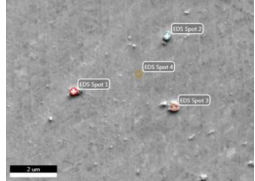| FEMORAL STEM (EXTERNAL) OF PROSTHESIS Co-o				FEMORAL STEM (INTERNAL) OF PROSTHESIS Co-o			
Element	Measurement 1 [wt%]	Measurement 2 [wt%]	Measurement 3 [wt%]	Element	Measurement 1 [wt%]	Measurement 2 [wt%]	Measurement 3 [wt%]
Mn	0.079 ± 0.009	0.080 ± 0.009	0.074 ± 0.009	Mn	0.72 ± 0.03	0.71 ± 0.03	0.70 ± 0.03
Fe	0.18 ± 0.01	0.18 ± 0.01	0.18 ± 0.01	Cr	28.2 ± 0.1	28.2 ± 0.1	28.2 ± 0.1
Ni	0.64 ± 0.01	0.63 ± 0.01	0.63 ± 0.01	Ni	2.27 ± 0.02	2.29 ± 0.02	2.29 ± 0.02
Ti	0.019 ± 0.004	0.021 ± 0.004	0.021 ± 0.004	W	0.16 ± 0.02	0.15 ± 0.02	0.15 ± 0.02
Cr	13.9 ± 0.1	13.9 ± 0.1	13.9 ± 0.1	Mo	5.63 ± 0.02	5.64 ± 0.02	5.63 ± 0.02
Co	23.6 ± 0.1	23.6 ± 0.1	23.6 ± 0.1	Fe	0.45 ± 0.01	0.45 ± 0.01	0.45 ± 0.01
Zr	0.33 ± 0.01	0.32 ± 0.01	0.33 ± 0.01	Nb	0.004 ± 0.003	0.003 ± 0.003	0.003 ± 0.003
Ga	0.002 ± 0.001	-	-	Zr	0.002 ± 0.002	0.003 ± 0.02	0.004 ± 0.002
Mo	1.96 ± 0.01	1.97 ± 0.01	1.97 ± 0.01	Co	62.6 ± 0.1	62.5 ± 0.1	62.5 ± 0.1
Nb	0.002 ± 0.001	0.003 ± 0.001	0.004 ± 0.001				
Rh	-	-	0.013 ± 0.005				

APPENDIX B - EDS measurements

Table B: This table lists the EDS measurements for prosthesis SS. Uncertainty for all values is ±0.01%. The given error represents error range for the determination of the correct element. *SE = Secondary electron imaging. *BSE=Backscatter electron imaging.

COLUMN A — PROSTHESIS SS (Neck)

Spot 1 – Dark particle

Element	Atomic% [%]	Weight% [%]	Error [%]
C	24.24	14.72	8.02
O	54.46	44.06	10.04
Ne	1.03	1.05	13.45
Al	0.70	0.96	7.93
Si	0.81	1.15	5.95
Cl	0.68	1.23	3.49
K	0.33	0.64	4.46
Ca	17.43	35.31	1.03
Fe	0.31	0.87	6.77

Spot 2 – Light particle

Element	Atomic% [%]	Weight% [%]	Error [%]
C	16.91	4.97	10.32
O	13.04	5.11	10.18
Cl	1.42	1.23	5.42
K	0.69	0.66	6.34
Ca	15.45	15.16	2.29
Cr	13.08	16.65	2.15
Eu	0.88	3.27	6.64
Mn	1.16	1.56	4.69
Fe	33.36	45.62	1.99
Ni	4.01	5.77	3.68

Spot 3 – Light particle

Element	Atomic% [%]	Weight% [%]	Error [%]
O	29.51	15.85	7.24
Mg	41.53	33.90	8.34
S	0.23	0.25	11.22
Cl	0.91	1.09	5.70
Cr	6.32	11.03	1.76
Mn	1.00	1.84	3.20
Fe	16.45	30.85	1.58
Ni	1.89	3.73	3.47

Spot 4 – Dark particle

Element	Atomic% [%]	Weight% [%]	Error [%]
C	21.84	5.74	10.14
Cr	18.92	21.53	1.66
Mn	3.43	4.13	2.39
Fe	49.31	60.26	1.81
Ni	6.50	8.35	3.50

Spot 5 – Bulk

Element	Atomic% [%]	Weight% [%]	Error [%]
Cr	24.39	23.01	1.69
Mn	4.49	4.48	2.42
Fe	62.64	63.48	1.88
Ni	8.48	9.04	3.47

COLUMN B — PROSTHESIS SS (Neck)

Spot 1 – Dark patch

Element	Atomic% [%]	Weight% [%]	Error [%]
C	71.82	42.34	8.89
O	9.51	7.47	13.25
Cr	5.23	13.35	6.69
Fe	13.44	36.85	5.01

Spot 2 – Dark patch

Element	Atomic% [%]	Weight% [%]	Error [%]
C	72.64	43.48	8.97
O	8.40	6.70	13.60
Na	1.45	1.66	18.96
Mo	0.34	1.60	25.53
Cl	0.53	0.94	20.08
Cr	4.37	11.33	6.66
Mn	0.56	1.54	29.09
Fe	10.75	29.93	5.00
Ni	0.96	2.81	25.69

Spot 3 - Bulk

Element	Atomic% [%]	Weight% [%]	Error [%]
Mo	1.19	1.99	26.97
Cr	23.80	21.53	4.92
Eu	1.91	5.05	36.96
Fe	65.18	63.34	4.16
Ni	7.92	8.09	15.85

COLUMN C — PROSTHESIS SS (Neck)

Spot 1 – Inside pore

Element	Atomic% [%]	Weight% [%]	Error [%]
O	57.13	42.24	8.93
Ne	0.14	0.13	24.62
Al	36.33	45.30	4.82
Ca	6.31	11.68	2.18
Pm	0.10	0.65	12.28

Spot 2 – Inside pore

Element	Atomic% [%]	Weight% [%]	Error [%]
O	42.27	24.23	8.63
Al	34.74	33.58	6.74
Ca	5.74	8.25	2.41
Cr	4.61	8.59	2.05
Mn	0.95	1.86	3.09
Fe	10.48	20.97	1.71
Ni	1.20	2.53	3.41

Spot 3 – Edge of pore

Element	Atomic% [%]	Weight% [%]	Error [%]
O	15.39	5.49	8.23
Al	13.95	8.40	8.74
Ca	2.48	2.22	3.64
Cr	16.23	18.84	1.80
Mn	3.05	3.74	2.68
Fe	43.38	54.08	1.82
Ni	5.51	7.23	3.43

Spot 4 – Edge of pore

Element	Atomic% [%]	Weight% [%]	Error [%]
CrK	24.00	22.64	1.71
MnK	4.45	4.43	2.44
FeK	63.28	64.11	1.87
NiK	8.28	8.82	3.61

Spot 5 - Bulk

Element	Atomic% [%]	Weight% [%]	Error [%]
C	0.73	0.16	73.15
Cr	24.12	22.89	1.69
Mn	4.37	4.38	2.43
Fe	62.56	63.76	1.88
Ni	8.22	8.81	3.48

COLUMN D (SE* image) — PROSTHESIS SS (Parallel cross section of stem)

Spot 1 – Light area in BSE**

Element	Atomic% [%]	Weight% [%]	Error [%]
N	24.43	6.98	10.76
Fe	21.30	24.25	8.07
Ne	5.42	2.23	11.65
Al	1.00	0.55	10.40
Nb	18.21	34.49	3.02
Cr	28.09	29.78	6.21
Mn	1.54	1.72	39.47

Spot 2 – Light area in BSE**

Element	Atomic% [%]	Weight% [%]	Error [%]
C	4.88	1.12	15.53
Fe	47.33	50.31	6.91
Ni	9.11	10.18	10.48
Al	0.62	0.32	30.39
Si	1.96	1.05	9.94
Mo	1.30	2.37	10.04
Cr	31.03	30.71	6.38
Mn	3.77	3.95	24.70

Spot 3 – Light area in BSE**

Element	Atomic% [%]	Weight% [%]	Error [%]
C	5.86	1.55	13.15
O	4.28	1.50	8.62
Fe	42.48	52.11	6.96
Ne	12.89	5.71	12.00
Al	0.90	0.53	19.37
Si	2.27	1.40	9.51
Mo	1.29	2.71	14.38
Cr	27.07	30.91	6.37
Mn	2.96	3.58	28.00

Spot 4 -Bulk

Element	Atomic% [%]	Weight% [%]	Error [%]
C	4.26	1.00	17.98
Fe	47.25	51.66	6.99
Ne	8.06	3.19	13.23
Ni	3.56	4.10	15.57
Al	0.56	0.30	30.20
Ta	0.39	1.39	9.29
W	0.08	0.27	60.84
Mo	1.04	1.95	12.05
Pb	0.17	0.70	39.17
Cr	31.36	31.93	6.15
Mn	3.26	3.51	27.64

APPENDIX B - EDS measurements

Table C: This table lists the EDS measurements for prosthesis Co. Uncertainty for all values is ±0.01%. The given error represents error range for the determination of the correct element. *SE = Secondary electron imaging. *BSE=Backscatter electron imaging.

COLUMN E — PROSTHESIS Co (Head)

Spot 1 – Dark patch

Element	Atomic% [%]	Weight% [%]	Error [%]
C	90.60	67.55	6.30
Co	2.55	9.32	6.32
Si	0.88	1.53	5.83
Mo	1.05	6.23	5.43
Ca	0.71	1.78	16.06
Cr	4.21	13.60	8.12

Spot 2 – Dark patch

Element	Atomic% [%]	Weight% [%]	Error [%]
C	53.06	34.04	7.55
N	16.21	12.13	11.07
O	15.92	13.60	9.41
Co	4.56	14.36	6.42
Si	3.18	4.77	4.43
Mo	0.93	4.77	4.98
Ca	1.11	2.37	7.53
Cr	5.03	13.97	6.81

Spot 3 – Dark patch

Element	Atomic% [%]	Weight% [%]	Error [%]
C	74.83	56.25	6.74
O	14.91	14.93	10.32
Co	0.96	3.54	9.39
Al	1.05	1.78	6.00
Si	2.31	4.05	4.69
Mo	0.65	3.90	11.58
Ca	2.20	5.51	6.99
Cr	3.08	10.03	9.16

Spot 4 – Bulk

Element	Atomic% [%]	Weight% [%]	Error [%]
C	4.07	0.93	15.48
O	4.84	1.47	8.85
Co	48.36	53.95	6.30
Si	2.38	1.27	8.64
Mo	3.20	5.82	6.42
Cr	37.15	36.57	5.91

COLUMN F — PROSTHESIS Co (Neck)

Spot 1 - Particle

Element	Atomic% [%]	Weight% [%]	Error [%]
O	27.86	17.37	10.96
Na	34.68	31.08	6.08
Mg	5.29	5.02	9.61
Mo	0.92	3.46	15.17
S	0.63	0.79	22.72
Cl	30.61	42.30	3.10

Spot 2 - Pore

Element	Atomic% [%]	Weight% [%]	Error [%]
O	57.57	37.18	7.24
Al	5.72	6.24	7.46
Si	22.64	25.67	4.86
Ti	0.95	1.84	22.52
Cr	5.61	11.78	7.37
Mn	3.43	7.61	12.51
Co	4.07	9.68	14.90

Spot 3 – Pore

Element	Atomic% [%]	Weight% [%]	Error [%]
O	60.26	42.26	7.06
Al	6.17	7.30	6.76
Si	25.37	31.23	4.45
Cr	4.10	9.33	9.24
Mn	4.10	9.88	12.07

Spot 4 – Bulk

Element	Atomic% [%]	Weight% [%]	Error [%]
O	4.42	1.28	16.83
Si	2.07	1.05	17.79
Mo	3.23	5.61	10.97
Cr	34.00	32.01	4.20
Co	56.27	60.04	4.61

COLUMN G — PROSTHESIS Co (Parallel cross section of stem)

Spot 1 - Particle

Element	Atomic% [%]	Weight% [%]	Error [%]
C	18.32	11.16	6.23
O	63.23	51.32	9.06
Ca	18.45	37.51	3.57

Spot 2 - Particle

Element	Atomic% [%]	Weight% [%]	Error [%]
C	96.89	88.16	4.20
Fe	2.48	10.50	5.67
Si	0.63	1.34	8.02

Spot 3 – Bulk

Element	Atomic% [%]	Weight% [%]	Error [%]
C	4.32	0.97	15.50
O	5.14	1.53	8.71
Co	40.38	44.36	5.67
Cu	13.45	15.93	8.47
Si	1.73	0.91	10.46
Mo	2.91	5.20	6.07
Cr	32.08	31.10	5.87

COLUMN H (SE* image) — PROSTHESIS Co (Neck)

Spot 1 – Dark area in BSE

Element	Atomic% [%]	Weight% [%]	Error [%]
O	70.25	57.58	6.82
Al	6.80	9.40	5.26
Si	22.95	33.02	3.99

Spot 2 – Dark area in BSE

Element	Atomic% [%]	Weight% [%]	Error [%]
O	58.28	38.95	6.97
Al	7.51	8.47	6.34
Si	22.95	26.93	4.81
Cr	4.97	10.78	8.07
Mn	3.53	8.10	12.76
Co	2.75	6.78	15.60

Spot 3 – Dark area in BSE

Element	Atomic% [%]	Weight% [%]	Error [%]
O	30.71	12.31	8.07
Al	3.38	2.29	12.86
Si	12.73	8.96	7.28
Mo	1.53	3.68	14.93
Cr	20.27	26.41	4.56
Co	31.39	46.35	5.15

Spot 4 – Bulk

Element	Atomic% [%]	Weight% [%]	Error [%]
O	4.58	1.33	16.11
Si	2.01	1.02	18.06
Mo	2.74	4.78	15.34
Cr	32.44	30.60	4.24
Co	58.23	62.27	4.46

APPENDIX B - EDS measurements

Table D: This table lists the EDS measurements for prosthesis Co-o. Uncertainty for all values is ±0.01%. The given error represents error range for the determination of the correct element.

COLUMN I — PROSTHESIS Co-o (Neck)

Spot 1 – Light area of patch
Element	Atomic% [%]	Weight% [%]	Error [%]
Co	28.12	25.84	6.81
Si	10.21	4.47	5.49
Mo	28.70	42.95	3.07
Cr	32.97	26.74	6.02

Spot 2 – Dark area of patch
Element	Atomic% [%]	Weight% [%]	Error [%]
C	17.83	4.78	9.68
O	8.53	3.04	7.88
Co	7.48	9.83	9.25
Mo	5.68	12.17	4.11
Cr	60.48	70.17	4.97

Spot 3 – Pore
Element	Atomic% [%]	Weight% [%]	Error [%]
C	0.93	0.23	69.84
O	4.08	1.32	9.08
Co	39.79	47.41	6.19
Si	2.06	1.17	9.02
S	18.12	11.74	4.21
Bi	0.26	1.12	28.66
Cr	26.73	28.10	5.93
Mn	8.02	8.91	14.32

Spot 4 – Bulk
Element	Atomic% [%]	Weight% [%]	Error [%]
C	4.30	0.98	15.31
O	5.18	1.57	8.87
Co	49.27	54.95	6.08
Si	2.99	1.59	7.85
Mo	3.94	7.15	5.64
Cr	34.32	33.77	5.88

COLUMN J — PROSTHESIS Co-o (Neck)

Spot 1 – Dark patch
Element	Atomic% [%]	Weight% [%]	Error [%]
C	52.50	20.69	8.57
O	6.49	3.41	8.41
Co	21.24	41.06	5.89
Si	1.62	1.49	7.62
Mo	1.66	5.23	7.43
Cr	16.49	28.12	6.03

Spot 2 – Dark patch
Element	Atomic% [%]	Weight% [%]	Error [%]
C	54.89	22.50	8.46
O	6.80	3.71	8.41
Co	20.42	41.06	5.81
Si	1.37	1.32	7.84
Mo	1.41	4.61	8.17
Cr	15.10	26.79	6.08

Spot 3 – Pore
Element	Atomic% [%]	Weight% [%]	Error [%]
C	59.69	26.68	8.31
O	7.45	4.44	8.70
Co	16.26	35.64	5.86
Si	1.62	1.69	6.45
Mo	1.57	5.62	6.44
Cr	13.41	25.94	6.01

Spot 4 – Bulk
Element	Atomic% [%]	Weight% [%]	Error [%]
C	4.29	0.98	15.21
O	4.95	1.50	8.63
Co	50.98	57.10	6.04
Si	2.64	1.41	8.11
Mo	2.77	5.04	6.78
Cr	34.38	33.97	5.90

COLUMN K — PROSTHESIS Co-o (Parallel cross section of stem)

Spot 1 – Particle in pore, dark
Element	Atomic% [%]	Weight% [%]	Error [%]
O	65.46	45.82	5.87
Br	3.95	13.81	2.78
Al	26.71	31.53	3.71
Cr	3.89	8.85	7.25

Spot 2 – Particle in pore, dark
Element	Atomic% [%]	Weight% [%]	Error [%]
O	67.72	47.14	6.03
Br	5.07	17.64	2.61
Al	24.17	28.37	3.78
Cr	3.03	6.86	7.67

Spot 3 – Inside pore
Element	Atomic% [%]	Weight% [%]	Error [%]
O	61.35	43.06	6.38
Al	11.41	13.51	4.20
Si	16.69	20.56	4.05
Ca	3.58	6.30	5.56
Cr	1.80	4.10	14.83
Mn	5.18	12.47	8.82

Spot 4 – Inside pore
Element	Atomic% [%]	Weight% [%]	Error [%]
C	0.63	0.34	33.75
O	64.42	46.39	6.16
Al	7.75	9.41	4.33
Si	17.56	22.20	3.89
Ca	2.92	5.28	5.88
Cr	1.77	4.13	14.75
Mn	4.95	12.25	8.74

COLUMN L — PROSTHESIS Co-o (Neck)

Spot 1 – Light particle
Element	Atomic% [%]	Weight% [%]	Error [%]
C	12.12	3.47	11.16
O	17.09	6.51	6.81
Co	35.68	50.08	5.82
Al	5.47	3.52	7.21
Si	4.17	2.79	6.58
Mo	2.00	4.58	8.49
Cr	23.46	29.05	5.91

Spot 2 – Light particle
Element	Atomic% [%]	Weight% [%]	Error [%]
C	4.16	1.01	15.42
O	10.75	3.50	6.99
Co	45.13	54.04	6.01
Al	2.68	1.47	9.36
Si	3.34	1.90	7.26
Mo	2.47	4.82	8.66
Cr	31.47	33.25	5.79

Spot 3 – Light particle
Element	Atomic% [%]	Weight% [%]	Error [%]
C	6.81	1.77	12.79
O	14.19	4.93	6.78
Co	41.77	53.40	5.89
Al	2.85	1.67	9.03
Si	4.82	2.94	6.60
Mo	2.05	4.28	9.14
Cr	27.51	31.03	5.90

Spot 4 – Bulk
Element	Atomic% [%]	Weight% [%]	Error [%]
O	5.49	1.62	8.36
Co	53.36	57.92	6.05
Si	2.43	1.26	8.99
Mo	2.62	4.63	7.13
Cr	36.09	34.57	5.86

APPENDIX C - Surface roughness measurements

Table E: The table below lists all surface roughness measurements for prostheses SS and Co. The uncertainty of the non average measurements are all ± 1 unit at the last given decimal placement. The uncertainty of the average values are based on a continuous uniform distribution and given with two standard deviations. The yellow color represents prosthesis SS and the blue color represents prosthesis Co.

FEMORAL HEAD – PROSTHESIS SS

Test	Ra	Unit	Rq	Unit	Rz	Unit	Profile length	Unit
1	429.47	nm	589.98	nm	2.5061	µm	2.1447	mm
2	382.96	nm	511.57	nm	2.2	µm	2.2167	mm
3	414.05	nm	537.44	nm	2.4365	µm	2.4286	mm
4	438.78	nm	566.5	nm	2.4774	µm	2.4063	mm
Average	420±30 (416.32 ±32.23)	nm	550±50 (551.37 ±45.27)	nm	2.4±0.2 (2.41 ±0.18)	µm		

FEMORAL NECK – PROSTHESIS SS

Test	Ra	Unit	Rq	Unit	Rz	Unit	Profile length	Unit
1	96.085	nm	128.73	nm	535.87	nm	463.79	µm
2	101.34	nm	127.37	nm	372.23	nm	417.58	µm
3	95.596	nm	130.82	nm	525.35	nm	527.42	µm
4	99.507	nm	151.1	nm	686.66	nm	775.14	µm
5	99.562	nm	146.89	nm	615.88	nm	624.26	µm
6	101.64	nm	145.21	nm	623.99	nm	799.97	µm
7	108.85	nm	147.78	nm	619.47	nm	772.64	µm
Average	100±8 (100.37 ±7.65)	nm	140±10 (139.70 ±13.70)	nm	600±200 (568.49 ±181.54)	nm		

FEMORAL STEM (TOP) – PROSTHESIS SS

Test	Ra	Unit	Rq	Unit	Rz	Unit	Profile length	Unit
1	127.21	nm	182.68	nm	590.59	nm	476.33	µm
2	122.31	nm	156.41	nm	645.37	nm	847.55	µm
3	120.29	nm	197.16	nm	706.14	nm	685.64	µm
4	131.72	nm	208.56	nm	727.02	nm	493.32	µm
5	119.75	nm	186.76	nm	628.97	nm	654.02	µm
6	124.53	nm	191.92	nm	963.73	nm	839.71	µm
7	134.74	nm	196.62	nm	928.15	nm	832.79	µm
Average	126±9 (125.79 ±8.65)	nm	190±30 (188.59 ±30.11)	nm	700±200 (741.42 ±215.43)	nm		

FEMORAL STEM (BOTTOM) – PROSTHESIS SS

Test	Ra	Unit	Rq	Unit	Rz	Unit	Profile length	Unit
1	107.97	nm	158.1	nm	623.83	nm	768.87	µm
2	140.24	nm	197.69	nm	892.9	nm	705.95	µm
3	127.44	nm	180.22	nm	702.88	nm	644.85	µm
4	113.57	nm	169.51	nm	760.57	nm	725.93	µm
5	121	nm	191.59	nm	590.83	nm	490.47	µm
6	110.83	nm	155.06	nm	665.14	nm	742.21	µm
7	110.92	nm	161.97	nm	655.01	nm	730.55	µm
Average	120±20 (118.85 ±18.63)	nm	170±20 (173.45 ±24.61)	nm	700±200 (698.74 ±174.40)	nm		

FEMORAL HEAD – PROSTHESIS Co

Test	Ra	Unit	Rq	Unit	Rz	Unit	Profile length	Unit
1	116.76	nm	158.04	nm	755.52	nm	1.0978	mm
2	139.91	nm	195.74	nm	911.95	nm	919.35	µm
3	143.21	nm	217.32	nm	905.34	nm	809.05	µm
4	140.18	nm	197.37	nm	866.22	nm	907	µm
5	133.73	nm	192.4	nm	808.35	nm	815.15	µm
Average	130±20 (134.76 ±15.27)	nm	190±30 (192.17 ±34.23)	nm	850±90 (849.48 ±90.31)	nm		

FEMORAL NECK – PROSTHESIS Co

Test	Ra	Unit	Rq	Unit	Rz	Unit	Profile length	Unit
1	469.25	nm	613.12	nm	2.5726	µm	857.06	µm
2	497.57	nm	653.15	nm	2.7765	µm	800.51	µm
3	456.25	nm	631.89	nm	2.2952	µm	777.4	µm
4	500.65	nm	651.27	nm	2.5855	µm	765.46	µm
5	611.26	nm	784.04	nm	3.1399	µm	657.39	µm
6	494.86	nm	653.89	nm	2.6906	µm	766.02	µm
Average	500±90 (504.97 ±89.50)	nm	700±100 (664.56 ±98.68)	nm	2.7±0.5 (2.68 ±0.49)	µm		

FEMORAL STEM (TOP) – PROSTHESIS Co

Test	Ra	Unit	Rq	Unit	Rz	Unit	Profile length	Unit
1	315	nm	397.33	nm	1.6587	µm	849.35	µm
2	360.9	nm	454.2	nm	1.7285	µm	845.72	µm
3	329.44	nm	424.98	nm	1.5608	µm	513.12	µm
4	390.13	nm	502.34	nm	1.9656	µm	695.11	µm
5	422.29	nm	523.24	nm	1.988	µm	749.78	µm
6	315.63	nm	438.31	nm	1.7831	µm	791.68	µm
Average	360±60 (355.57 ±61.94)	nm	460±70 (456.73 ±72.69)	nm	1.8±0.3 (1.78 ±0.25)	µm		

FEMORAL STEM (BOTTOM) – PROSTHESIS Co

Test	Ra	Unit	Rq	Unit	Rz	Unit	Profile length	Unit
1	527.27	nm	656.02	nm	2.4378	µm	732.33	µm
2	555.48	nm	707.86	nm	2.9096	µm	678.27	µm
3	576.09	nm	728.88	nm	2.6013	µm	639.04	µm
4	463.04	nm	613.62	nm	2.5913	µm	714.37	µm
5	456.34	nm	589.13	nm	2.6099	µm	614.56	µm
6	380.47	nm	460.57	nm	1.7572	µm	731.5	µm
Average	500±100 (493.12 ±112.94)	nm	600±200 (626.01 ±154.91)	nm	2.5±0.7 (2.48 ±0.67)	µm		
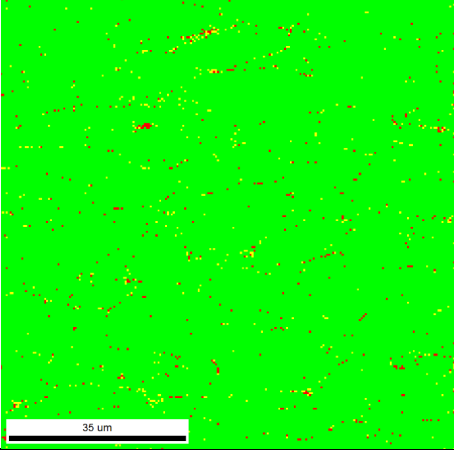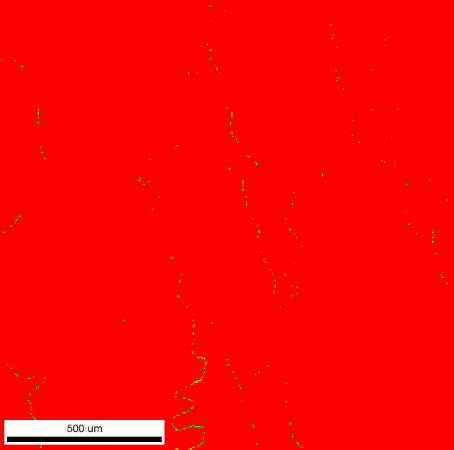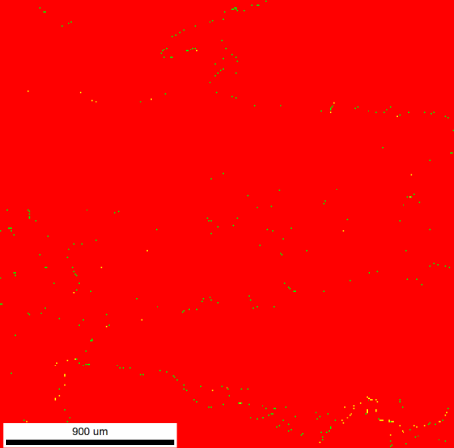
APPENDIX C - Surface roughness measurements

Table F: The table below lists all surface roughness measurements for prosthesis Co-o. The uncertainty of the non average measurements are all ± 1 unit at the last given decimal placement. The uncertainty of the average values are based on a continuous uniform distribution and given with two standard deviations. The green color represents prosthesis Co-o.

FEMORAL NECK (TOP) – PROSTHESIS Co-o

Test	Ra	Unit	Rq	Unit	Rz	Unit	Profile length	Unit
1	338.4	nm	413.9	nm	1.8029	µm	854.37	µm
2	296.15	nm	363.44	nm	1.4751	µm	692.08	µm
3	328.51	nm	401.57	nm	1.5837	µm	695.47	µm
4	284.2	nm	358.3	nm	1.4913	µm	697.45	µm
5	344.51	nm	433.76	nm	1.7745	µm	713.1	µm
6	256.96	nm	310.65	nm	1.2649	µm	787.95	µm
Average	310±50 (308.12 ±50.55)	nm	380±70 (380.27 ±71.08)	nm	1.6±0.3 (1.57 ±0.31)	µm		

FEMORAL NECK (BOTTOM) – PROSTHESIS Co-o

Test	Ra	Unit	Rq	Unit	Rz	Unit	Profile length	Unit
1	315.2	nm	449.13	nm	1.8365	µm	866.08	µm
2	332.44	nm	406.7	nm	1.6677	µm	854.38	µm
3	256.55	nm	309.48	nm	1.1715	µm	746.94	µm
4	316	nm	397.25	nm	1.5018	µm	673.07	µm
5	287.95	nm	363.72	nm	1.343	µm	691.01	µm
6	330.91	nm	444.15	nm	1.5557	µm	753.04	µm
Average	310±40 (306.51 ±43.82)	nm	400±80 (395.07 ±80.63)	nm	1.5±0.4 (1.51 ±0.38)	µm		

FEMORAL NECK (BUST) – PROSTHESIS Co-o

Test	Ra	Unit	Rq	Unit	Rz	Unit	Profile length	Unit
1	301.44	nm	371.94	nm	1.5125	µm	831.65	µm
2	292.96	nm	404.18	nm	1.7413	µm	837.77	µm
3	318.76	nm	392.94	nm	1.5126	µm	683.9	µm
4	295.18	nm	352.43	nm	1.2688	µm	696.73	µm
5	347.41	nm	427.82	nm	1.5991	µm	648.37	µm
6	291.56	nm	390.07	nm	1.5505	µm	754.08	µm
Average	310±30 (307.89 ±32.25)	nm	390±40 (389.90 ±43.53)	nm	1.5±0.3 (1.53 ±0.27)	µm		

FEMORAL STEM – PROSTHESIS Co-o

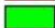| Test	Ra	Unit	Rq	Unit	Rz	Unit	Profile length	Unit
1	229.99	µm	268.34	µm	792.14	µm	1.7138	cm
2	286.45	µm	347.01	µm	901.62	µm	2.445	cm
3	264.46	µm	335.2	µm	1.1097	mm	2.9552	cm
Average	260±30 (260.30 ±32.60)	µm	320±50 (316.85 ±45.42)	µm	900±200 (934.49 ±183.34)	µm		
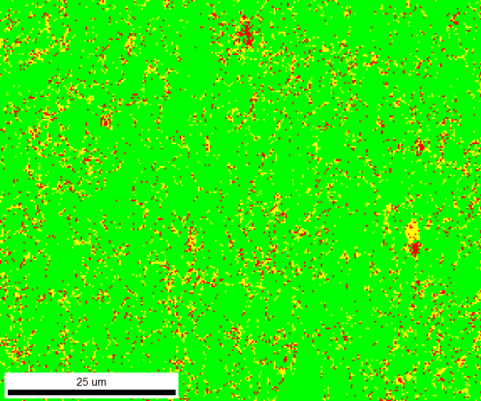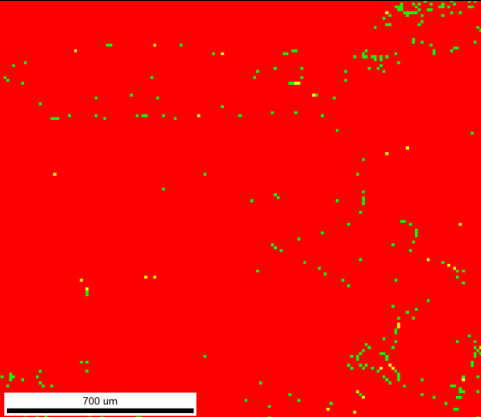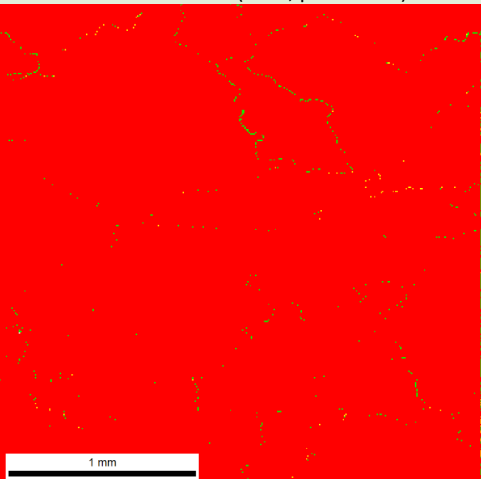
APPENDIX D - EBSD phase maps

Table G: The table below displays phase maps for the EBSD scans of the perpendicularly cut stem section for all prostheses. The yellow table color represents prosthesis SS, the blue table color represents prosthesis Co and the green table color represents prosthesis Co-o.

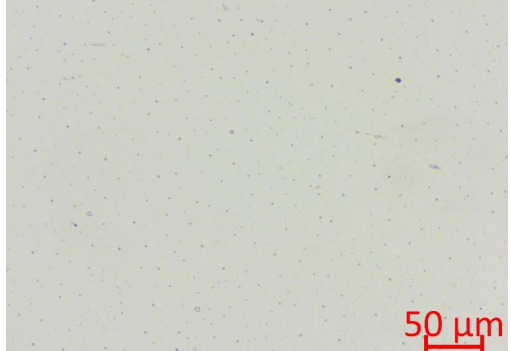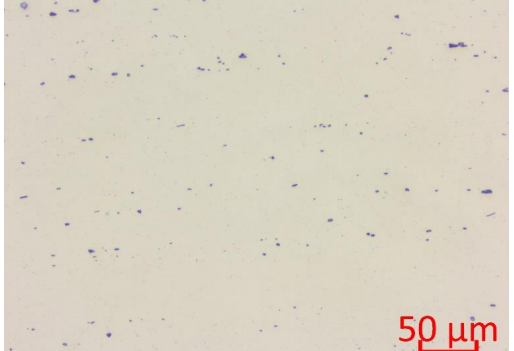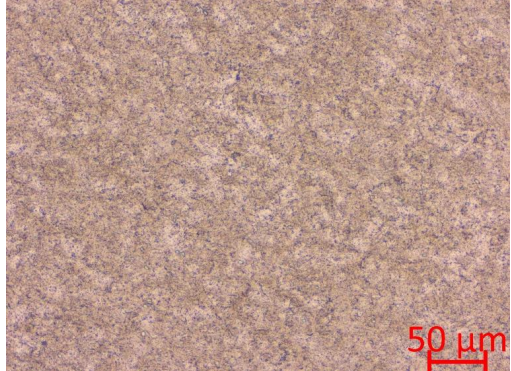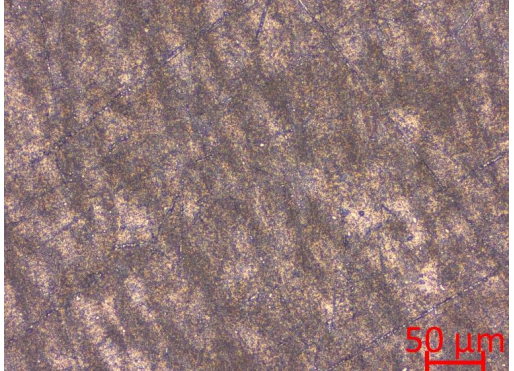| PROSTHESIS SS (stem, perpendicular cut)	Color representation
PROSTHESIS Co (stem, perpendicular cut)	Color representation
PROSTHESIS Co-o (stem, perpendicular cut)	Color representation

APPENDIX D - EBSD phase maps

Table H: The table below displays phase maps for the EBSD scans of the parallel cut stem section for all prostheses. The yellow table color represents prosthesis SS, the blue table color represents prosthesis Co and the green table color represents prosthesis Co-o.

PROSTHESIS SS (stem, parallel cut)	Color representation
	Phase — Total Fraction — Partition Fraction Iron (Alpha) — 0.047 — 0.047 Iron (Gamma) — 0.867 — 0.867 Chromium Iron Carbide — 0.086 — 0.086
PROSTHESIS Co (stem, parallel cut)	**Color representation**
	Phase — Total Fraction — Partition Fraction Face Centered Cubic — 0.987 — 0.987 HCP generic — 0.011 — 0.011 Body Centered Cubic — 0.001 — 0.001
PROSTHESIS Co-o (stem, parallel cut)	**Color representation**
	Phase — Total Fraction — Partition Fraction Face Centered Cubic — 0.994 — 0.994 HCP generic — 0.005 — 0.005 Body Centered Cubic — 0.001 — 0.001

APPENDIX E - Light microscope images

Table I: The table below displays the final results of the attempts to etch prosthesis SS. All photos are at 20x enlargement.

No etchant, head	Nital etchant, head
Marble's etchant, head	Murakami's etchant, neck
Adler's etchant, Perpendicularly cut stem (5 seconds)	Adler's etchant, Parallel cut stem (5+10 seconds)

APPENDIX F - Hardness measurements

Table J: The table below lists hardness measurement results, along with the average values, for all prostheses. The yellow color represents prosthesis SS, the blue color represents prosthesis Co and the green color represents prosthesis Co-o. (PA) indicates *parallel* cross section, (PE) indicates *perpendicular* cross section, (t) indicates *top* and (b) indicates *bottom*. The uncertainty of the average values are based on a continuous uniform distribution and given with two standard deviations.

HARDNESS PROSTHESIS SS					
Placement	Test 1 [HV]	Test 2 [HV]	Test 3 [HV]	Test 4 [HV]	Test 5 [HV]	Average [HV]
Head	267.5 ± 0.1	264.7 ± 0.1	263.0 ± 0.1	266.5 ± 0.1	264.0 ± 0.1	265 ± 3 (265.14 ± 2.60)
Neck	339.8 ± 0.1	339.4 ± 0.1	348.6 ± 0.1	348.7 ± 0.1	343.6 ± 0.1	344 ± 5 (344.02 ± 5.37)
Stem (PA)	354.6 ± 0.1	354.1 ± 0.1	347.1 ± 0.1	342.7 ± 0.1	332.5 ± 0.1	350 ± 10 (346.20 ± 12.76)
Stem (PE)	379.8 ± 0.1	370.8 ± 0.1	385.7 ± 0.1	382.6 ± 0.1	387.7 ± 0.1	380 ± 10 (381.32 ± 9.76)
HARDNESS PROSTHESIS Co					
Placement	Test 1 [HV]	Test 2 [HV]	Test 3 [HV]	Test 4 [HV]	Test 5 [HV]	Average [HV]
Head	322.1 ± 0.1	318.8 ± 0.1	311.8 ± 0.1	322.1 ± 0.1	328.5 ± 0.1	320 ± 10 (320.66 ± 9.64)
Neck	320.4 ± 0.1	299.9 ± 0.1	302.3 ± 0.1	311.1 ± 0.1	314.7 ± 0.1	310 ± 10 (309.68 ± 11.84)
Stem (PA)	298.2 ± 0.1	273.0 ± 0.1	299.3 ± 0.1	278.4 ± 0.1	285.5 ± 0.1	290 ± 20 (286.88 ± 15.18)
Stem (PE)	302.8 ± 0.1	307.7 ± 0.1	292.1 ± 0.1	287.8 ± 0.1	296.3 ± 0.1	300 ± 10 (297.34 ± 11.49)
HARDNESS PROSTHESIS 3 Co-o					
Placement	Test 1 [HV]	Test 2 [HV]	Test 3 [HV]	Test 4 [HV]	Test 5 [HV]	Average [HV]
Neck (t)	346.1 ± 0.1	327.6 ± 0.1	350.7 ± 0.1	331.1 ± 0.1	335.3 ± 0.1	340 ± 10 (338.16 ± 13.34)
Neck (b)	322.0 ± 0.1	333.1 ± 0.1	338.6 ± 0.1	336.6 ± 0.1	329.5 ± 0.1	330 ± 10 (331.96 ± 9.58)
Bust	333.6 ± 0.1	316.8 ± 0.1	315.4 ± 0.1	329.3 ± 0.1	316.8 ± 0.1	320 ± 10 (322.38 ± 10.51)
Stem (PA)	309.0 ± 0.1	334.3 ± 0.1	326.9 ± 0.1	325.0 ± 0.1	313.2 ± 0.1	320 ± 10 (321.68 ± 14.61)
Stem (PE)	303.3 ± 0.1	315.3 ± 0.1	291.4 ± 0.1	310.9 ± 0.1	307.2 ± 0.1	310 ± 10 (305.62 ± 13.80)

Table K: The table below lists the measured diameters that the values in Table J are based on. The yellow color represents prosthesis SS, the blue color represents prosthesis Co and the green color represents prosthesis Co-o. (PA) indicates *parallel* cross section, (PE) indicates *perpendicular* cross section, (t) indicates *top* and (b) indicates *bottom*. All values in Table K below has an uncertainty of ±0.01 μm.

Prosthesis SS										
Test	1		2		3		4		5	
	D1 [μm]	D2 [μm]	D1 [μm]	D2 [μm]	D1 [μm]	D2 [μm]	D1 [μm]	D2 [μm]	D1 [μm]	D2 [μm]
Stem (PA)	161.68	161.68	160.82	162.80	162.43	164.41	164.78	164.16	167.38	166.57
Stem (PE)	157.04	155.43	160.82	155.43	156.85	153.20	157.10	154.19	156.79	152.46
Neck	165.33	165.03	165.27	165.27	163.29	162.86	164.04	162.05	164.84	163.66
Head	188.05	184.28	188.42	185.82	189.23	186.26	188.18	184.83	188.61	186.20
Prosthesis Co										
Test	1		2		3		4		5	
	D1 [μm]	D2 [μm]	D1 [μm]	D2 [μm]	D1 [μm]	D2 [μm]	D1 [μm]	D2 [μm]	D1 [μm]	D2 [μm]
Stem (PA)	176.66	175.98	182.17	186.38	175.30	176.66	184.40	180.56	179.26	181.12
Stem (PE)	172.89	177.03	175.18	171.96	176.42	179.88	177.65	181.31	175.42	178.33
Neck	169.11	171.09	173.82	177.84	173.57	176.66	171.52	173.69	169.92	173.32
Head	171.28	168.00	166.57	174.50	169.98	174.87	168.43	170.84	167.81	168.18
Prosthesis Co-o										
Test	1		2		3		4		5	
	D1 [μm]	D2 [μm]	D1 [μm]	D2 [μm]	D1 [μm]	D2 [μm]	D1 [μm]	D2 [μm]	D1 [μm]	D2 [μm]
Stem (PA)	173.44	172.95	164.53	168.49	166.94	169.85	171.28	166.51	175.18	168.93
Stem (PE)	174.74	174.93	173.57	169.36	178.52	178.21	173.26	172.08	174.74	172.70
Neck (t)	160.82	166.51	167.93	168.49	164.34	160.82	169.61	165.03	168.24	164.28
Neck (b)	171.83	167.50	165.77	167.87	166.82	164.10	167.25	164.65	170.53	164.90
Bust	169.92	163.48	170.91	171.22	169.42	173.44	167.75	167.81	170.04	172.08

APPENDIX G - Tensile measurements

Table L: The table below lists the full results of the tensile tests performed on each prosthesis. The yellow color represents prosthesis SS, the blue color represents prosthesis Co and the green color represents prosthesis Co-o. The uncertainty of the average values are based on a continuous uniform distribution and given with two standard deviations.

TENSILE PROPERTIES – PROSTHESIS SS				
Value	Test 1	Test 2	Test 3	Average
Ultimate tensile strength [MPa]	1175.09 ± 0.01	1227.54 ± 0.01	1202.77 ± 0.01	1200±30 (1201.80±30.28)
Young's modulus [GPa]	14.96 ± 0.01	16.19 ± 0.01	16.53 ± 0.01	15.9±0.9 (15.89±0.91)
Yield strength at 0.2% elongation [MPa]	565.08 ± 0.01	883.08 ± 0.01	886.35 ± 0.01	800±200 (778.17±185.49)
TENSILE PROPERTIES – PROSTHESIS Co				
Value	Test 1	Test 2	Test 3	Average
Ultimate tensile strength [MPa]	824.06 ± 0.01	814.65 ± 0.01	848.39 ± 0.01	830±20 (829.03±19.48)
Young's modulus [GPa]	15.37 ± 0.01	16.56 ± 0.01	15.81 ± 0.01	15.9±0.7 (15.91±0.69)
Yield strength at 0.2% elongation [MPa]	535.45 ± 0.01	491.64 ± 0.01	468.90 ± 0.01	500±40 (498.66±38.42)
TENSILE PROPERTIES – PROSTHESIS Co-o				
Value	Test 1	Test 2	Test 3	Average
Ultimate tensile strength [Mpa]	642.01 ± 0.01	646.44 ± 0.01	651.52 ± 0.01	647±5 (646.66±5.49)
Young's modulus [GPa]	16.41 ± 0.01	15.57 ± 0.01	15.87 ± 0.01	16.0±0.5 (15.95±0.48)
Yield strength at 0.2% elongation [MPa]	482.62 ± 0.01	479.72 ± 0.01	484.78 ± 0.01	482±3 (482.37±2.92)

Table M: The table below displays the engineering stress-strain curves for all prostheses. These are based on the grip separation in the tensile test machine.
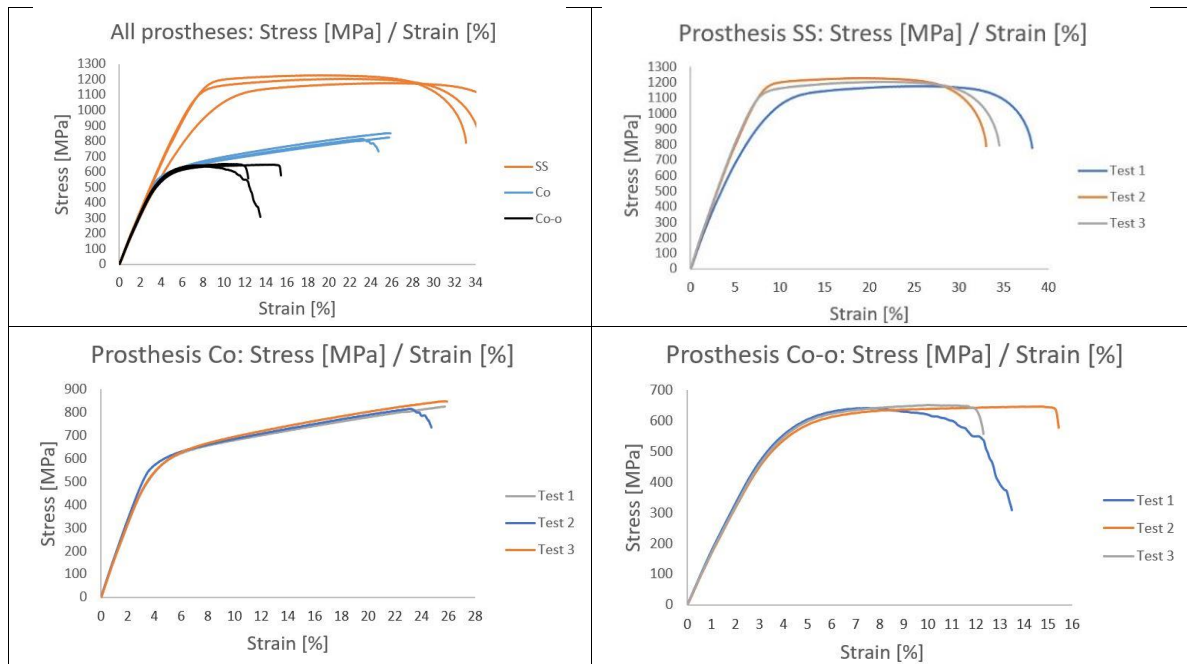
APPENDIX G - Tensile measurements

Table N: The table below displays the engineering stress-strain curves for all prostheses. These are based on a laser video extensometer.